Kinetics of Water Mediated Proton Transfer in the Atmosphere

Dissertation

handed in for the obtainment of the PhD degree

at Leopold-Franzens-Universität Innsbruck

by

MSc Thomas Lörting

28th July 2000

Preface

My first and most important thanks goes to my family, especially to my parents (Mama and Papa), my sister Simone and my brother Andreas, who died much too early, for many important and happy hours in my life and for giving me the opportunity to do what I am doing.

I am very much indebted to my supervisor Klaus Liedl, who first taught me the basics of research, especially how to use literature research for the planning of one's own research, and provided me with insight into state-of-the art theoretical chemistry and second gave me the opportunity to do research on my own initiative.

"Thank you" to Ingrid and Dieter for many discussions on principles and details, which were very helpful.

Maybe the following adaption of a *Paul Simon and Art Garfunkel* song called "Sounds of Science" appeals to those of you who feel critical with university life and the place of science in the world we live in.

I wonder which of the two sides of the "neon god" science shines more.

"Sounds of Science"

Hello darkness, my old friend,
I've come to talk with you again,
Because a vision softly creeping,
Left its seeds while I was sleeping,
And the vision that was planted in my brain
Still remains
Within the sound of science.

In restless dreams I walked alone
Narrow streets of cobblestone,
'Neath the halo of a street lamp,
I turned my collar to the cold and damp
When my eyes were stabbed by the flash of a neon light
That split the night
And touched the sound of science.

And in the naked light I saw
Ten thousand people, maybe more.
People talking without speaking,
People hearing without listening,
People writing songs that voices never share
And no one dare
Disturb the sound of science.

"Fools" said I, "You do not know
Science like a cancer grows.
Hear my words that I might teach you,
Take my arms that I might reach you."
But my words like silent raindrops fell,
And echoed
In the wells of science.

And the people bowed and prayed
To the neon god they made.
And the sign flashed out its warning,
In the words that it was forming.
And the sign said, "The words of the prophets
are written on the subway walls
And tenement halls."
And whisper'd in the sounds of science.

Contents

Chapter 1

Introduction

1.1 Todays Environmental Problems Originating in the Atmosphere

The three environmental problems originating in the atmosphere that are named nowadays probably most often are long-time ozone depletion, acid rain and global warming due to greenhouse-gases. Commonly, all of the three mentioned problems have started to become "problems" after the start of the industrial revolution, when anthropogenic emissions of pollutant gases increased rapidly. Furtheron, these three issues have in common that they are dominated by chemical reactions in the atmosphere, particularly in the stratosphere at a height between 10 and 50 kilometers.[1] In the following the chemical and physical model leading to the mentioned disturbances will be presented.

1.1.1 Acid Rain

An important discovery of environmental chemistry in the last twenty years was the recognition of acid rain and unusually high acidity of lakes. In Figure 1.1 on page 8 the measured

6

acidity of Sweden's lakes is depicted. Interestingly the lowest pH is observed in the south-west region, which is exposed to air circulation from the United Kingdom and Germany. These two nations are highly burdened with sulfur- and nitrogen-oxides. The deposition of these acid-oxides is made responsible for the observed high acidity. Major consequences of continuing low pH are, according to the National Acid Precipitation Assessment Program (NAPAP), strongly decreasing biodiversity and enhanced solubility of poisonous metals, e.g., aluminum.

The most important species in clouds and precipitation is the hydronium ion (H_3O^+). The presence of atmospheric carbon dioxide and the chemical equilibrium between carbonic-acid and the hydrogencarbonate ion in aqueous solution results in a natural pH of 5–6. Precipitation may be termed acidic, therefore, only if the the concentration of H_3O^+ exceeds 10^{-5} mol/l, i.e., pH<5. The aqueous sulfates and nitrates acidify the large amounts of rainwater deposits[2] down to a pH of 4 in most industrial areas, which is significantly lower than 50 years ago. The most acidic fog observed in Los Angeles showed a pH of as low as 1.7, which corresponds to a diluted strong acid. Especially concrete buildings suffer under such conditions. The dramatic increase in anthropogenic sulfur emissions observed over the past decades and the resulting environmental effects have made necessary governmental Sulfur Protocols in the United States, Europe and Asia, e.g., the Montreal Protocol and the Kyoto convention, which now start to result in a recovery of surface waters.[3,4] Besides HNO_3/NO_3^-, HCl/Cl^-, H_2SO_4/HSO_4^-, H_2CO_3/HCO_3^- and NH_4^+/NH_3, i.e., the inorganic acid/base pairs, also organic acids, like formic acid and acetic acid, and formaldehyde have been detected in rainwater.[5] The acidity of the atmospheric water droplets is determined by the composition of the condensation nuclei, from which they originated, and the surrounding trace gases. Due to the higher solubility of SO_2 as compared to NO· and NO₂· in water the "acid-rain chemistry" of the two most important acids, namely sulfuric acid and nitric acid, is quite different. Whereas nitric acid forms in the gas-phase and is dissolved
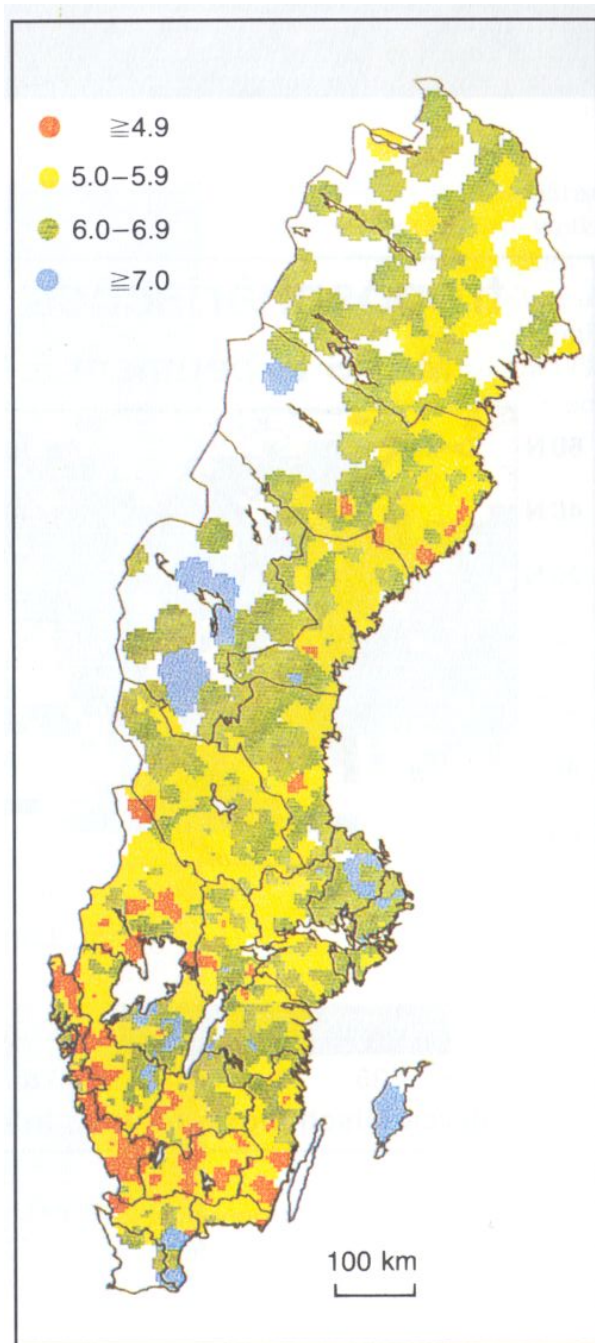
Figure 1.1: The acidity of Swedish lakes in 1985 as determined by the Swedish Environmental Protection Board. Green and blue areas show "natural" pH values above 6.0, whereas yellow and red areas show pH values lower than 6.0 due to industrial contamination. Taken from the atmospheric chemistry book by T. E. Graedel and nobel laureate Paul J. Crutzen.[1]
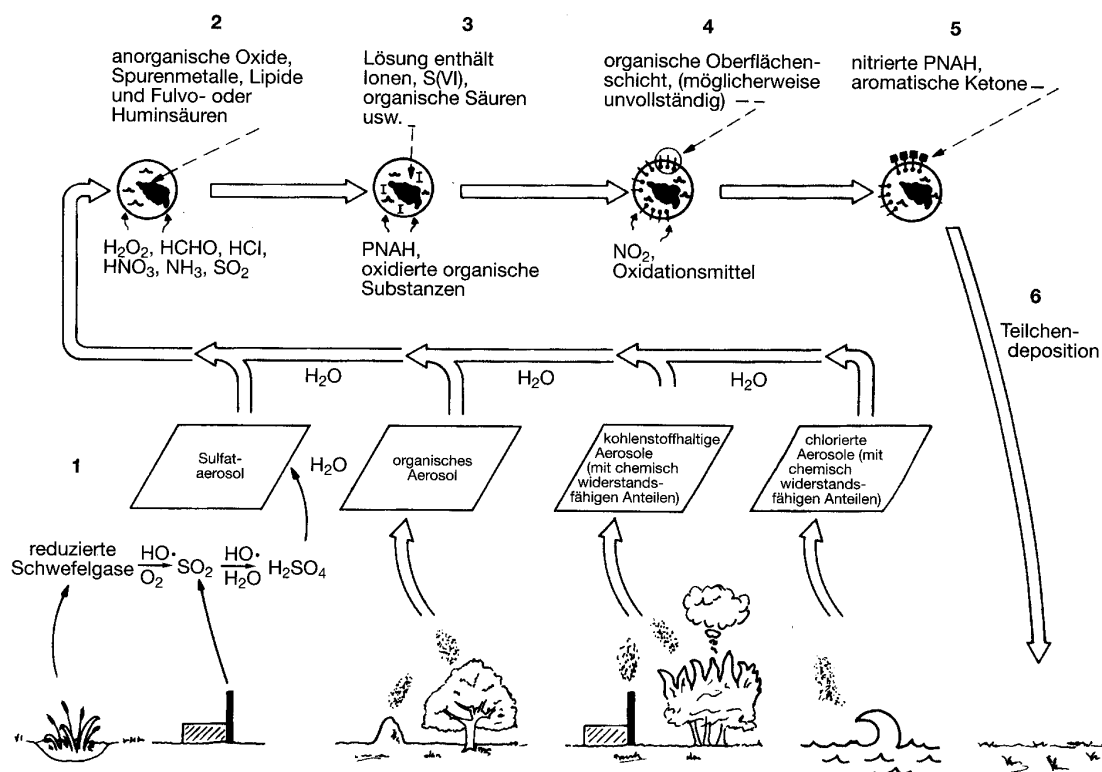
Figure 1.2: Schematic depiction of atmospheric aerosol particle chemistry starting with emission (stage 1), agglomeration (stage 2), dissolving soluble gases (stage 3), incorporation of amphipilic components (stage 4), reactions with the hydrophobic outer part (stage 5) and ending up with particle deposition (stage 6). Taken from the atmospheric chemistry book by T. E. Graedel and nobel laureate Paul J. Crutzen.[1]

as an acid, sulfuric acid forms inside a drop by oxidation with hydrogen peroxide or ozone of dissolved sulfur dioxide.

A typical atmospheric cycle starting from emission and ending up with particle deposition is depicted in Figure 1.2. One can distinguish between three major sources of emission seen under number 1 in Figure 1.2, namely a) spume producing chloride-aerosol, b) mechanical processing of solid surfaces, e.g., drop of foliage or wind-moved dust and c) burning of fossil fuel and biomass producing soot (carbon-aerosol). Independent of their source the smallest aerosol particles aggregate and take up water vapor to reach stage 2

in Figure 1.2. Now the particle has a solid core coated in an aqueous shell. Next, water soluble gases like HCl, formaldehyde, ammonia, nitric acid, sulfur dioxide or hydrogen peroxide enter this shell, which leads to a complex reactive mixture (stage 3). Now, relatively insoluble species gather on the surface of the particle, especially if they contain both a hydrophobic and hydrophilic subunit like, e.g., n-decanol (stage 4). The new organic border layer can react with the surrounding gases. In this manner ketones are built from arenes, and nitrified arenes are produced from reaction of $NO_2\cdot$ with polynuclear aromatic hydrocarbons (stage 5). In the last stage 6 these complicated particles are deposited on the surface. In most cases only the stage 6 particles can be undertaken a chemical analysis. So it is very difficult to know details about the underlying chemical mechanism. My interest is especially in the reactions between stage 1 and stage 2 involving agglomeration and reaction with water. It is supposed that the transformation between gaseous species to liquid/solid species, i.e., condensation, involves the formation of molecular clusters. These clusters are supermolecules formed when some small molecules are held together by weak interactions, e.g., hydrogen bonding or van-der-Waals forces. Weakly bound molecular complexes containing a varying number of molecules ("clusters"), e.g., $SO_2\cdot3H_2O$, can be viewed, therefore, as bridging the gap between single gas-phase molecules and condensed phases like crystalline clouds extending over hundreds of meters.[6] Therefore, they are studied very often in the context of aggregation and condensation. My special interest is the conversion of sulfur dioxide to sulfates raining down Earth's surface in a vast amount.

The Sulfur Cycle

More than 100 million tons of sulfur are emitted per year mainly in the form of dimethyl sulfide (DMS),[7–9] H_2S and sulfur dioxide (SO_2).[1,10,11] A global atmospheric sulfur balance[12] is depicted in Figure 1.3 on page 12. The balance is largely dominated by industrial processes resulting annually in 70 megatons (Mt) of sulfur. A quarter of this amount is

redeposited on the sea due to the influence of wind, weathering and transport by rivers, which leads to increasing acidification of the sea. The natural emission above the landmass amounts to just 2 Mt for comparison. From the oceans much more sulfur is emitted naturally (15–30 Mt) in the form of DMS due to microbiological processes involving algae. About 90% of this amount reenters the sea, so that the natural and anthropogenic deposit approximatively equals. Vulcanoes and fumaroles emit an uncertain amount of up to 11 Mt, which is clearly less than all anthropogenic emissions.

The precursor substances DMS and H_2S are oxidized subsequently to SO_2, which by itself is oxidized following the Stockwell-Calvert mechanism[13] to sulfur trioxide by reaction with the hydroxyl radical and O_2 to SO_3,[14–17] which is in turn hydrated to form sulfuric acid (H_2SO_4) and sulfates (SO_4^{2-}). The latter play a major role in the process of cloud formation as good cloud condensation nuclei.[18–20] Especially "Polar Stratospheric Clouds" (PSC) form from such sulfate nuclei.[16,21–24] The so formed sulfate aerosols increase Earth's reflectance of solar radiation ("albedo") by about 1–2 W/m^2, and thus favor global climate cooling.[7,25–29] It is therefore difficult to rigorously prove a global climate warming induced by anthropogenic emissions. More adversely, the total annual natural[30] and anthropogenic[7,10,11] emission of sulfur is the major source of acid rain.[3,4] Changes of the sulfur cycle not only alter Earth's albedo and the pH of our rain, but are also directly related to climate change, volcanism and tectonics on Venus[31] and presumably also on the Jupiter moons Europa[32] and Io.[33] The chemistry of the involved processes is highly dependent on the amount of water available, i.e., on the relative humidity.[19,34,35] Especially the rate and the product distribution of the atmospheric oxidation of SO_2 to sulfuric acid, occurring predominantly within these cloud droplets, is strongly affected by the hydration state. The production rate and amount of the acidic compounds involved under different conditions of humidity are quantities that would be required for a better understanding of the recovery process.
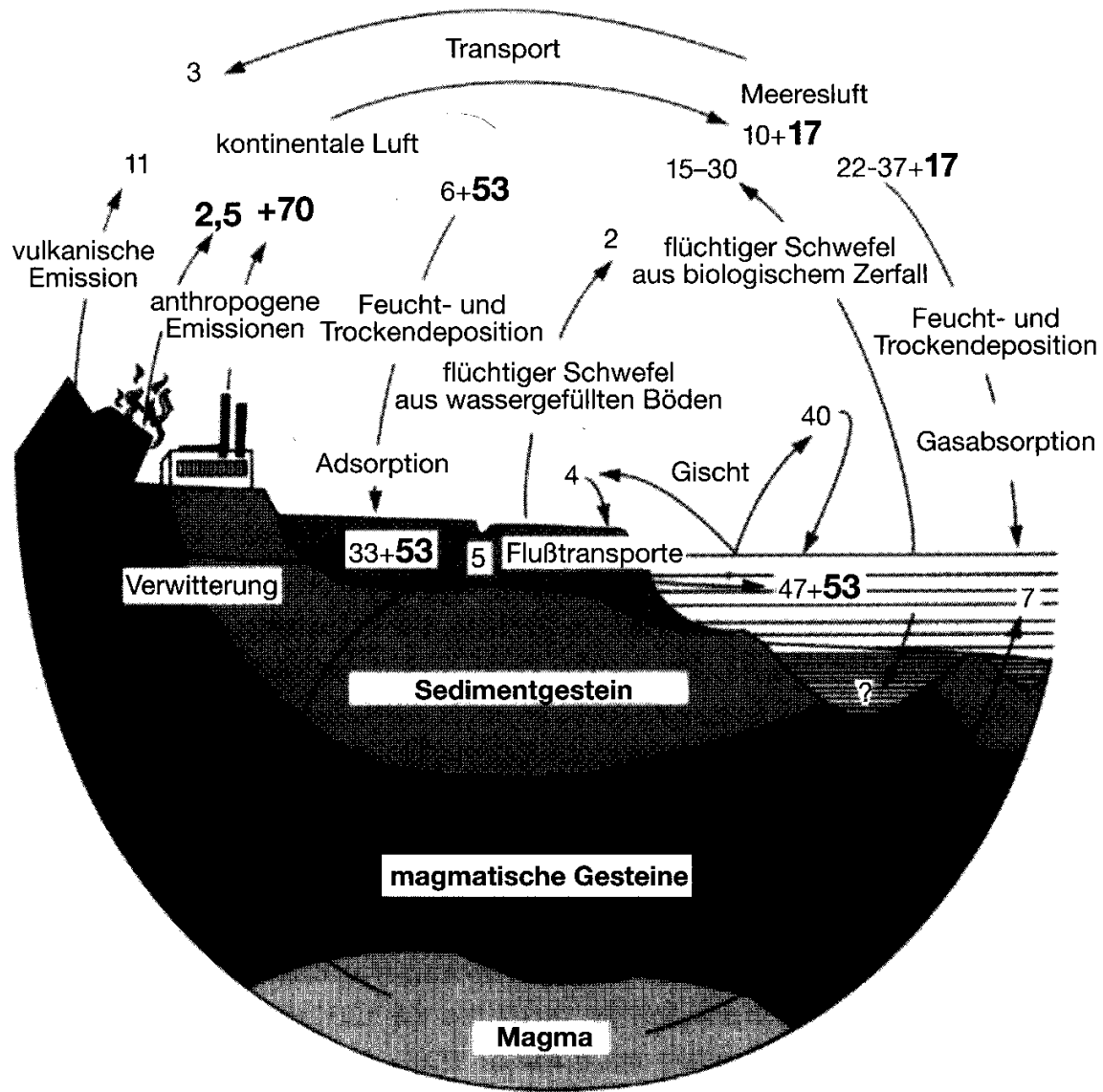
Figure 1.3: A global atmospheric sulfur cycle in megatons per year. Small and large font numbers correspond to the natural and anthropogenic contribution, respectively. Numbers were taken from the book of L. Granat et al.[12] Figure taken from the atmospheric chemistry book by T. E. Graedel and nobel laureate Paul J. Crutzen.[1]
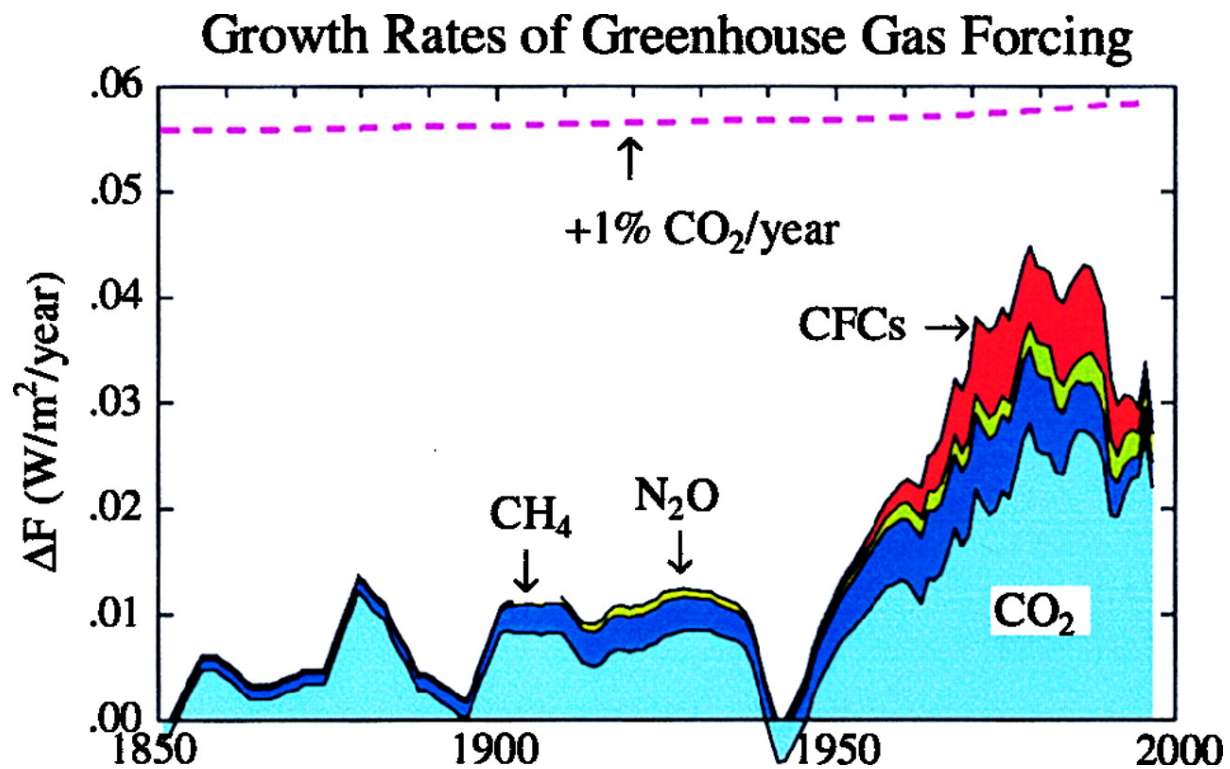
Figure 1.4: Growth rates of greenhouse gas forcing from the year 1850 to the year 2000. Contributions from carbon dioxide (light blue), methane (deep blue), laughing gas (green) and chlorofluorocarbons (red). Note that the additional contribution of the most important greenhouse gas (according to the Global Hydrology and Climate center of the NASA) is missing, namely water, which shows a contribution similar to the one of N_2O.[1] Taken from a publication by Hansen et al.[36]

1.1.2 Anthropogenically Induced Global Warming?

The fundamental source of energy for most terrestrial processes, especially for the climate, is the uptake of sunlight. In case of an equilibrium the amount of uptaken radiation must be compensated by thermal, infrared irradiation from Earth. However, because of human activities the amount of irradiation can be significantly altered. Especially anthropogenically forced increases of carbon dioxide (1990: 26 Mt emission), which is the most prominent greenhouse gas, are of central relevance in this context. An increase in its concentration first reduces terrestrial backscattering to space, as a great portion is arrested in the tropo-

sphere (0–10 km height). In turn this yields increased surface temperatures. The radiative forcing is the amount of reduction of infrared radiation per unit increase of a certain gas. Methane (1990: 0.3 Mt emission) shows a radiative forcing that is very high. It is even 25 times higher than the forcing exerted by CO_2, as this gas adsorbs in spectral regions where no other gases of our atmosphere adsorb. A unit increase, therefore, leads to a much more drastic reduction of the outgoing infrared radiation. Increasing the CO_2 concentration from 250 to 500 ppmv leads to a global warming effect of 3.3 W/m^2, whereas an increase in methane from 1 to 4 ppmw result in a warming of 1.3 W/m^2. The highest radiative forcings, being more than a factor of 1000 higher than the forcing exerted by additional CO_2, are found for chlorofluorocarbons (CFCs, 1990: 1 Kt emission) and N_2O (1990: 6 Kt emission).

In Figure 1.4 on the preceding page the contributors to the total radiative forcings are depicted for periods between 1850 and 1990. Whereas in the 19th century carbon dioxide was responsible for nearly all of the forcing, nowadays CFCs, CH_4 and N_2O contribute by more than a third. The total forcing has increased from <0.1 W/m^2 in the 18th century to >0.5 W/m^2 in the late 20th century.[37] Assuming a continuous increase in greenhouse gases the global temperature will increase by 3–6 K till 2100, whereas since 1765 an increase of less than 1 K was found.[37] This leads directly to the prediction of sea-levels raised by 45 cm in the year 2070. A synergistic effect back coupled to the global warming is the increased water concentration in the atmosphere, which brings an additional contribution to global warming, as water clusters are potent greenhouse-gases.[6] It was stated, therefore, that water is the most dangerous greenhouse-gas.[1] Nevertheless, there are many positive and negative feedback mechanisms, like enhanced cloud formation, reduced precipitation in clouds, increased cloud coverage, chemical reactions, biotic feedback that are very difficult to predict quantitatively.[38–40]

One effect that tends to reduce the global climate forcing results from anthropogenic
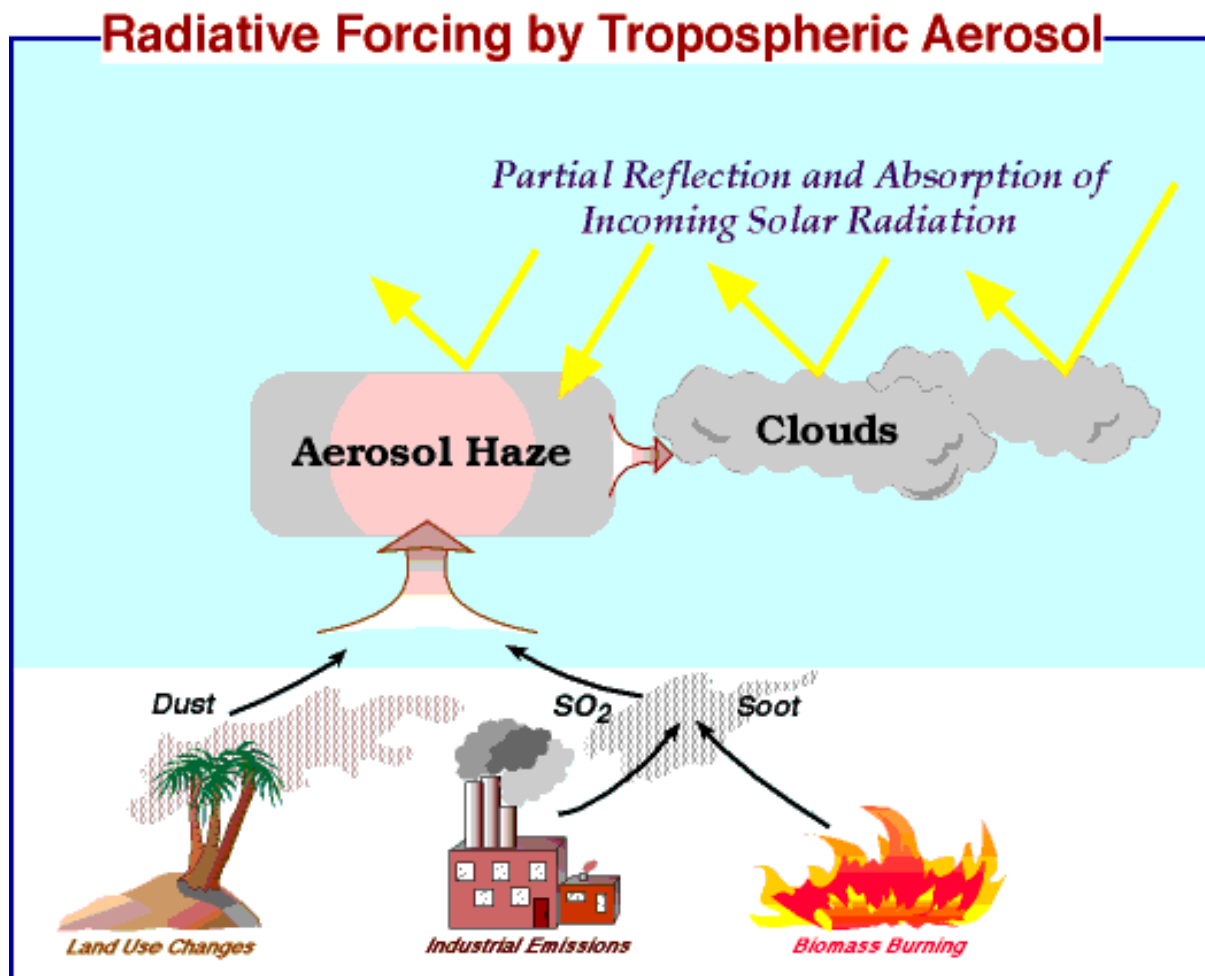
Figure 1.5: Partial reflection and absorption of incoming solar radiation by tropospheric aerosols formed from SO_2 and soot emissions. Taken from the Atmospheric Chemistry Research Program of NOAA's Pacific Marine Environmental Laboratory.

SO$_2$ emissions.[25-29] Besides the adverse effects (i.e., acid rain as mentioned above, destruction of the biosphere and higher optical density) SO$_2$ emissions result in a negative radiative forcing, because incoming solar radiation is partially reflected and absorbed by the tropospheric aerosols as depicted in Figure 1.5 on the page before. The positive forcings of greenhouse gases, the negative forcings exerted by sulfate aerosols and clouds as well as the balanced natural forcings are depicted in Figure 1.6 on the following page. A secondary (indirect) forcing effect ("forced cloud changes") accompanying sulfate aerosol is plagued with a fivefold uncertainty. An increase in sulfate below a cloud increases the number of cloud droplets and thus also the clouds brightness, which in turn increases the reflectivity. It can be seen that the forcings are nearly quantitatively caused by human activities. For that reason it is clear that these global forcings arise mainly from the more industrialized northern hemisphere, whereas the contribution from the southern hemisphere is more or less negligible.

The counterbalance observed in all these forcings renders it difficult to prove a global warming nowadays. So it was stated that a climate index indicates that climate change is apparent only in a few regions in Asia and western North America, but in most places climate trends are too small to stand out above year-to-year variability.[41] However, as already noted the global area with obvious climate change will increase notably in the next few years.

1.1.3   Ozone Depletion

The "ozone hole" was recognized for the first time in 1985.[42] This recognition has resulted in a wealth of studies on the chemical reactions and physical mechanisms involved in ozone depletion and rebuilding.[43-47] Loss of ozone was observed by balloon and satellite measurements above the McMurdo station in Antarctic spring, when the stratosphere is warmed up by the incident sunlight, especially in the months from September to December.[48] At
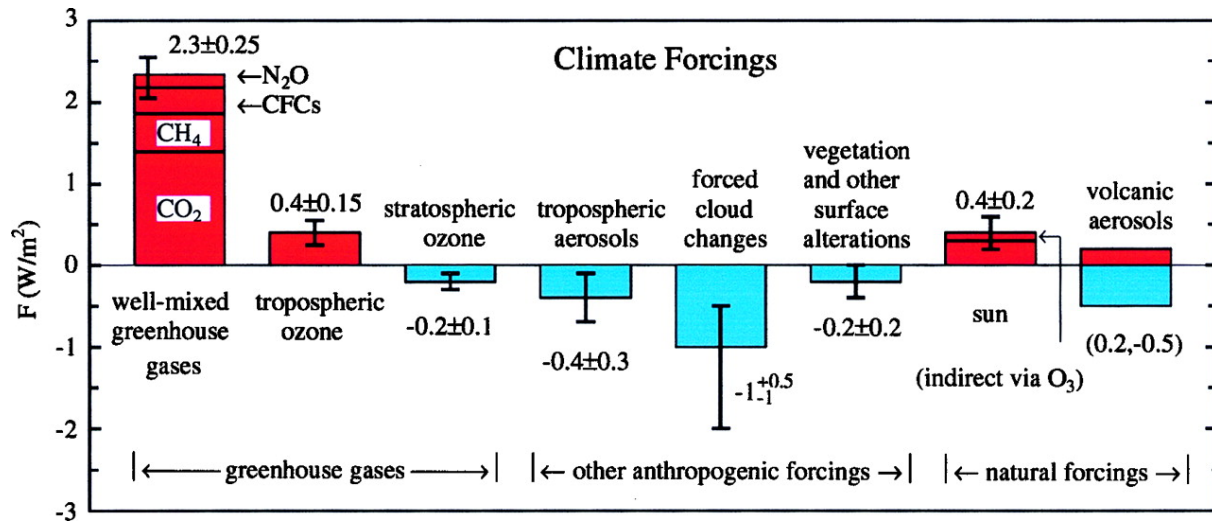
Figure 1.6: Positive (red) and negative (light blue) climate forcing from 1850 to 1998 caused by greenhouse-gases, anthropogenically induced clouds and aerosols, and natural happenings. Taken from a publication by Hansen et al.[36] The influence of water is not taken into consideration.

the end of August a total column of 274 Dobson units was measured, whereas at the end of October the column was reduced to 148 Dobson units. In the following months the ozone levels recovered again. However, the trend over the years as depicted in Figure 1.7 on page 19 is indicative of the decline of about 7% per decade in the vertical profile of ozone over the last 30 years.[49] This decline is attributed to human influence, especially the emission of chlorine containing substances, e.g., CFCs, as a clear anticorrelation between ClO· and ozone could be demonstrated.[50] As these record low levels of column ozone can directly be correlated with the occurrence of "Polar Stratospheric Clouds" (PSC),[21,51] the mechanism that is thought to be responsible for the depletion involves chemical reaction on frozen particles found in PSCs. PSCs form in the dark polar winter at temperatures below about 200 K in a height of 10–20 km[23] and disappear when the temperature raises. The PSC lifetime, i.e., the average time an air mass is exposed to temperatures below the condensation point of PSCs, was found to be between one and twenty days depending on the composition of the specific PSC type.[40] The composition of the PSCs seems to be a

ternary solution of water, sulfuric acid and nitric acid.[21,22] However, the major component in all types of PSC is water occurring at least with a relative abundance of 56% in type I (water-rich) PSCs[51] and with almost 100% in type II (water-ice) PSCs. During the time of their occurrence chlorine reservoir species ($ClONO_2$, HCl) are converted to active chlorine compounds ($HOCl$, Cl_2).[52–56] In spring these active species are photolyzed by the incident sunlight to chlorine radicals ($Cl\cdot$, $ClO\cdot$), which immediately start to deplete the protecting ozone layer above Antarctica.[43,44,57]

On the other hand there is hardly any decline in the ozone layer above the more industrialized midlatitudes. It was unclear for a long time why especially the poles are concerned with ozone depletion. Then it has been observed that the heterogeneous reactions on PSC[22–24] are much more efficient in performing the required conversions than the homogeneous gas-phase reactions.[52,56] Additional ozone destruction potential in PSCs comes from the sequestering of the $NO\cdot$ and $NO_2\cdot$ precursor HNO_3 on their surface at low temperatures of 180 K, thus leading to denitrification of the atmosphere,[40] whereas the $ClO\cdot$ and $Cl\cdot$ pre-cursor substances $HOCl$ and Cl_2 are released at the same temperatures. This has the effect that less radical recombination to reservoir species is possible, and a larger amount of radicals will attack the ozone layer. Not enough, the situation is getting worse because of the pole centered air circulation system, the polar vortex, which arrests $ClO\cdot$ rich air for months above Antarctica.

Ozone (O_3) is the central species in stratospheric chemistry, although its concentration does not exceed 10 ppmv (10 volume units under 1 million volume units) anywhere. The central importance comes from its ability to absorb a great portion of biologically damaging UV-radiation and its interaction with other stratospheric components. It is built from molecular oxygen in the stratosphere through photodissociation induced by UV-sunlight
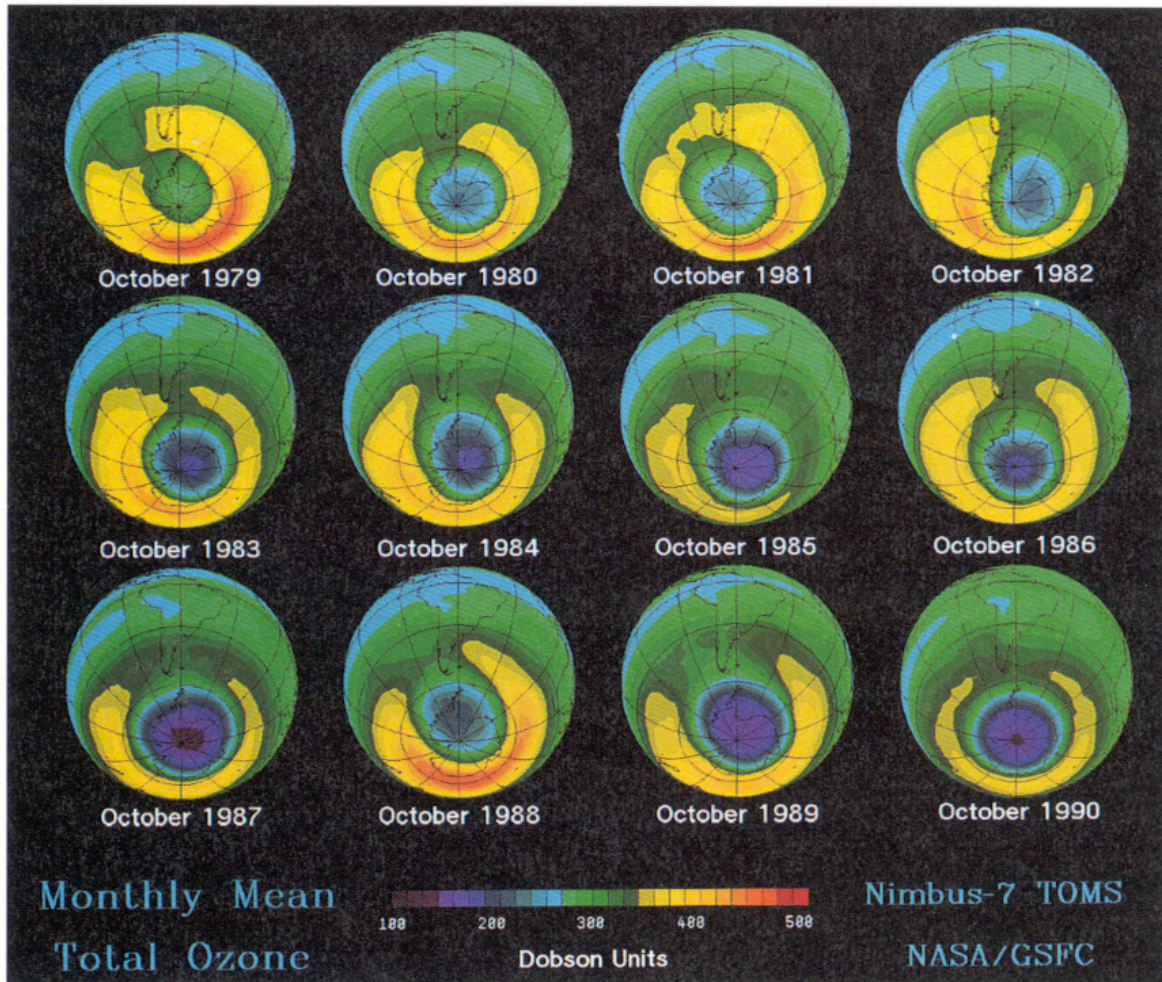
Figure 1.7: October mean values between 1979 and 1990 of total column ozone observed in the stratosphere above the southern hemisphere. Data were determined by Total Ozone Mapping Spectrometry (TOMS) on board of the National Aeronautics and Space administration satellite Nimbus7. Taken from the atmospheric chemistry book by T. E. Graedel and nobel laureate Paul J. Crutzen.[1]

of a wavelength $\lambda <242$ nm:

$$O_2 \overset{h\nu}{\rightarrow} O + O \tag{1.1}$$

$$O_2 + O \rightarrow O_3 \tag{1.2}$$

Because most of the oxygen in the atmosphere is found as O_2 there must consequently be mechanisms destroying O_3 and leading to O_2. For 40 years the mechanism proposed by Chapman in 1930

$$O_3 \overset{\lambda<1140 \text{ nm}}{\rightarrow} O + O_2 \tag{1.3}$$

was considered to be solely responsible for this conversion. In the last 30 years it was found that small components play a crucial role as catalysts destroying ozone

$$X \cdot + O_3 \rightarrow XO \cdot + O_2 \tag{1.4}$$

$$O + XO \cdot \rightarrow X \cdot + O_2. \tag{1.5}$$

X· and XO· were proposed by Paul J. Crutzen in 1970 to be especially NO· and NO_2· formed in the stratosphere from surface emissions of laughing gas (N_2O). However, oxidation of NO· to nitric acid in the troposphere greatly reduces the catalytical potential of NO·. A second species capable of acting as such a catalyst is the hydroxyl radical (OH·) that is

formed from the reaction of water with single oxygen atoms:

$$H_2O + O(^1D) \rightarrow 2HO\cdot. \tag{1.6}$$

The third, most important, catalytic cycle was proposed in 1974 by Stolarski and Cicerone to involve chlorine. One year later M. Molina and Rowland found the connection of this mechanism with chlorofluorocarbons, which have an enormously long life-time in our atmosphere of 60–120 years as they are resistant to reactions with OH$\cdot$. The lighter species CFCl$_3$ and CF$_2$Cl$_2$ are very mobile and reach the stratosphere in only a few years, where solar radiation (λ <260 nm) photolyzes these species in the presence of O$_2$ to CO$_2$, HF and Cl$\cdot$ or ClO$\cdot$. The two radicals show the largest contribution, nowadays, to ozone destruction, as nearly 100% of CFCs are transported to the stratosphere. Additional sources of chlorine are methylchloride (CH$_3$Cl) from algae and tropical burning of biomass as well as eruptions of vulcanoes. The natural concentration of stratospheric chlorine amounts to 0.6 ppbv, whereas the industrial contribution amounts to 3.0 ppbv.

An important natural restriction to stratospheric ozone destruction results from the reaction of the X$\cdot$ catalysts among each other, for example

$$ClO\cdot + NO_2\cdot + M \rightarrow ClONO_2 + M. \tag{1.7}$$
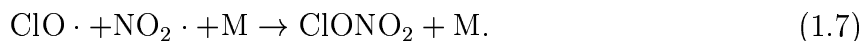
This leads to so-called reservoir species not capable of fractionizing O$_3$. Prominent members of these reservoir species are chlorine nitrate (ClONO$_2$), hydrogen chloride (HCl) or nitric acid (HNO$_3$). The bewildering array of reactions involving these four main catalytic ozone destroying cycles and the involved chemical transformations are depicted in Figure 1.8 on the following page.
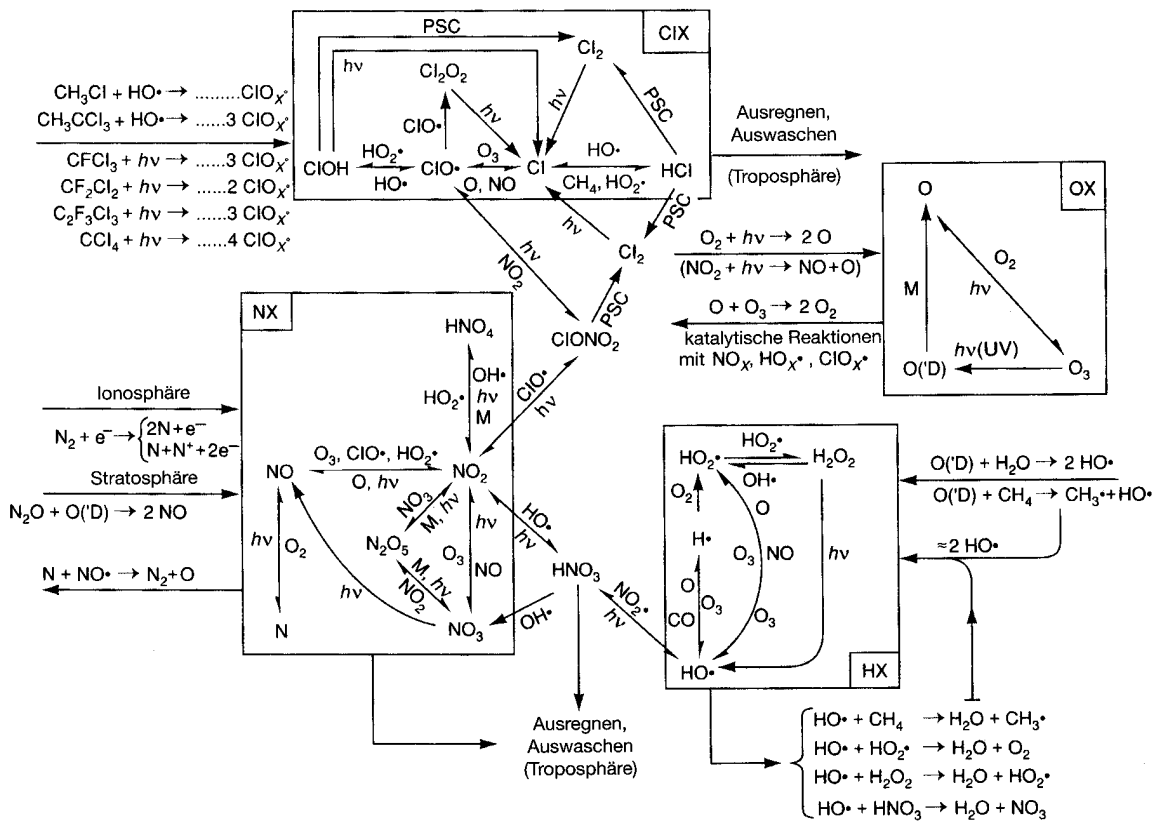
Figure 1.8: Catalytic cycles of stratospheric ozone destruction and reactions connecting the four cycles. Also included are tropospheric and (the very small) ionospheric contributions. PSC stands for reactions on the surface of polar stratospheric clouds. Taken from the atmospheric chemistry book by T. E. Graedel and nobel laureate Paul J. Crutzen.[1]

1.2 Some Open Questions to be Answered

1.2.1 Conversion of Sulfur Dioxide to Sulfates

DMS is oxidized to SO_2 at a model-frequency of $0.7{\times}10^{-5}$ s^{-1}, which by itself is oxidized following the Stockwell-Calvert mechanism[13] at a rate of $1.3{\times}10^{-5}$ s^{-1} to sulfur trioxide by reaction with the hydroxyl radical and O_2.[14-17] Next, SO_3 is hydrated to form sulfuric acid (H_2SO_4) and sulfates (SO_4^{2-}).[18-20] Especially "Polar Stratospheric Clouds" (PSC) form from such sulfate nuclei.[16,21-24] These PSC provide a catalytically active surface for reactions converting chlorine and bromine reservoir species to halogen radicals directly capable of attacking Earth's protecting ozone layer.[46,51,52,55-59] The detailed mechanisms and reaction rate constants for these processes are keys for understanding the gas to particle conversion,[16] which can be assessed from both the experimental and theoretical side.[14] An alternative mechanism that can be imagined is direct hydration of SO_2 to sulfurous acid and subsequent oxidation to sulfate.

In this work the focus is on the mechanism of the atmospheric hydration of SO_2 to H_2SO_3 and SO_3 to H_2SO_4 and the corresponding reaction rate constant following the reaction schemes:

$$SO_2 + nH_2O \rightleftharpoons SO_2 \cdot nH_2O \rightleftharpoons H_2SO_3 \cdot (n-1)H_2O, \qquad (1.8)$$

$$SO_3 + nH_2O \rightleftharpoons SO_3 \cdot nH_2O \rightleftharpoons H_2SO_4 \cdot (n-1)H_2O, \qquad (1.9)$$

where n is the length of the water bridge. It is now well established that the second part of the reaction, i.e., the unimolecular isomerization, has a substantial activation barrier,

which is overcome by the pre-association reaction acting as driving force.[60] In molecular beam studies the decay of SO_3 has been attributed mostly to the complexation of one H_2O and one SO_3 moiety, which rapidly isomerizes to H_2SO_4.[61,62] The conversion time set an upper limit of $+13$ kcal/mol on the reaction barrier to unimolecular isomerization.[62,63] The bimolecular hydration rate constant corresponding to this process was determined to be about $9.1 \times 10^{-13} cm^3 s^{-1}$ as early as 1975.[64] Newer studies carefully eliminating heterogeneous wall reactions have inferred upper limits of $2.4 \times 10^{-15} cm^3 s^{-1}$ and $5.7 \times 10^{-15} cm^3 s^{-1}$ for the homogeneous reaction.[34,65,66] All these studies assume a linear dependence of the SO_3 loss rate on water vapor pressure. More recent gas-phase studies yielded a second-order dependence of this rate with respect to water vapor pressure[34,67] implying the involvement of water-dimers.[35] Experiments under both turbulent[35] and laminar[68] flow conditions yielded a nitrogen pressure independent conversion rate constant of SO_3 to sulfuric acid of 2.0–$3.0 \times 10^{-31} cm^6 s^{-1}$ at 300 K.

Concerning the reaction energetics, especially the activation barrier to the hydration coupled with proton transfer, experimental information is missing. From the theoretical side it has been established that the reaction barrier in the 1:1 complex is rather high (23.2–29.0 kcal/mol).[69–72] Involvement of the water-dimer instead of a single water molecule leads to a reduction of the predicted barrier to 7.4–12.4 kcal/mol.[71,72] The possibility that even higher hydrates are responsible for the reaction chamber results and/or the atmospheric reaction has not received much attention in the literature. A careful investigation of the reaction path and rate for the different hydrates taking into account quantum effects like tunneling is also missing in the literature to the best of my knowledge. In summary, the open questions are:

- How many water molecules are involved in the atmospheric conversion of sulfur dioxide to sulfates?

- Does atmospheric hydration precede oxidation or not?

- What influence has quantum mechanical tunneling on the reaction path?

- What is the exact reaction path?

- Why has sulfurous acid $\{H_2SO_3\}$ never been detected?

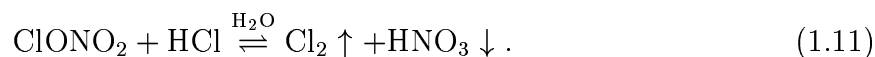- What consequences can be expected on further increasing atmospheric SO_2 and H_2O levels?

In order to get at least an idea on the answers to these questions I performed a calculation on the dynamics of this hydration in the presence of up to n=3 water molecules by variational transition state theory and multidimensional tunneling methods.

1.2.2   Converting Chlorine Reservoir Species to Active Species

The importance of PSCs in depleting ozone results from the rapid[73] absorption of chlorine nitrate and hydrogen chloride together with their subsequent hydrolysis on the cloud surface by the vast amount of contained water according to the reactions

$$ClONO_2 + H_2O \overset{H_2O}{\rightleftharpoons} HOCl \uparrow + HNO_3 \downarrow \tag{1.10}$$

and

$$ClONO_2 + HCl \overset{H_2O}{\rightleftharpoons} Cl_2 \uparrow + HNO_3 \downarrow . \tag{1.11}$$

In the absence of PSCs the chlorine nitrate hydrolysis takes place at much slower reaction rates.[55] The hydrolyses involving the acidic cloud components have been shown

to take place with a much smaller efficiency.[56, 74] Thus, the PSCs can be seen much more as liquid water than an acidic ternary mixture or concentrated sulfuric acid.[55] Especially the dielectric constant is very similar to the one of liquid water. The products of the reaction are nitric acid (presumably in the form of a contact ion pair $[H_3O^+][NO_3^-]$) and hypochlorites, which are easily photolyzed to the strong Cl· and ClO· radicals in springtime.[1, 75] These radicals can be desorbed to the gas phase at 155 K, whereas nitric acid remains in the condensed phase.[76] Therefore, the PSCs not only act as source of chlorine radicals, but also as a sink of NO_x radicals, which normally protect the ozone layer by destroying the active chlorine species.[57] A detailed knowledge of the rate constants and the mechanisms involved in ozone depletion is inevitable for predicting future ozone levels, especially for predicting the year in which the "ozone hole will shut" because of governmentally forced reductions of chlorine emissions as manifested e.g. in the "Montreal Protocol of Substances That Deplete the Ozone Layer" entering into force on January 1, 1989.[77] In summary similar questions like the ones on sulfur dioxide hydration can be formulated:

- Which of the two reactions is more important to understand ozone depletion?

- How many water and/or HCl molecules are required to reproduce model rate constants found appropriate for present day ozone variations?

- What is the exact reaction path?

- What is the influence of tunneling on the rates?

- What kind of consequences are expected on increasing halogen and water concentration in the atmosphere?

- Why is the homogeneous reaction much less efficient in promoting ozone depletion than the heterogeneous reaction on PSCs?

It was my intention to seek for answers to these questions by theoretical chemistry methods, as described in the following chapters.

Chapter 2

Methods

2.1 Theoretical Chemistry

It is often the case that experiments approach a technical limit beyond which it is impossible to gather "chemically" meaningful information. For example it was long believed to be impossible to obtain spectroscopic data on species along a reaction path other than the equilibrium structures. Recent advances in "Femtochemistry", for which Ahmed Zewail was awarded the 1999 nobel-price in chemistry,[78,79] and the technique of supersonic-jet cooling in combination with Terahertz spectroscopy, invented in the group of Richard Saykally, have made this possible at least for some selected ultrafast reactions, e.g., tautomerization in DNA model base-pairs[80–82] and the proton dynamics in selected cyclic water clusters.[83–90] However, such techniques are still far from being generally applicable. Especially, when the reaction educts and the reaction by itself are not well defined it is still considered impossible nowadays to gather detailed experimental information on the electronic structure along the reaction coordinate. The here studied processes are a typical example for such a situation. Undefined water content of the reaction complexes, lack of data on the concentration of the different species at different altitudes and the impossibility to imitate the exact atmospheric

pressure, composition and temperature conditions in a certain apparatus hamper detailed experimental insight to atmospheric chemistry.

When experimental chemistry reaches its limit, theoretical chemistry comes into play. Whereas it is hardly possibly to prepare defined reaction conditions in the laboratory, it is very easy to do so on the computer. It is also very easy to "freeze in" transition states on the computer for a long time, whereas they disappear in fact within a femtosecond. The critical point in theoretical chemistry concerns the usefulness and reliability of the model used. A model can be called reliable as long as the predictions are at least close to the experimental findings. It is assumed that if the model reproduces known experiments well it will also predict the outcome of unfeasible experiments well. In the following the model used for the prediction of the mechanism and the reaction rate constant at different temperatures for the different atmospheric reactions will be presented. The chapter after this one will deal with the verification of the model used on the example of double proton transfer in carboxylic acid dimers. Such dimers are well suited for this validation due to the wealth of both experimental and theoretical studies on this topic. Especially advantageous is the availability of studies on the kinetics of this reaction by various optical, scattering and NMR techniques. Such studies are rare for the atmospheric reactions described in Chapter 4.

2.2   Theory of Reaction Dynamics

Widely used approaches to calculate reaction rate constants are collision theory[91] and transition state theory (TST).[92-94] The latter has already been accommodated for its use in computer models.[95-99] Hence, I have chosen an advanced variant of the TST approach. A description more detailed than the following, involving all algorithmic details and all important equations, can be found in my master thesis.[100]

In TST the reaction rate is obtained *a priori* only from information about the reactants and the transition state or, more generally spoken, the bottleneck of the reaction. The products themselves contribute not to the evaluation of the rate constant k, as a major point of theory is the "no recrossing assumption", i.e., each trajectory that reaches the energetically highest point on the reaction path is assumed to be converted to products and trapped there on the potential energy surface (PES). This assumption is not fulfilled in reality, and trajectories in fact can recross the highest point several times. Therefore the TST rate constant provides only an upper limit for the experimental rate constant. By varying the location of the hypersurface, dividing reactants from products and minimizing the computed k and thus minimizing recrossing, this error can be reduced drastically. This approach is called variational transition state theory (VTST) and can provide considerably better agreement with experiment than pure TST.[96,98]

Nevertheless, this strategy still fails to describe non-classical trajectories tunneling through a barrier. Especially when the curvature of the PES near the transition state is large, the rate constants without inclusion of quantum-mechanical tunneling methods can be considerably wrong.[96,98] The amount of tunneling is taken into account by multiplying the pure variational rate constant $k^{CVT}(T)$ with a transmission coefficient κ, where the superscript CVT indicates that a canonical ensemble was assumed for the calculation. Depending on the curvature of the minimum energy path (MEP), which is defined as the steepest descent path in mass-weighted Cartesian coordinates connecting saddle points and minima,[101] different quantum-mechanical methods can be used to take into account the nuclei's quantum properties. The minimum energy path semiclassical adiabatic ground state (MEPSAG) method is appropriate, if the tunneling path coincides with the MEP.[102] Therefore it is also called the zero curvature method (ZCT), because a one-dimensional, straight reaction path is assumed. As the reaction path is in fact curved, tunneling is assumed to occur on the path defined by the classical turning points on the concave side of

the MEP ("anti-bobsleigh effect"). This type of calculation is called centrifugal-dominant small curvature semiclassical adiabatic ground state (CD-SCSAG) method, a small curvature tunneling (SCT) approach.[103] For light atom transfer reactions the reaction path curvature is very large and the centrifugal dominant approximation breaks down. In the large curvature ground state approximation, version 3 (LCG3),[96,104] a large curvature tunneling (LCT) method, it is assumed that the short distance between tunneling start and end point forces the system to take straight paths between these two points. As the end points can be far away from the transition state, a much wider area of the hypersurface far away from the steepest-descent path is traversed, which is called the "reaction swath".[105–107] Clearly defined, the reaction swath is the region on the concave side of the reaction path extending beyond the transverse vibrational turning points and/or beyond the local radius of curvature. Motions over the swath are initiated by vibrations orthogonal to the MEP as well as parallel to it. Sudden tunneling along straight line paths over the swath may provide the most effective tunneling mechanism for a system of high reaction-path curvature, e.g., the bimolecular transfer of a light atom between two heavy atoms. The effective potential for tunneling over the adiabatic part of the swath is obtained from Hessian calculations on the MEP, whereas the effective potential for nonadiabatic regions (those beyond the vibrational turning points and/or the local radius of curvature) are obtained from single-point energy calculations along those portions of the path.[96,104,108]

The LCG3 approximation includes contributions from all straight-line tunneling paths with equal kinetic energy in reaction coordinate motion at the pre- and post-tunneling configuration coordinate by using a quasiclassical distribution function to average over paths with different end-points. Especially at low temperatures, κ can deviate from one (i.e., no tunneling) considerably and change calculated rate constants by several orders of magnitude. Depending on the nature of the PES, κ can also vary strongly with the level of sophistication of tunneling inclusion. For strongly bent PES the differences between κ^{ZCT},

κ^{SCT} and κ^{LCT} can rise to several orders of magnitude even at room temperature.[109,110] The maximum value of κ (SCT) and κ (LCT) is called κ (μOMT), where μOMT stands for microcanonical optimized multidimensional tunneling.

One should be aware that calculations can only lead to results comparable to experiment for a wide range of temperatures, when the provided PES is accurate enough. Due to limitations in resources, it is hardly possible to calculate the whole PES in terms of *ab-initio* calculations and it is, therefore, necessary to find a cheaper method for a good description of the hypersurface as described in the following sections. The detailed mathematical procedures and computational formulas are discussed elsewhere.[96,98,100]

2.3   Generation of Reaction Hypersurfaces

The reaction barrier of proton transfer does not only depend on the energetics when the proton is moved alone, but also on the relaxation of the not directly participating heavy atom skeleton as found for several different intramolecular hydrogen bridges.[111–119] Therefore, the energy of the system depends on a large number of coordinates and can only be understood by means of a high-dimensional potential energy surface (PES).[105,120–122] The choice of the method affordable for the PES critically depends on the number of explicitly described atoms in the system. As the reaction rate strongly depends on the barrier, it is desirable to know this value as exactly as possible. The stationary points of the systems, therefore, should be evaluated properly incorporating electron correlation. If no additional hypersurface information is computationally feasible application of pure transition state theory[92,93] with Wigner tunnel correction[123] is possible only. Variational transition state theory (VTST) requires the calculation of the steepest-descent path from the TS to the minima in mass-scaled coordinates (scaling mass of 1 amu). All figures in the "Results" chapter as well as all text segments dealing with reaction coordinates (and Bohr) refer to

this mass-scaled coordinate system. For the purpose of calculating the steepest-descent path various integrators have been developed, e.g., Page-McIver,[124] Euler[125] and some related ones.[126–130] All of them require the calculation of many points along this path. It is therefore hardly possible to afford the same high-level of theory as for the stationary points. An unique hypersurface is gained from interpolating between these two according to a sophisticated logarithm of ratios scheme.[131] On these hypersurfaces various paths are possible connecting educts and products. Some are short but exhibit rather high potential differences, others are longer but flatter. Furtheron, classical over-barrier jumps are unlikely for movement of the lightest particle in the periodic table. Instead quantum mechanical tunneling plays an enormously important role especially at low reaction temperatures.[132] It is the task of the theoretical chemist to localize paths fulfilling these criteria best, i.e., to find the least-action path. This extreme value problem of seeking the best path is known as the "multidimensional tunneling" problem.[133] Compared to omitting microcanonical optimized multidimensional tunneling (μOMT) a proper treatment yields proton exchange rates higher by orders of magnitude especially at low temperatures, but even at room temperature.[108,126,134] Such rate constants are in good agreement with experiments, especially when high-level PES are used.[110,135–139]

2.4 Electronic Structure Methods

As the results critically depend on the underlying reaction hypersurface, it is worth spending a few words on the electronic structure methods used for the calculation of points on these hypersurfaces. Theoretical chemistry can be divided in two major areas, namely the quantum mechanics (QM) area and the molecular mechanics (MM) area. Molecular mechanics relies on the assumption that the total energy of the reaction system can be summed up from contribution arising from non-optimal configurations of different atomic groups. In

this manner bond-length, bond-angle, dihedral, van-der-Waals, hydrogen-bonding energy terms are summed up depending on the positions of the atom nuclei. This is computationally rather easily to manage, and, therefore, systems containing many thousands of atoms can be treated fairly easy. The disadvantages are that a force-field containing many different atom types has to be parametrized before the system of interest can be investigated, accuracy is quite low and bond-breaking and bond-making (i.e., a chemical reaction) can not be described. On the other hand quantum mechanics directly solves the (time-independent) electronic Schrödinger equation by numerical methods in order to find the electronic energy for a certain atomic arrangement. These methods require not an *a priori* parametrization and are, therefore, called *ab initio* methods. The disadvantage of these methods is that it is very time-consuming to perform such calculations. With present implementations of the QM-methods, as e.g. in GAUSSIAN98,[140] and present days computers it is affordable to calculate the electronic energy of systems containing about 20 atoms in a reasonable time of, say, a month, when using methods that take electron correlation effects carefully into account. From this last sentence it is clear that the quantum mechanical methods can be divided in many subgroups of different accuracy and time expenditure. There are many textbooks giving a good overview on this topic, e.g., the book written by Levine[141] or the book written by Jensen.[142] All of these methods employ the Born-Oppenheimer approximation stating that the heavy nuclei stay statically in their positions, while the light electrons move very fast into favorable positions. The electrons are only allowed to move in certain areas in space determined by the so-called basis-set, which is a set of (mostly) atom centered functions. The computationally unfeasible limit of an infinite basis-set results in the lowest possible electronic energy reachable by a certain method. The methods differ in their way of taking the electron-electron interactions into account. The most easy way to do so is to neglect it at all, as is done in Hartree-Fock theory. Other approaches start from the Hartree-Fock solution to the wave-function, which

is perturbed by the action of an operator, in order to take electron correlation into account. These methods are called Møller-Plesset calculations up to different order, e.g., MP2 or MP4. Coupled cluster methods work with cluster operators converting the wave-function in such a way that excited Slater determinants contribute to the wave-function. E.g., CCSD(T) allows for single, double and perturbative triple excitations. Other approaches, called multideterminant approaches, introduce configuration interaction, i.e., the possibility that electronically excited states contribute to the wave-function. However, all of these methods are computationally too intensive and scale unfavorably with increasing system-size in order to be a useful method for the generation of a reaction surface of many hundred point in a 10 atomic system. Therefore, I only used MP2, CCSD(T) and G2(MP2) methods in order to calculate energies for the stationary points on the hypersurface. For the wealth of points on the surface I used hybrid density functional theory employing a medium sized basis-set containing both diffuse and polarization functions. This method is comparable in computational cost with Hartree-Fock calculations and shows a fortuitous, but systematic, error cancellation when using medium sized basis-sets. Hybrid density functional theory relies on the Hohenberg-Kohn theorem, which states that it is possible to calculate all ground-state molecular properties from the electron probability density. The Kohn-Sham equations tell one how to calculate the exact electronic ground-state energy. This equation contains the exchange-correlation energy, for which a rigorous solution is impossible. Many approximate functionals have been developed in a rather empirical manner for the exchange-correlation energy. There seems to be no systematic way of improving this contribution. Most of these functionals are derived from the homogeneous electron gas and involve the local spin-density approximation for molecules. Hartree-Fock theory can be viewed as a special (unaccurate) example of density functional theory. In hybrid density functional theory the exchange-correlation is calculated as a linear-combination of the Hartree-Fock exchange and the exchange-correlation functional. A hybrid density

functional calculation, therefore, is only slightly more expensive than a Hartree-Fock calcu-
lation and a useful method for the calculation of many points on the reaction hypersurface.
I have chosen to employ Becke's 3 parameter functional containing also a non-local corre-
lation developed by Lee, Yang and Parr (B3LYP). The three parameters in this functional
are optimized in order to get the best agreement with the known energies of a molecule
test set (the G1 test set).

2.5   Procedure

Geometry optimization of the equilibrium structures and the transition states was per-
formed both by hybrid density functional theory (B3LYP/6-31+G(d))[143] and second-order
many-body perturbation theory (MP2/aug-cc-pVDZ)[144] as implemented in Gaussian98.[140]
The nature of these stationary points was verified by diagonalization of the Hessian ma-
trix. All transition states exhibit a single negative eigenvalue. Coupled cluster with single,
double and perturbational triple excitation energies at geometries found by application
of second-order Møller Plesset perturbation theory (CCSD(T)/aug-cc-pVDZ//MP2/aug-
cc-pVDZ)[144–146] and by Gaussian-2 theory using MP2, i.e., G2(MP2),[147] served as verifi-
cation of the generally high performance of hybrid density functional theory B3LYP for
hydrogen-bonded clusters[107, 148–150] and as benchmark for the reaction energetics, especially
the reaction barrier.

The path of steepest-descent (MEP, IRC)[127, 128] was evaluated in a mass-scaled coordi-
nate system[101] using a reduced mass of 1 amu starting from the transition state (TS) at
B3LYP/6-31+G(d) level[143, 148, 151] with the aid of the path integrator of Page-McIver[124, 125]
and a stepsize of $\Delta s = 0.05$ Bohr (1 Bohr corresponds to 0.53 Å). The Hessian was updated
every third point in both directions. Altogether about 900 points at B3LYP/6-31+G(d)
level of theory were computed on the MEP according to the techniques implemented in

Polyrate8.2[152, 153] and using the path convergence parameters found to be successful for the much more critical "pure" proton transfer reactions.[106, 107] Additionally a grid of 600 points was calculated in the reaction swath at the same level of theory for the calculation of the LCT correction. The reaction path and especially the reaction barrier obtained from hybrid density functional theory were adjusted to the G2(MP2) results by an interpolation procedure[110, 131, 134, 154] that has already proven to give results very close to experiments.[149] The reaction rate for the unimolecular isomerization step was obtained from classical variational transition state theory (CVTST)[92] corrected semiclassically to describe non-classical barrier penetration, i.e., tunneling, and reflection.[96, 98, 105, 106] These non-classical effects were quantified by the microcanonical optimized multidimensional tunneling method (μOMT)[108] as implemented in Polyrate8.2.[152, 153]

The effect of the pre-equilibria on the reaction rates for a homogeneous reaction was taken into account by calculating the association constant of the water molecules and guest molecules in the initial unimolecular complex[155] and multiplying them with the unimolecular reaction rate constants. This procedure ensures that the effect of a potential energy minimum, i.e., hydrogen-bonded complex, on both the activation energy and the tunneling correction factor is taken into account properly.[156] The Gibbs free energies required to obtain the equilibrium constants were gathered by calculating partition functions for the involved species using B3LYP/6-31+G(d).

Chapter 3

Validation of the Method

3.1 Proton Transfer in Carboxylic Acid Dimers

Any model that is used to predict something has the drawback that it is just a model relying on assumptions and approximations. In the case of variational transition state theory corrected for multidimensional tunneling such approximations are besides others the Born-Oppenheimer assumption of electrons instantaneously reacting on changes in nuclear coordinates, the reaction path separability assuming that the transition from educts to products occurs along a single reaction coordinate separable from all other 3N-1 degrees of freedom in an N-atom system, the assumption that there is just a single transition state, the assumption of electronic adiabaticity, i.e., that no electronic transitions occur along the reaction path. In order to test whether these assumptions and approximations are justified, comparison with reliable experimental results has to be sought. For the multiple proton transfer reactions investigated in this study carboxylic acid dimers seemed to be a good example for the validation of the method, especially because a wealth of experimental studies is available on formic, acetic and benzoic acid dimers. For all of these dimers the most favorable orientation is the planar dimer as depicted in Figure 3.1.
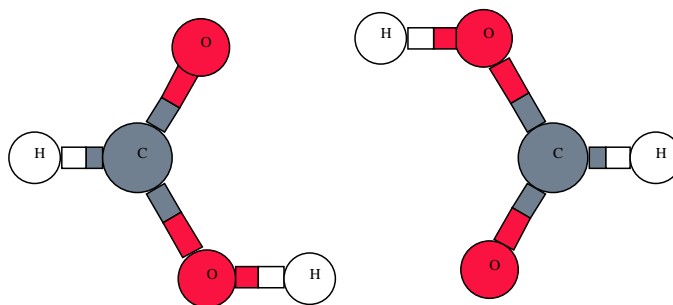
Figure 3.1: Hydrogen bonded dimer of formic acid as existant both in condensed phases and the gas-phase.

3.2   Previous Experimental and Theoretical Studies

The synchronous double proton transfer in carboxylic acid dimers is long known and has been studied thoroughly. For a long time experiments focused on equilibrium properties, e.g., determination of geometries of the monomers and dimers and the energetic stabilization upon dimerization using IR-, Raman- and microwave spectroscopy as well as electron diffraction.[157–161] These measurements were soon followed by theoretical investigations.[162–167] Studies of the dynamics have been possible by means of T_1-NMR spin-lattice relaxation spectroscopy. The fully symmetric double well potential found theoretically in isolated dimers is modulated in the condensed phase of benzoic (p-toluic) acid dimers to an asymmetry of about 0.10–0.24 kcal/mol.[160, 161, 168–171] In these experiments the apparent activation energy for the hydrogen transfer at room temperature has been determined to be 1.15–1.44 kcal/mol. All atoms together are dislocated by 0.69–0.80 Å during the reaction, which occurs with a frequency between 2.6×10^9 and 3.7×10^{10} s^{-1} for differently meta and para substituted benzoic and aliphatic acid dimers.[168, 170, 172] These results have been confirmed by inelastic neutron scattering measurements.[173, 174] At low temperatures (15–50 K) the apparent activation energy goes down to 0.18–0.30 kcal/mol. Different non-

aromatic carboxylic acid dimers exhibit an about ten times slower interchange than the benzoic acid dimer.[175] In crystals of benzoic acid dimers the deviation from centrosymmetry, i.e., the energy asymmetry of the double-well potential, can be removed by doping with guest heteroaromatic molecules (e.g. 10^{-4} mol/mol thioindigo).[176–180] The tunneling matrix element and isomerization rate are practically unaffected by the nature of these guest dyes.[172,174,177] All studied substituents of the acid dimers yield similar results, except ortho-substituted aromats.[170,181] The most precise determination of the tunnel-matrix element by fluorescence line narrowing at 1.4–4.2 K yields $\Delta = 0.32 \pm 0.03$ cm^{-1} together with a zero-temperature proton tunneling rate of $k_0 \approx 2 \times 10^8$ s^{-1} in the doped crystals.[182] In mixed acetic-fluoracetic acid dimers the splitting was estimated from microwave rotation spectra as early as 1964 to be between 0.5 and 5.0 cm^{-1}.[158] The temperature T_c below which tunneling predominates the over-barrier mechanism is found to be between 50 and 120 K in different experimental studies, but tunneling also remains relevant in the mainly classically activated high-temperature limit.[113,176,183,184]

From the theoretical point of view the experiments show that the description of the dynamics by one-dimensional models is insufficient as the exchange in the benzoic acid dimer is influenced by several normal-modes.[113,185] Namely, in the first excited state of a heavy atom rocking mode the exchange is 56 times faster than in the ground state.[186] Shortening of the OO-distance by external pressure also increases reaction rates.[183,187] Such an increase has been found computationally for excitation of the interdimer-stretch and the CO_2 rocking mode in the formic acid dimer as enlarged tunneling splittings corresponding to increased reaction rates ($k_0 \propto \Delta^2$).[172]

Early estimates for the reaction barrier of the formic acid dimer were about 15 kcal/mol at Hartree-Fock level of theory[111,188,189] and 12 kcal/mol at MCPF and CISD level of theory.[188,190] Nowadays, the highest level of theory available is a G2* calculation based on MP2/6-31G(d,p) geometries and on single point energy corrections at MP2, MP4 and

QCISD(T) level with large basis sets containing diffuse and polarization functions.[191] The barrier obtained by this G2* approach is 5.20 kcal/mol with zero-point correction and 8.94 kcal/mol without. The apparent discrepancy of the rather high theoretical and rather low experimental exchange barrier estimates was attributed to "transitions between OHO-fragment vibrational levels under the action of random forces of the surrounding" and "proton tunneling promoted by the low-frequency mode excitations" in a two-dimensional study.[185] However, there is no quantitative data accounting for the difference between bare barrier height and apparent activation energy. Here, the factors contributing to the lowering of the apparent activation energy will be presented in a reaction path dynamics study directly obtained from *ab-initio* data. In contrast to other studies the approach used in this work is full-dimensional rather than three-dimensional[190, 192, 193] and full *ab-initio* rather than relying on a specially parametrized semiempirical hypersurface,[191] which is important for a proper description of a wide region of the potential energy surface (PES).[106] I further studied the transfer reaction of systems containing one (HD) and two (DD) deuterons instead of the carboxylic protons. Additionally, the first correlated calculation of the exchange barrier in the benzoic acid dimer is presented.

3.2.1 Tunneling Splitting

For further comparison to experiment the tunneling-splitting Δ_0 has been estimated from the data of the reaction path calculation. Namely, the ground-state tunneling probability P^Q at zero-temperature and the equilibrium reaction-coordinate double-well potential frequency ω_0 can be utilized for this purpose:[107, 194, 195]

$$\Delta_0 = (\frac{\omega_0}{\pi}) \times \sqrt{P^Q}$$

Therefore, the zero-level tunneling splitting is related to the low-temperature limit of the tunneling correction. It is hence temperature-independent and can be compared directly with molecular beam experiments, which involve measuring pure transitions between two well-defined quantum states. These "rough estimates" have been quite successfully used to predict ground-state splittings Δ_0.[196–198] Data for the transfer in $(HF)_2$ obtained from reaction path calculations (0.44 and 0.61 cm^{-1})[199] are comparable to accurate quantal calculations (0.43–0.66 cm^{-1})[200,201] in predicting the experimental value (0.66 cm^{-1}).[202] As the sudden straight line paths are expected to be the most probable reaction mechanism yielding the highest rates, the LCG3 tunneling probability has been used for this estimate. However, if more precise information like mode-specific splittings are desired other approaches to obtain tunneling-splittings have to be applied.[195,203–210]

3.3   Results Obtained by VTST

3.3.1   Reaction Rate and Mechanism

As can be seen in Figure 3.2 on the next page the highest tunneling corrections stem from the direct corner-cutting (LCT) approximation, which is reasonable for the mass-combination of the transfer studied. The reaction thus takes place by first following the MEP some way up starting from the minima in order to decrease the OO-distance. When the system has reached an orientation where the potential in the swath is favorable it crosses the dividing surface in a straight manner by directly following the OH-stretch direction. Typically, this orientation is near to the TS at high temperatures (i.e., OO-distance reduction of nearly 0.3 Å) and near to the minimum structure at low temperatures (i.e., OO-distance reduction of less than 0.1 Å). The representative tunneling energy is 1.0 and 2.0 kcal/mol below the saddle at 300 and 100 K, respectively. A similar mechanism of a preliminary hydrogen bond compression has also been found in some other systems show-
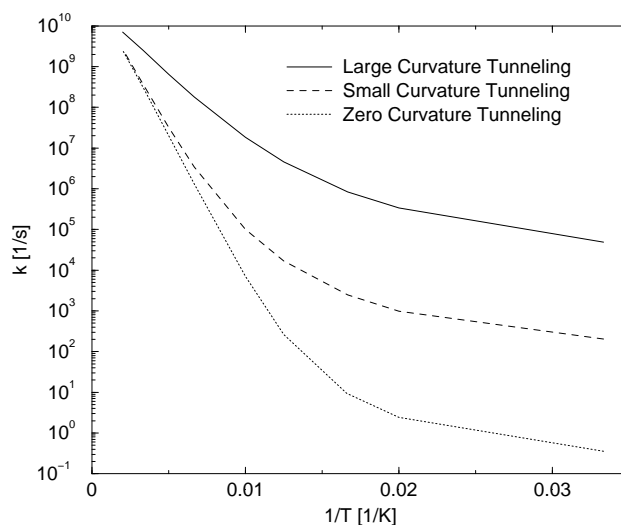
Figure 3.2: Reaction rate constants for the concerted proton exchange in $(HCOOH)_2$ at MP2///B3LYP level employing different tunneling corrections.

ing multiple hydrogen transfers.[115,116,118,119,211] In comparison to the LCT rate constants obtained directly from VTST at AM1-SRP level of theory[191] my predictions are higher by two orders of magnitude at 200 K and one at 300 K as predicted qualitatively previously.[106] The difference is on the one hand due to the much steeper ridge of the reaction swath[106,107,212] at AM1-SRP level and on the other hand due to the AM1-SRP barrier higher by 0.7 kcal/mol.

3.3.2 Importance of Tunneling up to Room-Temperature

The crossover-temperature T_c between the high- and low-temperature regimes is found to be between 70 and 100 K from the change between the two linear regions in the Arrhenius plot. Already the ZCT approximation provides a good estimate for T_c, although the intermediate region is broader compared to the LCT result. Especially the latter compares very well with the experimental curves.[113,176,183,184] Below T_c tunneling predominates clearly as can be seen from the small amount of heavy atom movement. Above T_c tunneling

still plays a major role. Namely, a proton tunneling distance of more than 0.4 Å is found at the representative LCT path (300 K). A similar result has been obtained by Kim.[191] The total displacement between the two minima of 0.63 Å compares very well with the recent neutron scattering result of 0.686 Å.[172] More than half of the total hydrogenic motion occurs, therefore, in the classically forbidden tunneling region even at ambient temperature.

The associated tunneling splitting is estimated to be $\Delta_0 = 0.09$ cm^{-1}. This is an order of magnitude higher than the one found employing a three-dimensional PES.[190] It has been suggested that the adiabatical treatment of the strongly and linearly coupled low frequency CO_2 rocking mode[111,172,208,209] is the reason for the small splitting found in this study.[193,208]   However, comparing the employed MCPF barrier of 12.0 kcal/mol with the G2* barrier of 8.9 kcal/mol[191] the difference rather seems to emerge from the too high barrier.   Other low-dimensional studies yielded splittings of 1.8 cm^{-1} (Makri, Miller[213]) and 0.3 cm^{-1} (Chang et al.[189]) for the ground-state but seem to suffer from neglecting skeletal motion and thus give an unphysical low effective mass.

3.3.3   Isotopic Substitution

The results for the LCT isotope effects on the rate compare not very well with the experiments.[113,168,170] Obviously they are suffering from the fact that the straight line paths are poor approximations for the deuterated species. However, the found kinetic isotope effect in the small curvature tunneling regime shows a similar tendency to the experiment.[113] While the curve for the ratio of k(HH) to k(HD) approaches $\sqrt{2}$ at high temperatures, higher values at lower temperatures are found due to enhanced tunneling. A similar behavior is calculated for the ratio of k(HD) to k(DD) with the exception that it starts from lower values at low temperatures and drops slower to $\sqrt{2}$ at increasing the temperature.

The stronger decrease of the OD vs. the OH stretching frequencies in the minimum

structure compared to the TS causes an increase in the zero-point corrected B3LYP/6-31+G(d) barrier from 3.97 to 4.68 and 5.44 kcal/mol from the HH to the HD and DD species, respectively.

3.3.4   Apparent Activation Energy

The reduction of these zero-point corrected barriers due to tunneling is shown in Figure 3.3 on the following page. Earlier attempts to reproduce the experimental results[168,170–172] suffered from uncorrelated barriers, incompletely optimized transition states showing too long OO-distances and from omitting tunneling.[111,188,189,214] The curves given here are in considerably better agreement, but still slightly higher than the experimental results, i.e., 1.4 kcal/mol at room temperature.[113,168,170] The task arising from Figure 3.3 on the next page is to find the reasons for the remaining small differences. I surmise that some further effects account for the remaining discrepancy:

Correlated Barrier in the Benzoic Acid Dimer

First, the barrier for benzoic acid dimer (BAD) is lower than for formic acid dimer (FAD). For BAD the barrier seemed to be lower by about 2 kcal/mol judging from calculations not taking into account electron correlation, which was unfortunately the highest level of theory available in the literature for the system of 128 electrons.[214] Thus I provide here to the best of my knowledge the first correlated barrier for the proton exchange in BAD. Namely, at B3LYP/6-31+G(d) level of theory the barrier is 7.40 kcal/mol, meaning a barrier reduction of 0.99 kcal/mol compared to FAD caused by the phenyl substituent. The main reason for the lower barrier is that the OO-distance is reduced from 2.72 Å (FAD) to 2.68 Å (BAD) in the minima, but not affected in the TS, i.e., 2.43 Å for both. The "presumably underestimated" experimental ground-state barrier[113] contributes further to a better matching between the two activation energy plots.
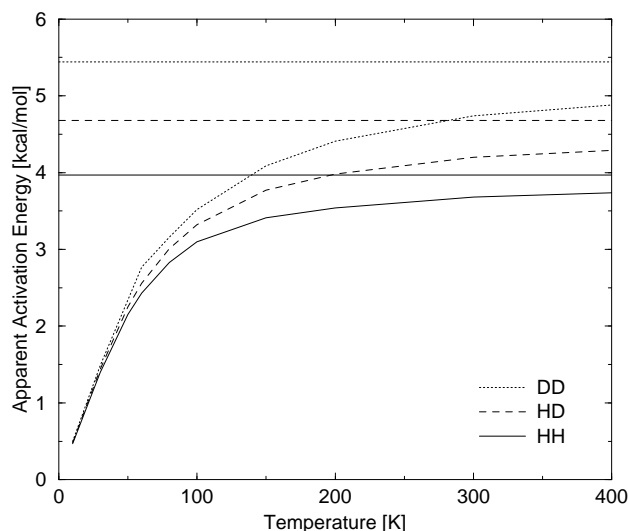
Figure 3.3: Isotope effect on apparent activation energy of intermolecular proton exchange in $(HCOOH)_2$ [HH], $(HCOOH)(HCOOD)$ [HD] and $(HCOOD)_2$ [DD] at B3LYP/6-31+G(d) level with small curvature tunneling correction from ground-state. For comparison the zero-point corrected barriers are shown (straight lines).

Additionally, incoherent transfer is important for some experimental results. This theoretical study focuses on the coherent transfer that has been realized experimentally through the doped systems of benzoic acid dimers. The effects arising on the transition to incoherent transfer are not subject of the present study. Although I do not believe that the small energy asymmetry can influence the here presented results drastically, especially at temperatures above 100 K, presently many steps are taken towards a more complete understanding of dynamics in the condensed phase.[215–219]

Vibrational Excitation

Finally, excitation of vibrations due to the thermal bath of neighboring molecules can lead to a considerable increase in the rate constants.[113, 172, 185, 186, 209] It is thus necessary to investigate the normal-modes participating in the reaction in order to identify the modes accelerating the reaction on excitation. Therefore, the MEP was recalculated in another
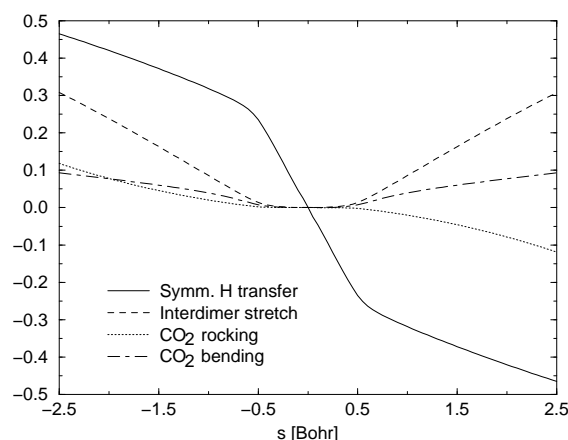
Figure 3.4: Minimum energy path for the concerted hydrogen exchange in $(HCOOH)_2$ in D_{2h} (TS) normal-mode mode basis (see Figure 3.6 on page 50). All other normal-modes exhibit coefficients lower than 0.05.

coordinate system using the 24 vectors of vibration at the transition state as basis. The multiples of each vector needed to reach a special point on the MEP from the TS are called a set of coefficients.[106, 220] Analyzing these set of coefficients along the whole MEP one can assert that mainly four vectors (i.e., normal modes) are relevant for the proton exchange. The coefficients of these important normal-modes are depicted in Figure 3.4. I thus agree with a previous study[208] that at least a four-dimensional treatment is necessary for a correct description of the dynamics. These four dimensions are the synchronous hydrogen transfer (OH-stretch), interdimer-stretch, CO_2 rocking and CO_2 bending modes (cf. Figure 3.6 on page 50). The OH-stretch mode contributes to the reaction for the whole process, whereas the other three modes do not participate near the TS (-0.5–0.5 Bohr), i.e., they are just assisting prior to the actual hydrogen transfer by reducing the OO distance. The rate of transfer is, therefore, strongly influenced by excitation of these modes. Raising the OH-stretch from the ground state to the first excited state leads to a shortening of the OO-distance by 0.073 Å and an increase of the tunneling-splitting by a factor of 10–100 as predicted from spectra of carboxylic acid bimolecules.[158] In contrast to a previous study it is
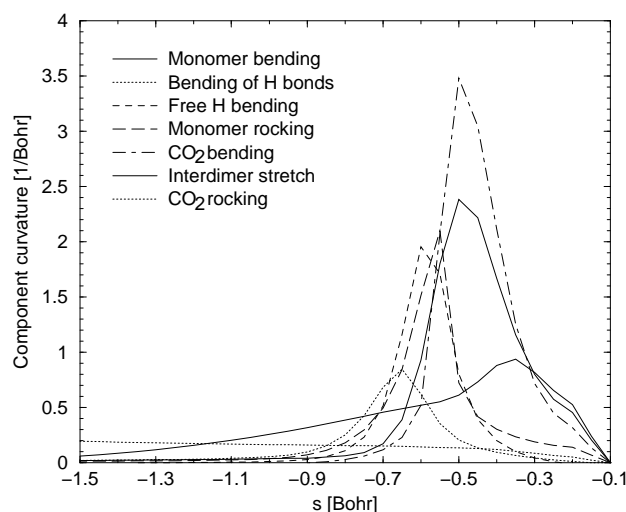
Figure 3.5: MP2///B3LYP curvature couplings to the minimum energy path.

found that motions of other symmetry than A_g or B_{3g} like the asymmetric hydrogen transfer coordinate (B_{1g}) contribute not to the coherent reaction.[190] The corresponding coefficients are perfectly zero, while other A_g or B_{3g} modes show contributions lower than 0.05 along the whole path. However, the representative LCT-path is in qualitative agreement with the most probable path (MPP) found by Shida et al.[190,192]

The curvature couplings of the various modes to the intrinsic reaction coordinate are depicted in Figure 3.5. The same modes as in Figure 3.4 on the page before are found to be relevant. The OH-stretch mode is missing as it is the transfer coordinate by itself. The remaining modes are essentially the same as those found by Benderskii et al.[208] These modes have only small non-zero normal-mode coefficients, but the coupling constant becomes as large as 2.4 Bohr^{-1} for the monomer rocking. Most of the modes show maximal coupling between 0.3 and 0.7 Bohr where also the gradient reaches a maximum. Only the coupling of the CO_2 rocking mode increases continuously towards the entrance channel of the reaction. Excitation of modes curvature coupled to the reaction path enhances the reaction rate due to an increased energy flow to the reaction coordinate.[96,101,120,205] Therefore, the

CO_2 rocking is perfectly suitable for accelerating the transfer in its vibrationally excited states in the entrance channel. The other modes can enhance the reaction in later stages of the reaction, even in the part of the reaction where direct corner cutting occurs, because the modes of Figure 3.5 on the preceding page are as well coupled to the LCT paths. The characterization of all relevant normal-modes is shown in Table 3.1 and Figure 3.6 on the following page. For the minima all slow and fast modes are within 10% and 3% of the experimental[159] result at B3LYP/6-31+G(d) level of theory, respectively.

Description	ν	μ	Γ
monomer rocking	1751	4.1	B_{3g}
bending of H bonds	1639	1.1	A_g
free H bending	1406	1.1	B_{3g}
monomer bending	1400	6.6	A_g
CO_2 bending	737	6.6	A_g
interdimer stretch	491	9.2	A_g
CO_2 rocking	231	12.5	B_{3g}
symm. H transfer	1324i	1.1	B_{3g}

Table 3.1: Frequency ν [cm^{-1}], reduced mass μ [amu] and irreducible representation Γ of the normal-modes important for the HH-transfer at the transition state as predicted from B3LYP/6-31+G(d).

In summary this study shows what is required to reach an accuracy within the experimental error limits. First, the full-dimensional nature of the reaction path needs to be considered, i.e., no vibrational degrees of freedom may be frozen out. Second, the electronic structure methods need to contain electron correlation effects. Third, the reaction barrier needs to be known to the best possible accuracy. Fourth, multidimensional optimized tunneling corrections need to be employed. If attention is paid to all of these points the experimental results can be approached rather closely, so that smaller effects like vibrational excitation can be invoked to be responsible for the remaining discrepancies.
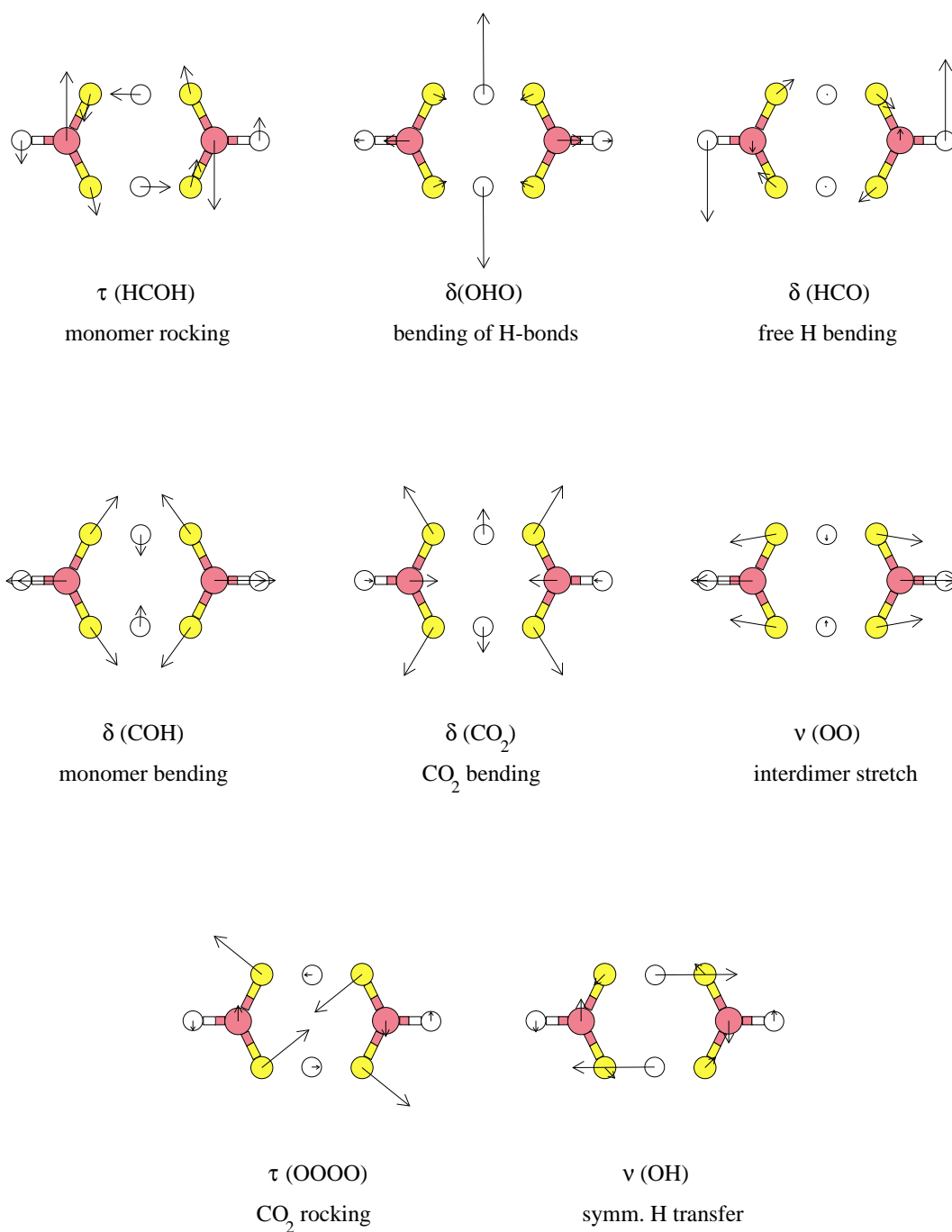
Figure 3.6: Normal-modes of the transition state participating actively in the concerted proton transfer in the formic acid dimer.

Chapter 4

Results

4.1   The Hydration of Sulfur Oxides

4.1.1   Sulfur Dioxide

Stationary Structures

The stationary structures, i.e., the educt minimum, the product minimum and the transition state, found after full geometry optimization utilizing the Berny algorithm as implemented in Gaussian98[140] at B3LYP/6-31+G(d) level of theory are depicted in Figure 4.1 on the next page. Additionally, a transition state optimized at the same level of theory interconverting H_2SO_3–$2H_2O$ structures is shown in Figure 4.2 on page 53. Calculations of the minimum energy paths utilizing the Page-McIver algorithm as implemented in Polyrate8[152] and shown in Figure 4.4 on page 55 resulted in slightly different product structures of $H_2SO_3 \cdot 1H_2O$ and $H_2SO_3 \cdot 2H_2O$ as shown in the mechanistic overview of Figure 4.3 on page 54. However, the conversion of these structures to the energetically lower lying H_2SO_3 structures depicted in Figure 4.1 on the next page just involves low-barrier reorientation of the water molecules. In the n=2 and n=3 cases additional stabilization
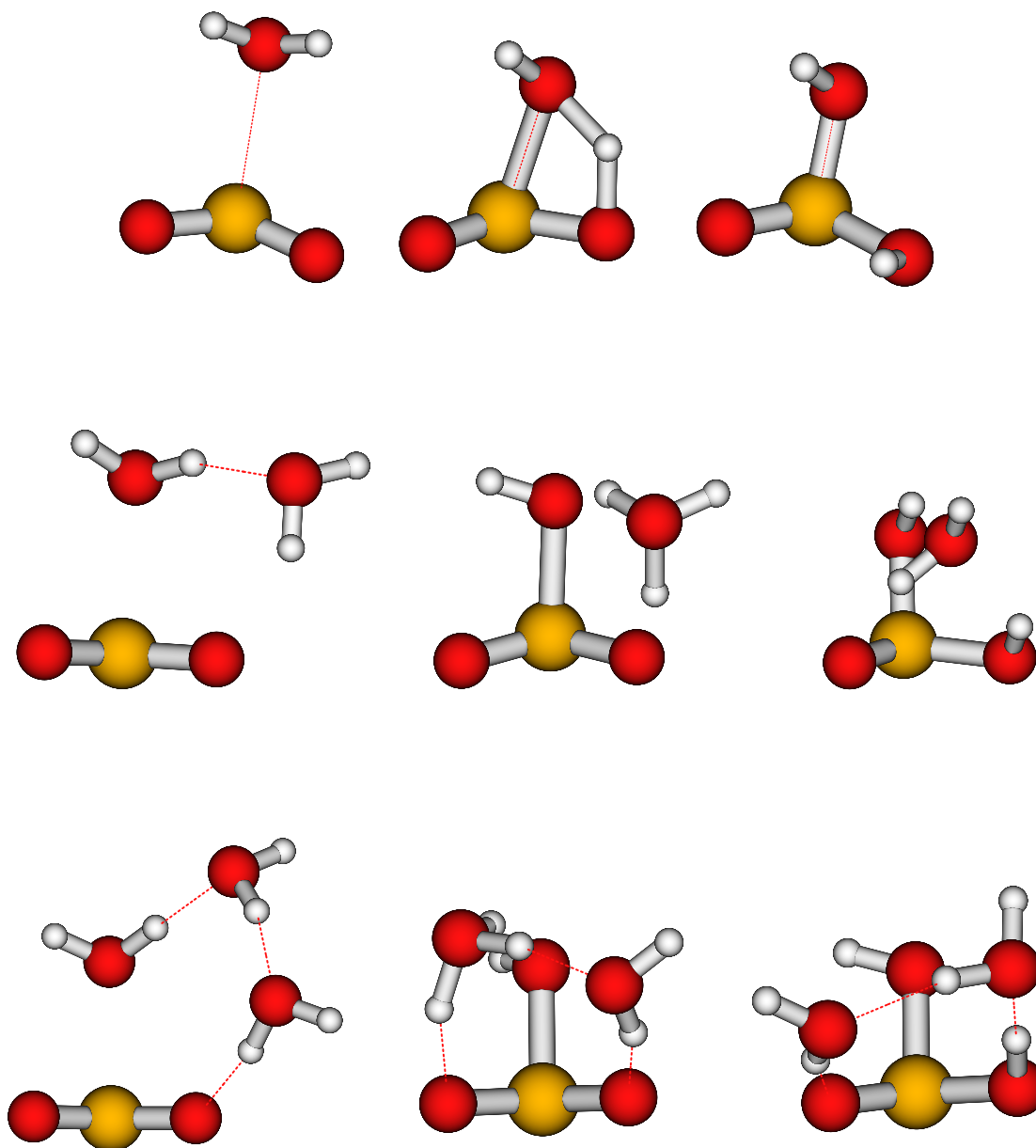
Figure 4.1: Stationary *in vacuo* structures involved in the conversion from sulfur dioxide to sulfurous acid in the presence of one (top), two (middle) and three water molecules (bottom) as found at B3LYP/6-31+G(d) level of theory.
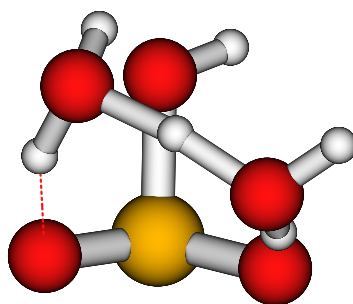
Figure 4.2: Transition state interconverting two isomers of the dihydrate of sulfurous acid as found at B3LYP/6-31+G(d) level of theory.

of 3 kcal/mol and 0.5 kcal/mol is found for this process, respectively, by comparing the values in Figure 4.4 on page 55 and Table 4.1 on page 62. A secondary transformation like this one accompanying the principal chemical reaction does not alter the observed forward rate constant as long as the secondary transformation involves a lower barrier than the principal reaction. Such a transformation only affects the backward rate constant and, therefore, also the equilibrium constant for the whole process.

Molecular Mechanism

Furtheron Figure 4.4 on page 55 reveals that all investigated reactions of sulfur dioxide to sulfurous acid involve concerted atomic movement, because no additional transition states besides the one at s=0.0 Bohr can be found. From the mechanistic viewpoint this means that the nucleophilic attack of oxygen on sulfur and all involved proton transfers happen in a single step without any intermediates. However, as demonstrated by the peak locations in Figure 4.6 on page 59 in the cases of multiple proton transfer encountered when two or three water molecules are present, the proton transfer step occur not synchronously,
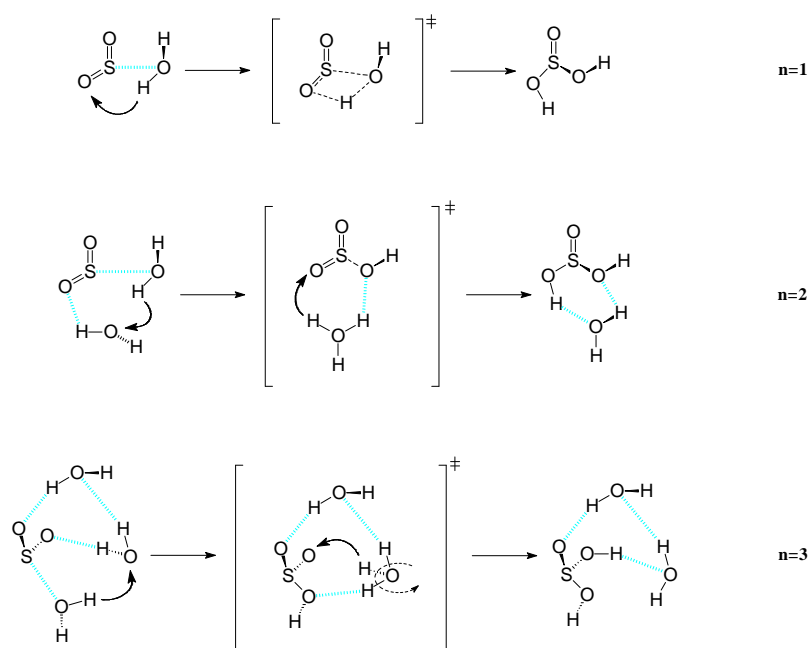
Figure 4.3: Molecular mechanism for the conversion of sulfur dioxide to sulfuric acid in the presence of one (n=1), two (n=2) and three (n=3) water molecules as found from the minimum energy path calculated at B3LYP/6-31+G(d) level of theory.
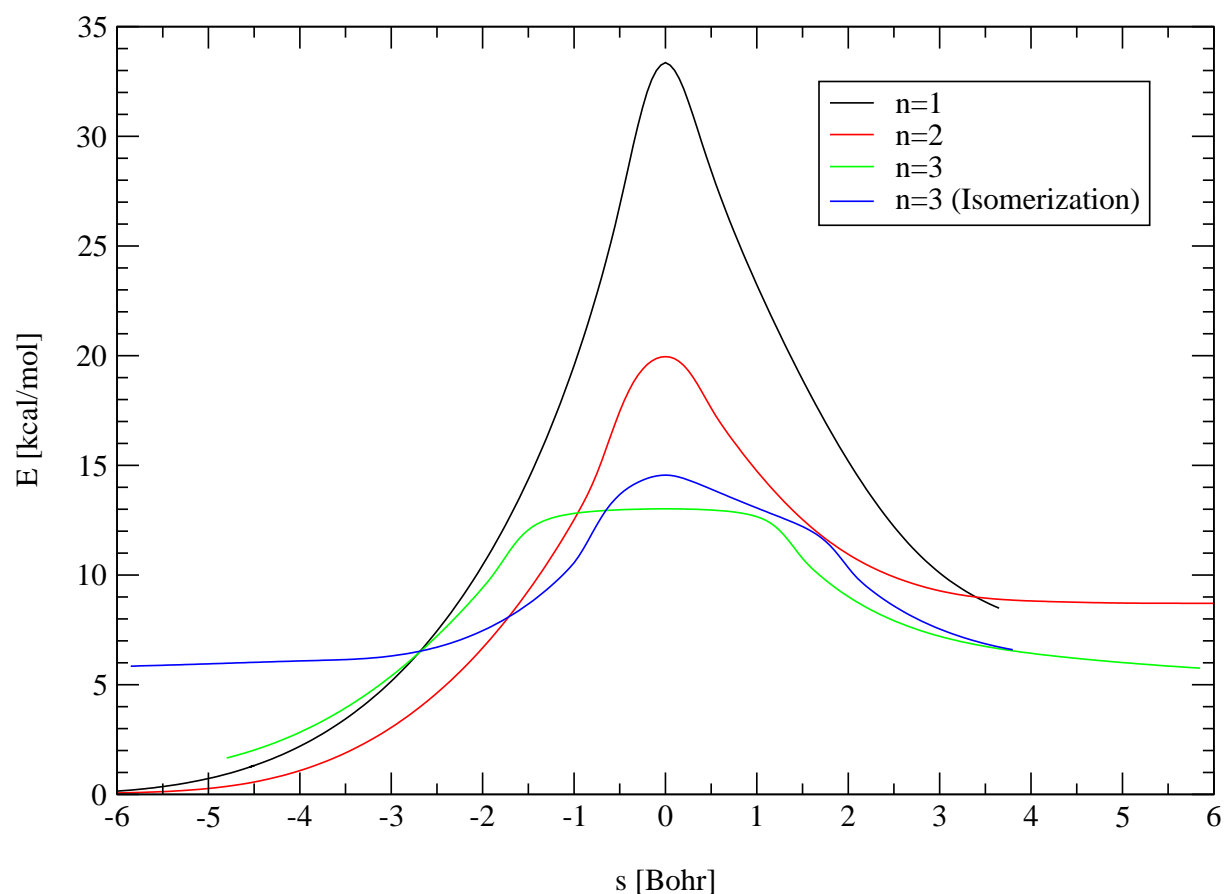
Figure 4.4: Electronic energy along the minimum energy path for the conversion from sulfur dioxide to sulfurous acid.

but rather asynchronously. Peaks in the frequency plots generally occur when the atomic movement corresponding to this frequency, i.e., the normal-mode, has a low reduced mass, which is the case for proton movements. Both for the n=2 and n=3 reactions two such peaks can be found along the reaction coordinate s, which indicates that two protons are transferred at different reaction coordinates. This is quite surprising for the SO_2 hydration involving three water molecules, as one could suspect the triple proton transfer along three water molecules to be favored most from ring strain considerations. Obviously the task of the third water molecule must be a different one.

In Figure 4.5 on the following page selected distances between pairs of atoms are depicted along the classical reaction coordinate, i.e., the minimum energy path, for the different hydration reactions of SO_2 and the isomerization of the instable dihydrate of sulfurous acid. On inspecting these plots some common features can be found. The protons involved in $OH \cdots O$ hydrogen bonds stay at a rather constant distance of slightly less than 1 Å from the donor oxygen atom for a great portion of the reaction coordinate. At the same time the O—O distance reduces from the equilibrium distance of 2.7–2.9 Å to about 2.5 Å. Then there is a point on the reaction coordinate where the proton suddenly starts the transfer to the acceptor oxygen atom, which can be seen in Figure 4.5 on the next page from the sudden increase of the proton distance to the acceptor oxygen atom. In case of the 1:1 complex of SO_2 with H_2O the favorable linear arrangement of the hydrogen bond can not be reached for steric reasons, and the proton is transferred at an O4—O2 distance of less than 2.5 Å. Whether the proton is transferred at an O—O distance of 2.5 Å can, therefore, be used as an indicator of steric strain. Such a strain is obviously absent for any proton transfer observed in the complexes of SO_2 with more than one water molecule. After the proton transfer has been accomplished the O—O distance again relaxes to the equilibrium distance of 2.7–2.9 Å. Obviously, the proton transfer is triggered by very short O—O distances. This phenomenon has been noted both by NMR methods and from electronic structure calculations for many different hydrogen bonds in the literature and received the name "hydrogen bond compression mechanism".[115,116,118,119] It has been shown in numerous publications that the potential describing the proton transfer process changes from a double-well potential involving a barrier to a single-well potential involving no barrier on decreasing the distance of the donor and acceptor atoms subsequently.[115,119,132,185,187,190,221–225]

This hydrogen bond compression mechanism, which works best in linear $OH \cdots O$ arrangements and O—O distances of 2.5 Å, explains why H9 is transferred to O10 rather than to O4, so that H_2SO_3 isomerization occurs. Whereas the O3–O4 atom pair can only
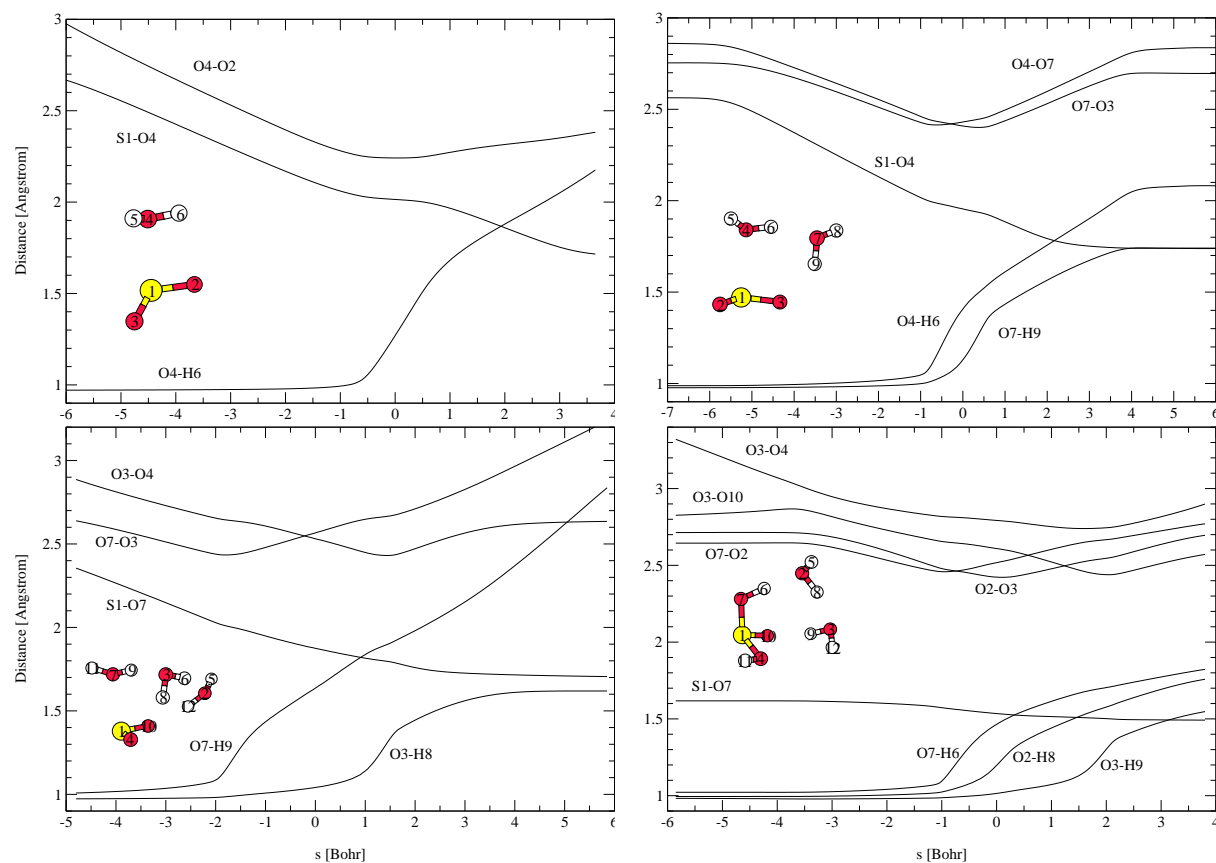
Figure 4.5: Distances [in Å] between selected two atoms along the minimum energy path [in Bohr] for the hydration of sulfur dioxide by one (top left), by two (top right) or by three (bottom left) water molecules and for the isomerization of "sulfurous acid" in the presence of two water molecules (bottom right). The numbering scheme is shown as inset in the respective plots.

reach a distance of 2.8 Å, the O3–O10 atom pair can reach a better orientation for hydrogen transfer. The hydrogen atom takes its way to the potential valley corresponding to the isomerization channel, therefore. The S1—O7 distance varies by only ≈0.1 Å corresponding to rehybridization from a formal single bond (S-O) to a double bond (S=O).

In case of a multiple proton transfer reaction all O—O distances vary at the same time, i.e., the process becomes highly cooperative. The accomplishment of the first proton transfer yields a H_3O^+ containing, instable transient species. To reach a stable state again, the next proton transfer is triggered and so forth. In Figure 4.5 on the preceding page it can be seen that the first proton is transferred before the transition state at negative s whereas the second (and third) proton is transferred at or after the transition state at non-negative s. This is validated from the reaction mechanisms shown in Figure 4.3 on page 54. At the transition state one "water" molecule can be found that has hydronium ion (H_3O^+) character for the n=2 and n=3 cases. The reaction coordinate differences of the proton transfer peaks are quite different for the n=2 and n=3 cases. In the n=2 case about 1 Bohr of atomic movement lies between the two proton transfer reactions, whereas in the n=3 case about 4 Bohr lie between them. According to IUPAC nomenclature such a behaviour is called *asynchronous*.[226] On inspecting the S—O distance, which decreases along the whole hydration coordinate, it becomes clear that the proton transfer is *concerted* with the nucleophilic attack.

The region between the proton transfers in Figure 4.4 on page 55 reveals that for the n=3 case the energy remains approximatively constant. On the other hand in the n=2 case the energy drops significantly on both sides of the transition state. This is also reflected in the "imaginary" frequencies in this region being between 900i cm^{-1} and 1000i cm^{-1} for n=2, and only between 100i cm^{-1} and 200i cm^{-1} for n=3. Clearly, the two double proton transfers of the n=2 and n=3 reactions must be mechanistically quite different. A comparative inspection of the structures along the reaction coordinates reveals that the
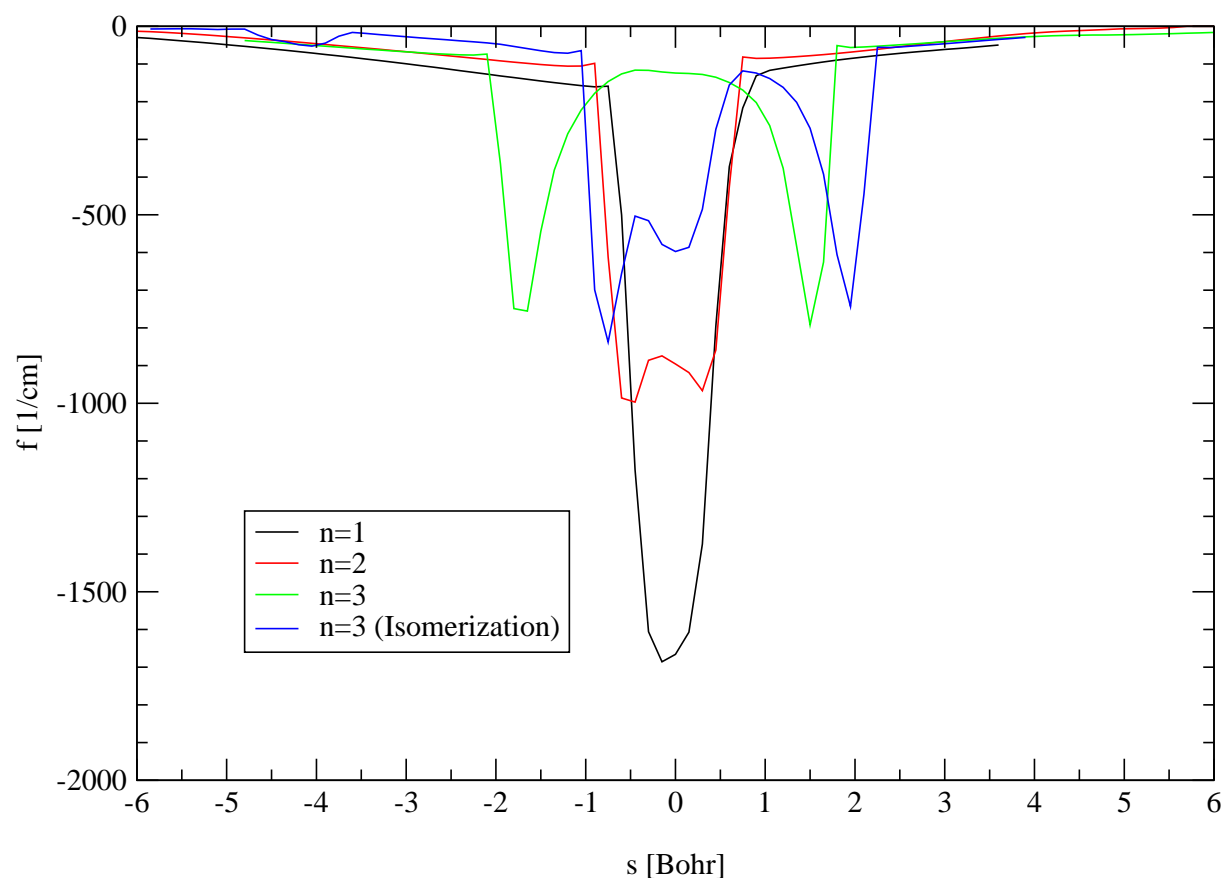
Figure 4.6: "Imaginary" frequency along the reaction coordinate. Negative s values correspond to H_2O–SO_2 like species, s=0 Bohr corresponds to the transition state, and positive s values correspond to H_2SO_3 like species.

n=2 case corresponds to the "classical" water mediated proton transfer along both water molecules, whereas in the n=3 case the "classical" water mediated proton transfer along three water molecules can not be found.

Instead the hydronium ion like subpart of the supermolecule performs a slight rotational movement as indicated in Figure 4.3 on page 54 in order to bring one proton to a position from which transfer to the neighbor oxygen atom is energetically favorable. Although the third water molecule acts as spectator, i.e., remains in about the same position during the whole reaction, it has the important function of stabilizing the H_3O^+ subunit by providing
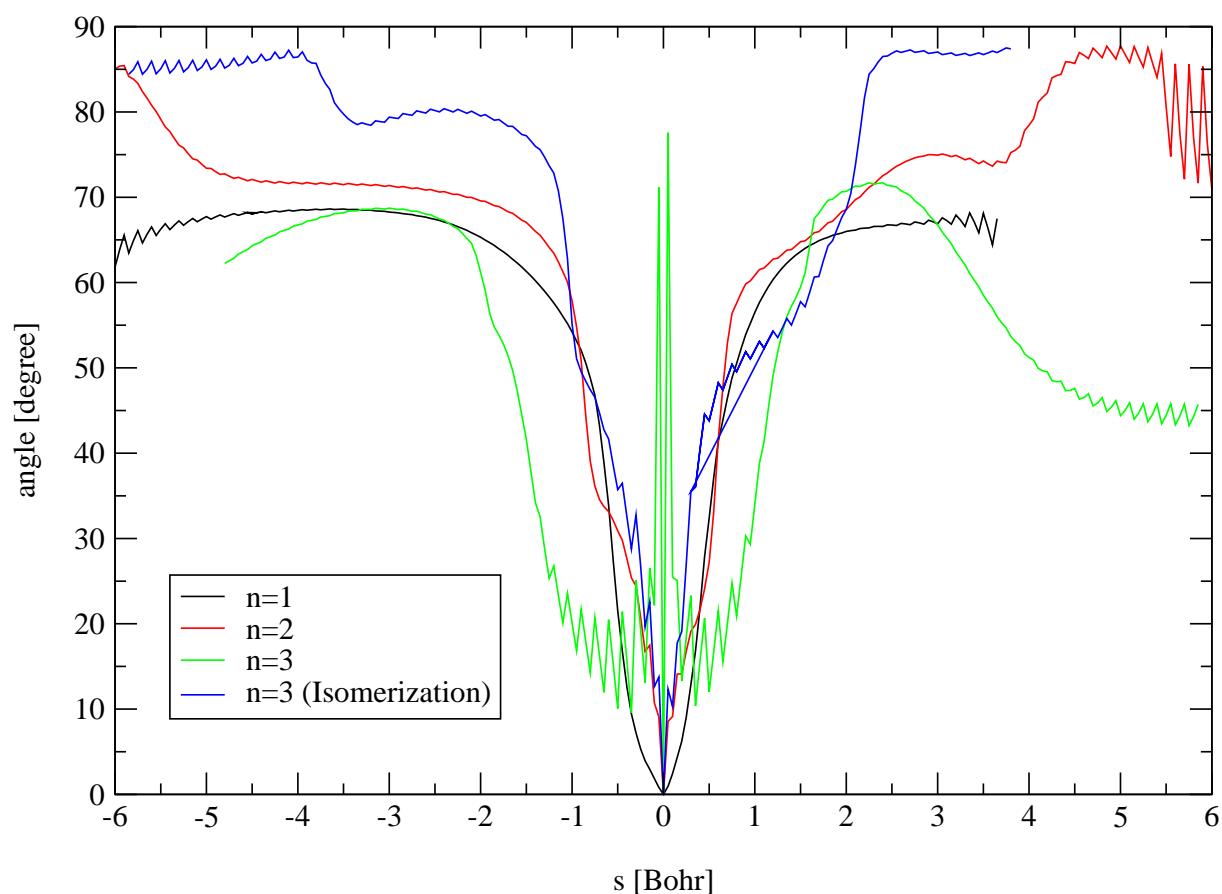
Figure 4.7: Angle between the reaction coordinate at the transition state, i.e., normal-mode vector of the "imaginary" frequency, and the gradient along the reaction path. Negative s values correspond to H_2O–SO_2 like species, s=0 Bohr corresponds to the transition state, and positive s values correspond to H_2SO_3 like species.

the oxygen atom, which acts as hydrogen bond acceptor. Figuratively spoken, this oxygen atom is the anchor for the second hydrogen bridge "rope" to which the molecular water "swing" carrying a proton is fastened. And when the "swing" reaches the highest point, the proton has gained enough energy to be able to "jump" to the oxygen atom.

The complicated nature of the reaction and the frequent turns of the reaction coordinate on the reaction hypersurface are demonstrated in Figure 4.7. This graph shows the relative orientation of the present reaction coordinate, i.e., the direction of the gradient, with

respect to the reaction coordinate at the transition state, i.e., the direction of the normal mode corresponding to the negative eigenvalue in the Hessian matrix. The noise in these curves can be found mainly near the stationary points of the reaction, where the gradient is very small and the direction of the gradient is numerically difficult to be described. Especially at the reaction coordinates of proton transfer the reaction angle suddenly changes from 0 degree to 60–80 degree. An angle of 90 degree implies orthonormality to the reaction coordinate at the transition state, i.e., a reaction coordinate that is uncoupled to the reaction coordinate at the transition state. However such an angle is never reached along the whole reaction coordinate. The need for the use of the full-dimensional tunneling model and the use of the full-dimensional hypersurface (as utilized in this work) for the description of the reaction directly follows from the highly coupled vibrational modes.

Reaction Energetics

From an energetic view of the hydration reactions (as summarized in Table 4.1 on the next page) it becomes clear that the reaction barrier clearly decreases in going from single proton transfer (n=1) to water mediated proton double proton transfer (n=2) and double proton transfer alleviated by a "molecular swing". This decrease from 34 kcal/mol to 22 kcal/mol is directly explainable by ring-strain in the transition state. Whereas in the case of n=1 an unfavorable four-membered transition state is encountered, a six-membered transition state is involved in the case of n=2, which is more free of ring strain. The lower ring strain of cyclobutane compared to cyclohexane amounts to 26 kcal/mol,[227] which is double the calculated barrier reduction. This is probably due to the sulfur atom, which is not restricted to a tetrahedral coordination geometry as is the case for carbon atoms due to the missing d orbitals. The reduction of the reaction barrier on going from n=2 to n=3 amounts to 7 kcal/mol. This reduction is supposedly due to the "molecular swing" mechanism bringing the system to an energetically favorable atomic arrangement in the

		B3LYP/ 6-31+G(d)	MP2/ aug-cc-pVDZ	CCSD(T)/ aug-cc-pVDZ	MP2/ aug-cc-pVTZ
n=1	SO_2/H_2O	5.26	4.50	5.00	4.34
	$SO_2 \cdot H_2O$	0.00	0.00	0.00	0.00
	TS	33.34	35.44	34.19	34.40
	H_2SO_3	6.94	11.59	6.82	9.00
n=2	$SO_2/2H_2O$	16.60	14.01	14.74	–
	$SO_2 \cdot (H_2O)_2$	0.00	0.00	0.00	–
	TS	19.96	22.95	22.12	–
	$H_2SO_3 \cdot H_2O$	5.77	9.38	4.47	–
n=3	$SO_2/3H_2O$	27.86	23.54	–	–
	$SO_2 \cdot (H_2O)_3$	0.00	0.00	–	–
	TS	13.02	–	–	–
	$H_2SO_3 \cdot (H_2O)_2$	5.52	8.31	–	–

Table 4.1: Electronic energies in kcal/mol for the hydration of SO_2 assisted by n=1, n=2 and n=3 water molecules, respectively. The first lines correspond to the separated SO_2 and nH_2O molecules, the second lines correspond to the $SO_2 \cdot nH_2O$ minima (set to 0.00 kcal/mol by definition), the third lines correspond to the transition states to the concerted nucleophilic attack/proton transfer reaction (TS), and the last lines correspond to the $H_2SO_3 \cdot (n-1)H_2O$ minima. CCSD(T) energies rely on MP2/aug-cc-pVDZ geometries.

transition state region.

As observed experimentally "sulfurous acid" is instable in any hydration state by at least 5 kcal/mol relative to loosely hydrated sulfur dioxide species. Zero-point correction tends to further increase this instability by approximately 1 kcal/mol. It is, therefore, highly unlikely that there are regions in the temperature, pressure diagram, in which "sulfurous acid" becomes stable. Nevertheless, it is still possible that oligomeric "sulfurous acid" $(H_2SO_3)_n$ species are approximately as stable as loosely hydrated sulfur dioxide species. Such a situation occurs for structurally similar carbon dioxide hydrates and carbonic acid dimers $(H_2CO_3)_2$.[165]

Another low-energy transition state that can be found in the $H_2SO_3 \cdot 2H_2O$ water system corresponds to the transfer of a hydrogen atom of "sulfurous acid" via double proton

transfer along a two water chain to the oxygen atom previously double bonded to the sulfur atom. Of course the educts and products of this isomerization are energetically equal as found also in Figure 4.4 on page 55. Nevertheless, this mechanism provides a possibility for oxygen isotope exchange. The marked *O atom moves from the hydroxy group (H*O)(O=S)(OH) to the double bonded position (HO)(*O=S)(OH). The reaction barrier to this process amounts to about 9 kcal/mol, which is clearly lower than all hydration barriers. However, using the SO$_2$·3H$_2$O complex as the zero of energy, as exemplified in Figure 4.4 on page 55, it becomes clear that the barrier-top for hydration lies lower by about 1.5 kcal/mol. When taking into account zero-point correction for both structures, the barrier-top to isomerization is even lower by 0.5 kcal/mol. This similarity in absolute energies of the transition states indicates that for the backward reaction there is a competition between isomerization and decomposition to sulfur dioxide. Indeed the geometries found on the minimum energy path are absolutely identical for both reaction channels between 6 Bohr and 4 Bohr. At the reaction coordinate of about 4 Bohr there is a point at which the system "decides" statistically or from the available distribution of thermal energy into vibrational excitations, which path will be tracked.

The Influence of Tunneling

In Table 4.2 on page 65 the magnitude of the quantum-mechanical tunneling correction κ to the classical rate constant is listed for the three hydration reactions of SO$_2$ and the isomerization mechanism (labeled Iso) described above at three temperatures (100, 200 and 300 K). There is a clear correlation between the magnitude of the imaginary frequency at the transition state depicted in Figure 4.6 on page 59 and the tunneling correction factor. For the lowest imaginary frequency observed, namely 124i cm^{-1} for the hydration involving three water molecules, tunneling is rather unimportant. In the dominant direct corner-cutting (LCT) mechanism the reaction is accelerated by a factor of 25.8 at 100 K.

At higher temperatures tunneling ceases, i.e., κ approaches 1.0. In comparison the isotope exchange mechanism is preferred by tunneling. This can be explained by the thinner energy barrier in Figure 4.4 on page 55 and the higher absolute value of the imaginary frequency, namely 597i cm^{-1}. Most tunneling enhancement is observed for the classically slowest reactions involving one and two water molecules. Especially at 100 K an acceleration factor of 10^{24} and 10^{8} is found from the calculation for n=1 and n=2, respectively. However, as seen in Figure 4.14 on page 79 this acceleration is still not sufficient to outweigh the classical disadvantage in terms of reaction rates.

Interestingly adiabatic corner-cutting (SCT) is the dominant tunneling mechanism for n=1 at all temperatures, which is indicative of energetically unfavorable geometries in the reaction swath. For n=2 the crossover from non-adiabatic (LCT) to adiabatic (SCT) corner cutting occurs at about 275 K. Due to the additional water molecules providing additional vibrational degrees of freedom the geometries encountered in the swath are comparatively less unfavorable.

Assuming uncertainties of 1 kcal/mol in the reaction barrier leading to uncertainties of a factor of 5 (300 K), 12 (200 K) and 150 (100 K) in the classical rate constant, it becomes clear that tunneling is a negligible effect for n=3 down to 100 K, important below about 250 K for n=2 and important even above room temperature for n=1. All Wigner tunneling corrections are very low and not significant within the above-mentioned error limits. Therefore, this method is not useful for quantifying tunneling corrections. The LCT tunneling corrections are not significantly higher than the SCT corrections. This is in strict contrast to the results found in carboxylic acid dimers,[149] cyclic HF[106,150] and water clusters.[107] Whereas these systems involve "pure" proton transfer reactions of reduced mass 1 amu, in the case of sulfur dioxide hydration heavy atom movement accompanies the reaction. This renders the proton transfer reactions "impure", so that the effective reduced mass becomes > 1 amu. This is the reason for the difference in the comparison of LCT

	Wigner	ZCT	SCT	LCT
	24.9	9.9×10^{17}	6.4×10^{23}	4.1×10^{21}
n=1	7.0	1.3×10^3	1.9×10^5	7.4×10^4
	3.7	13.3	76.4	27.1
	7.9	4.4×10^4	6.0×10^7	4.7×10^8
n=2	2.7	6.3	39.1	68.2
	1.8	2.1	4.2	3.3
	1.1	3.4	20.9	25.8
n=3	1.0	1.4	1.6	1.5
	1.0	1.2	1.2	1.2
	4.1	6.1	5.8×10^2	3.9×10^4
Iso	1.8	1.4	2.1	5.1
	1.3	1.2	1.3	1.4

Table 4.2: Tunneling correction factors κ at 100 K (top row), 200 K (middle) and 300 K (bottom) to the rate constants obtained from classical transition state theory for the reaction $SO_2 \cdot nH_2O \rightleftharpoons H_2SO_3 \cdot (n\text{-}1)H_2O$. B3LYP/6-31+G(d) was employed throughout. The Wigner correction[123] is calculated directly from the imaginary frequency at s=0 Bohr in Figure 4.6 on page 59 without using any information of the reaction path, zero-curvature tunneling (ZCT) involves tunneling along the minimum energy path, small-curvature tunneling (SCT)[228] involves adiabatic tunneling at the inner turning points of the concave side of the minimum energy path,[229] and large-curvature tunneling (LCT)[104] involves vibrationally non-adiabatic straight line tunneling through the reaction swath. The latter three corrections were all calculated employing the semi-classical approximation.[230]

and SCT tunneling corrections.

4.1.2   Sulfur Trioxide

Stationary Structures

The stationary structures after geometry optimization using the same method as for the SO_2 reaction systems are depicted in Figure 4.8 on page 67. Some of these stationary point structures have been characterized by experimental and/or computational techniques.[231–236] The IR spectrum of the 1:1 SO_3-H_2O complex predicted by hybrid density functional theory agrees with the results obtained by matrix-isolation in nitrogen.[231] Two

calculated bands above 3500 cm^{-1}, the 1340/1326 cm^{-1} doublet, the band at 1018 cm^{-1} and four bands between 460 and 560 cm^{-1} can be correlated directly with the observed spectrum. The geometry is reminiscent of a donor-acceptor complex, which is consistent with microwave-spectroscopy results.[232] The intermolecular S—O distance is predicted to be 2.395 Å instead of 2.432 Å, the out-of-plane distortion of the SO$_3$ part is 1.9 degree instead of 2.6 degree, and the angle between the C$_2$ axis of water and the intermolecular S—O axis is 108 degree instead of 103 degree. Also the reaction product sulfuric acid agrees well with microwave results.[237]

Concerning the global minimum of the 1:1 complex of sulfuric acid with water it is found that the water molecule is attached in a similar manner to sulfuric acid as was found both from independent *ab initio* calculations[233–235] and IR matrix isolation studies.[236] I do not find evidence for any ionic character of the 1:1 and also 1:2 sulfuric acid—water minima, which also agrees with the experimental[236] and theoretical findings.[238] On the other hand, the global minimum found here for the 1:2 complex differs from the one assumed in the literature to be the global minimum.[235] The cyclic arrangement of the two water molecules around sulfuric acid found here is favorable by 3.28 kcal/mol over the double chain structure noted in the literature.

Again a comparison of the optimized structures and the end-points of the minimum energy path as depicted in Figure 4.9 on page 68 reveals that low-barrier secondary transformations occur, which involve rearrangement of water in the sulfuric acid—water complex or torsional movement of the two hydroxy groups in sulfuric acid. From the energetic point of view these secondary rearrangements yield a further stabilization of sulfuric acid compared to sulfur trioxide–water of at most 3 kcal/mol.
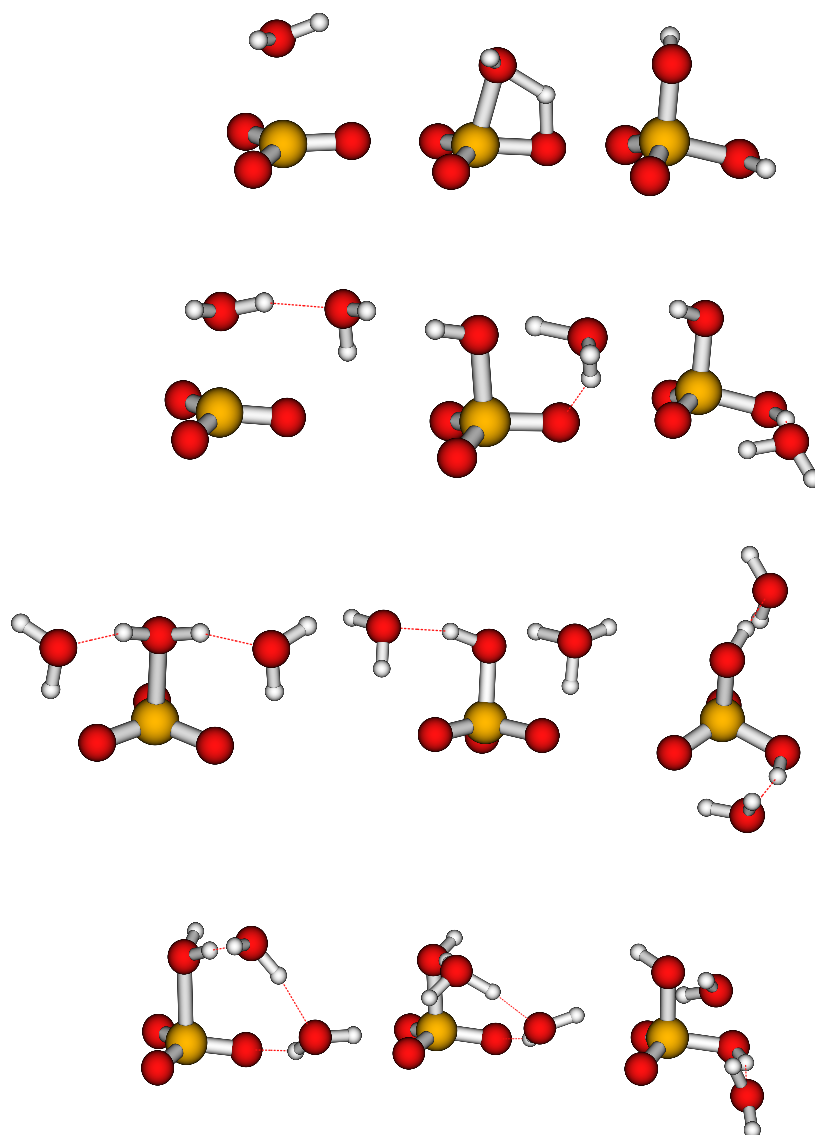
Figure 4.8: Stationary *in vacuo* structures involved in the conversion from sulfur trioxide to sulfuric acid in the presence of one (top), two (second from top), and three (second from bottom and bottom) water molecules as found at B3LYP/6-31+G(d) level of theory. The mechanism in the third row corresponds to water-mediated double proton transfer assisted by a rather rigid third water molecule. The mechanism in the bottom row corresponds to a single proton transfer, rotation of a H_3O^+ like transient subspecies, and a second single proton transfer.
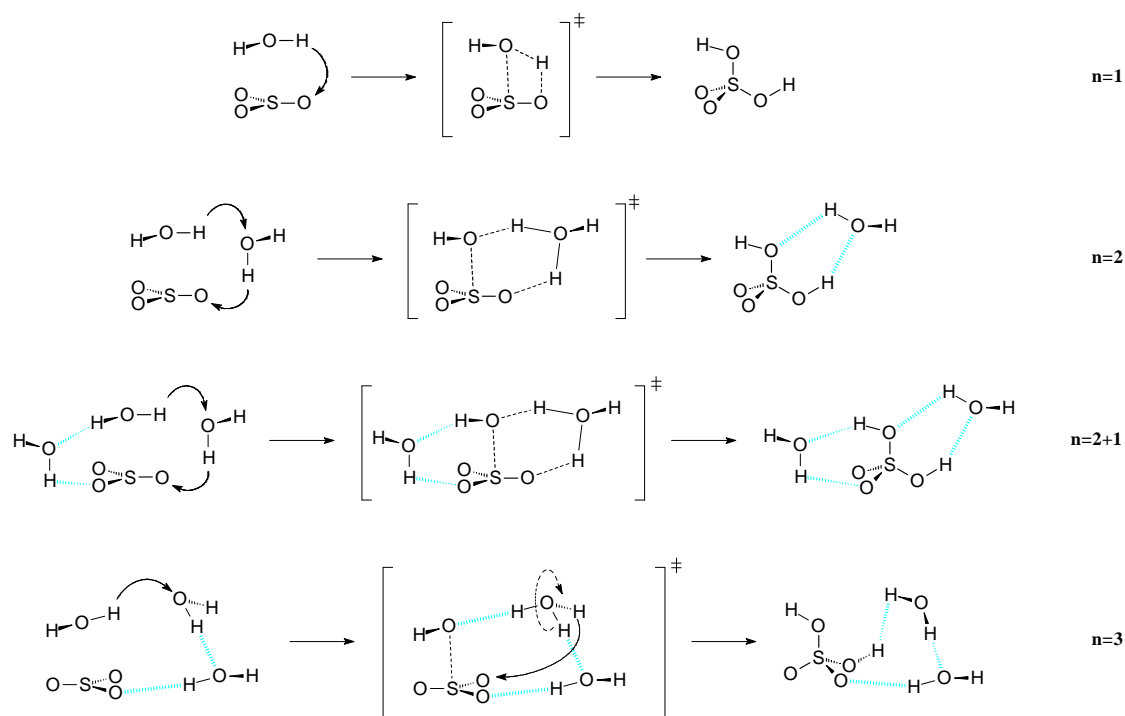
Figure 4.9: Qualitative representation of the stationary points of the different unimolecular isomerization steps of SO_3 hydration. Water addition concerted with a single proton transfer in the presence of a single water molecule (n=1), hydration concerted with water-mediated double proton transfer (n=2), hydration concerted with water-mediated double proton transfer in the presence of a third, microsolvating water molecule (n=2+1), and hydration concerted with the sequence proton transfer-rotation of H_3O^+-proton transfer in the presence of a third stabilizing water molecule (n=3).

Reaction Mechanism

In the case of one and two participating water molecules the reaction mechanisms are analogous to the proton transfers observed in the sulfur dioxide systems. The hydration involves the nucleophilic attack of a water oxygen to the sulfur atom *concerted* with the transfer of the water proton to an oxygen atom of SO_3 as can be seen in Figure 4.10 on the following page. Again the hydrogen bond compression mechanism is found, i.e., the proton is transferred when the O—O distance reaches the minimum value of 2.5 Å. In the 1:1 complex of SO_3 and H_2O this optimal arrangement can not be reached because of steric hindrance. The complicated coupled nature of the atomic displacement is exemplified in Figure 4.11 on page 71. On the course from the educt to the product the angle changes in total by 120–150 degree, which nearly corresponds to a complete turn to the opposite direction.

In the 1:2 complex the two proton transfer processes from the first water molecule to the second water molecule and from the second water molecule to the oxygen of sulfur trioxide occur not synchronously at the transition state, but *asynchronously*. The first proton is transferred before reaching the TS, the second one after having passed the TS, which yields a hydronium ion (H_3O^+) character of the transition state. The hydration of carbon dioxide, investigated by me with the same method, but in another context, is another reaction that exhibits similar mechanistic features.[239] On the other hand the tautomerization of the 7-azaindole dimer, which is also facilitated by the addition of water molecules, is likely to occur stepwisely.[81, 240]

When a six-atom (n=2) transition state is involved rather than a four-atom (n=1) the reaction barrier drops by 17 kcal/mol as shown in Figure 4.4 on page 55 and Table 4.3 on page 75. This is 4 kcal/mol more than the barrier reduction calculated in the SO_2 case, presumably because the flexibility of the sulfur atom is restricted by the presence of an
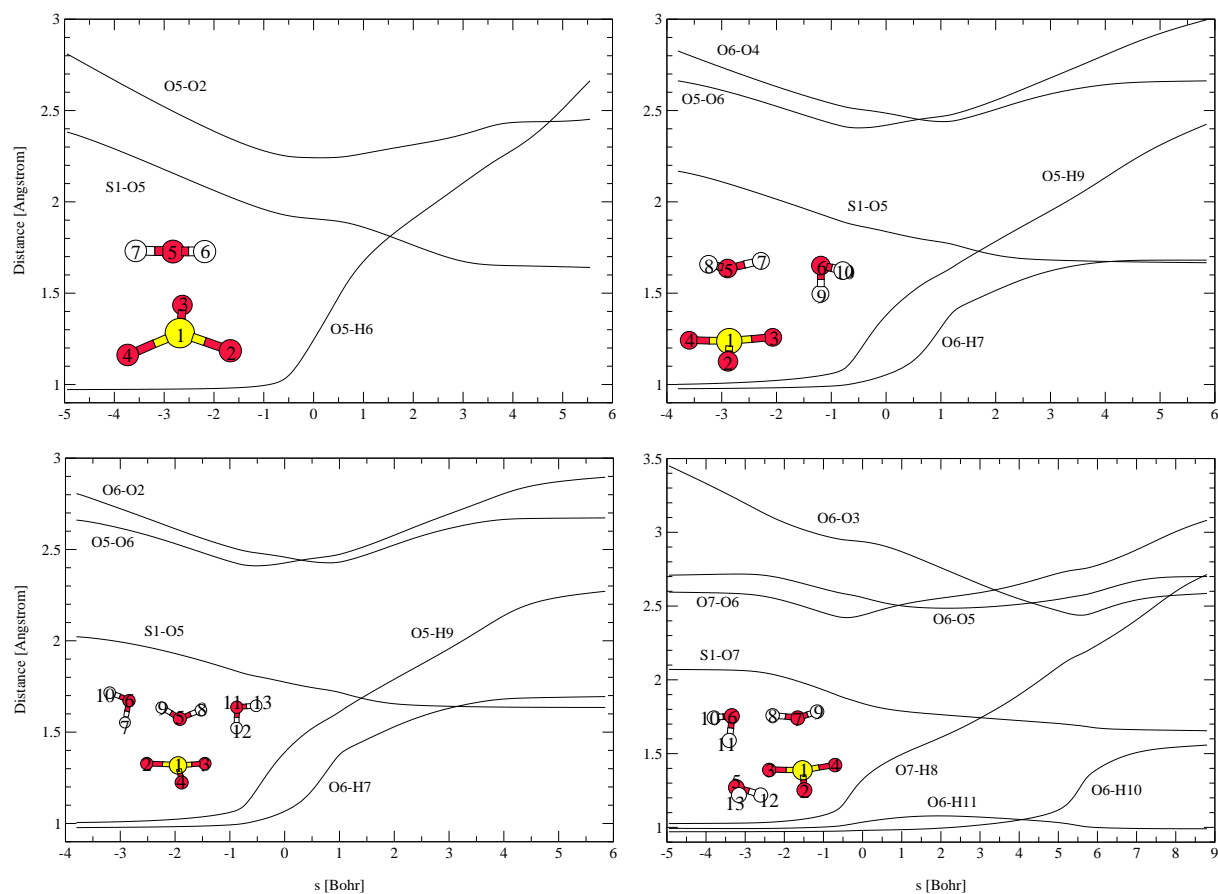
Figure 4.10: Distances [in Å] between selected two atoms along the minimum energy path [in Bohr] for the hydration of sulfur trioxide by one (top left), by two (top right), by two active and one passive (bottom left) or by three water molecules (bottom right). The numbering scheme is shown as inset in the respective plots.
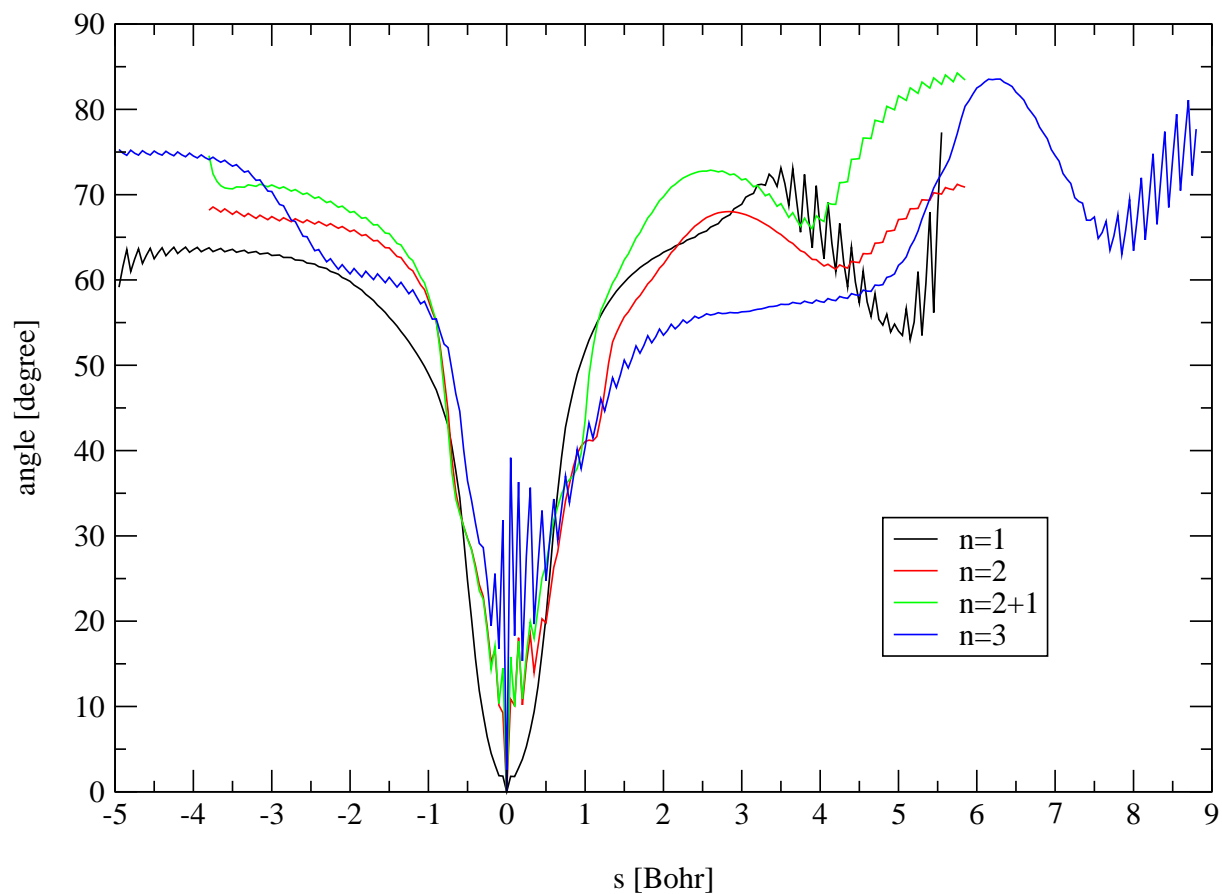
Figure 4.11: Angle between the reaction coordinate at the transition state, i.e., normal-mode vector of the "imaginary" frequency, and the gradient along the reaction path. Negative s values correspond to H_2O–SO_3 like species, s=0 Bohr corresponds to the transition state, and positive s values correspond to H_2SO_4 like species.
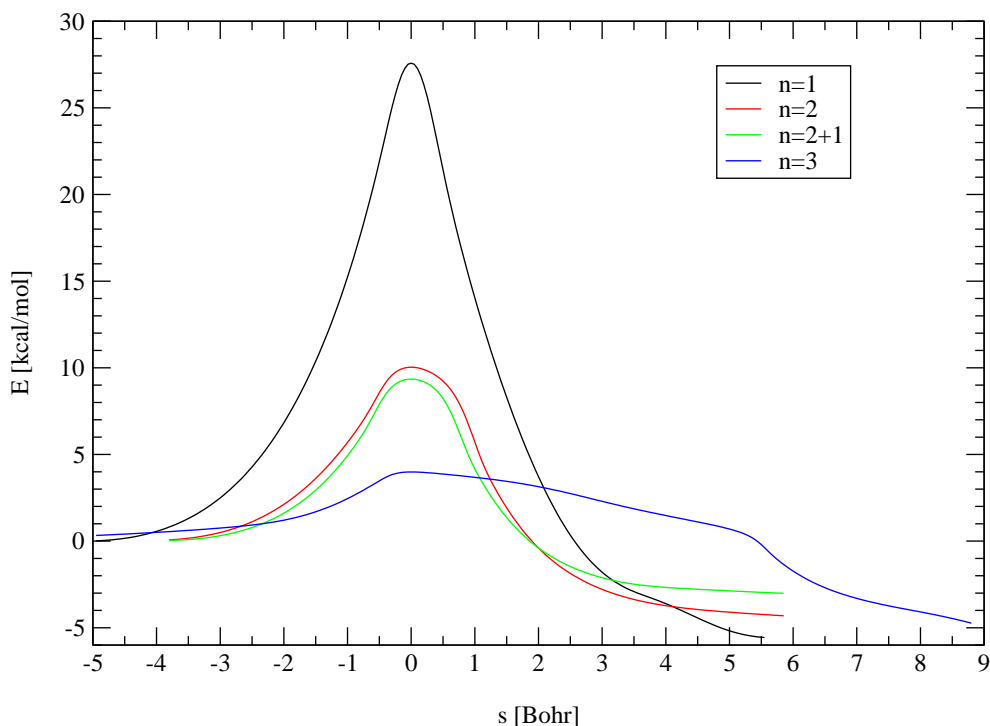
Figure 4.12: Energy along the classical reaction coordinate (MEP, IRC) as found at B3LYP/6-31+G(d) level of theory for the reaction $SO_3 + nH_2O \rightarrow SO_3 \cdot nH_2O \rightarrow H_2SO_4 \cdot (n-1)H_2O$.

additional oxygen atom.

Letting a third water molecule participate, two quite different mechanisms can be distinguished. The one termed n=2+1 hereafter is quite similar to the n=2 mechanism as can be seen from the coincidence of the corresponding curves in Figure 4.12 and Figure 4.13 on the next page. The third water molecule acts as "true spectator" in this case. Minor alterations of the hypersurface because of the third microsolvating water molecule result in a barrier reduction by 0.7 kcal/mol. However, because of the symmetry introduced by the third water molecule a second, equal reaction channel is opened. A symmetry factor of 2 enhances the forward rate constant, therefore.

As can also be seen from Figure 4.12 the reaction mechanism for the n=3 case is
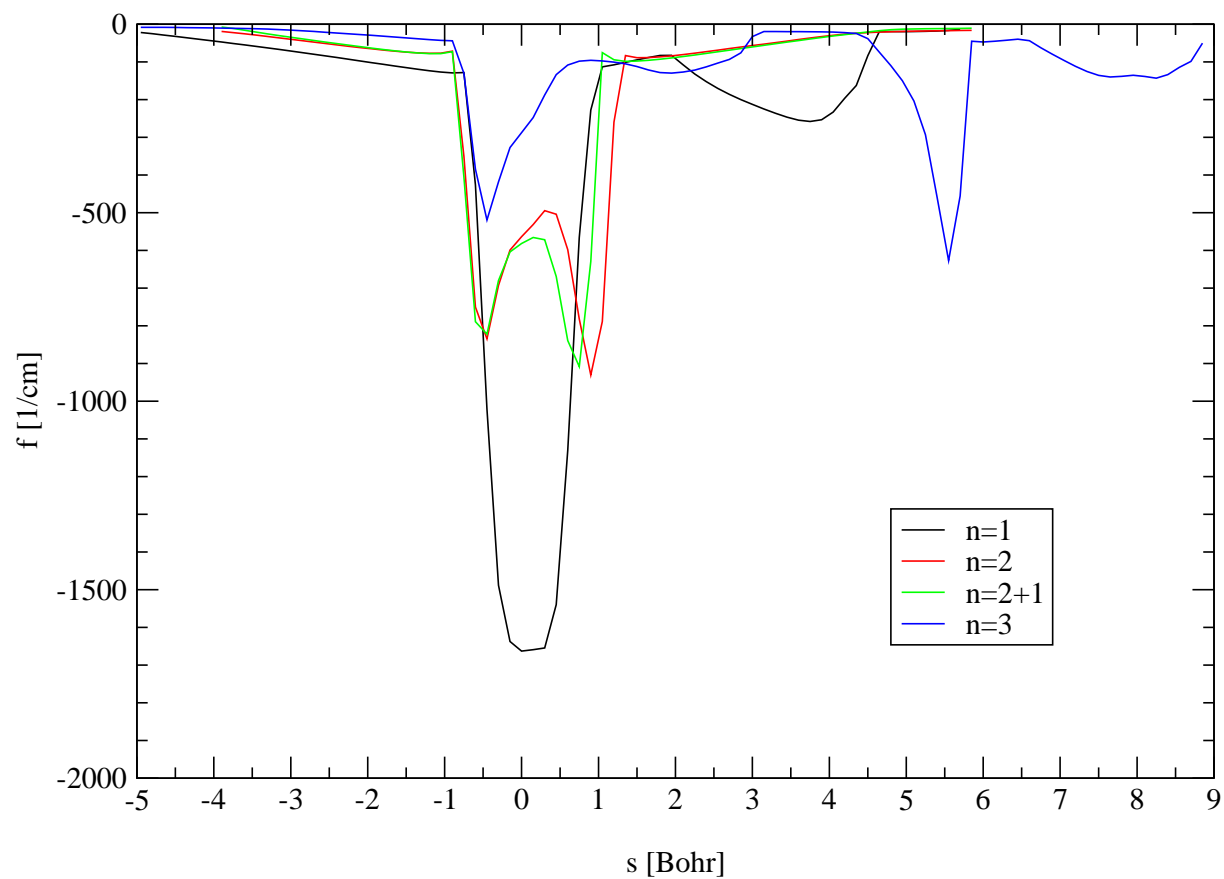
Figure 4.13: "Imaginary" frequency along the reaction coordinate. Negative s values correspond to H_2O–SO_3 like species, s=0 Bohr corresponds to the transition state, and positive s values correspond to H_2SO_4 like species.

substantially different from all other mechanisms seen in this figure. The flat region in the energy diagram between the transition state and 6 Bohr is accompanied by a bumpy, low imaginary frequency seen in Figure 4.13 on the page before. Inspecting the structures on the minimum energy path reveals that, similar to the n=3 reaction observed for sulfur dioxide, a "molecular swing" is the operative mechanism. Again the third water molecules has the function of fixating the H_3O^+ subspecies in a second hydrogen bonded "rope" enabling transient rotation of this subspecies. This "rope" function can be seen in Figure 4.10 on page 70. Whereas the O6—O5 distance remains rather constant after the transfer of the first proton, the O6—O3 distance is shortened. Atom H10 rotates into the O6—O3 line and is transferred, when the O6—O3 distance reaches 2.5 Å. A slight elongation of the O6-H11 bond is required to make this rotation energetically feasible. Instead of H11 being transferred to O5 the second proton switch involves H10 being transferred to O3, therefore.

Similar to the SO_2 case 7 kcal/mol of additional barrier reduction are observed for this kind of mechanism. A transition state to water-mediated proton transfer along all three water molecules could, despite extensive search, not be identified, and possibly does not exist on the $SO_3 \cdot 3H_2O$ hypersurface.

The Influence of Tunneling

On comparing Table 4.2 on page 65 with Table 4.4 on page 77 a lot of similarities can be found. On increasing the number of microsolvating water molecules the importance of quantum mechanical tunneling diminishes due to the broadening nature of the reaction barrier. This broadening can be seen in Figure 4.12 on page 72, but especially in the decrease of the "imaginary frequency" from 1663i cm^{-1} to 564i cm^{-1} (582i cm^{-1}) and 288i cm^{-1} for n=1, n=2 (n=2+1) and n=3, respectively. The analogous nature of the n=2 and n=2+1 types of reaction is evident from the very similar tunneling corrections in Table 4.4 on page 77, again. A significant rate enhancement because of tunneling is

		B3LYP/6-31+G(d)	MP2/aug-cc-pVDZ	CCSD(T)/aug-cc-pVDZ
n=1	SO_3/H_2O	9.96	8.72	9.09
	$SO_3 \cdot H_2O$	0.00	0.00	0.00
	TS	27.60	28.11	28.15
	H_2SO_4	-7.03	-3.74	-6.74
n=2	$SO_3/2H_2O$	22.48	19.40	19.81
	$SO_3 \cdot (H_2O)_2$	0.00	0.00	0.00
	TS	10.03	11.61	11.34
	$H_2SO_4 \cdot H_2O$	-7.71	-4.60	-7.70
n=2+1	$SO_3/3H_2O$	36.50	31.39	–
	$SO_3 \cdot (H_2O)_3$	0.00	0.00	–
	TS	9.35	–	–
	$H_2SO_4 \cdot (H_2O)_2$	-6.44	–	–
n=3	$SO_3/3H_2O$	36.43	31.12	–
	$SO_3 \cdot (H_2O)_3$	0.00	0.00	–
	TS	3.99	–	–
	$H_2SO_4 \cdot (H_2O)_2$	-3.22	–	–

Table 4.3: Electronic energies in kcal/mol for the hydration of SO_3 assisted by n=1, n=2, n=2+1 and n=3 water molecules, respectively. The first lines correspond to the separated SO_3 and nH_2O molecules, the second lines correspond to the $SO_3 \cdot nH_2O$ minima (set to 0.00 kcal/mol by definition), the third lines correspond to the transition states to the concerted nucleophilic attack/proton transfer reaction (TS), and the last lines correspond to the $H_2SO_4 \cdot (n-1)H_2O$ minima. CCSD(T) energies rely on MP2/aug-cc-pVDZ geometries.

observed for n=1 and for n=2 at temperatures clearly lower than 200 K only, which was also found for the hydrations of sulfur dioxide. The next similarity is found on comparing the different tunneling correction schemes among each other. Whereas for n=1 SCT is the dominant tunneling mechanism, LCT dominates at 100 K for n=2 (n=2+1). The Wigner tunneling correction is orders of magnitude too low at low temperatures, whereas it appropriate at high temperatures, where tunneling becomes unimportant. It is, therefore, highly recommended not to employ the simple Wigner tunneling correction scheme for proton transfer reactions. As a further consequence of the tunneling corrections in Table 4.2 on page 65 and Table 4.4 on the following page, it is not necessary to invest computer time for the calculation of the LCT correction in the case of "impure" proton transfer reactions. However, for "pure" proton transfer reactions such a calculation is very important in order to reach agreement with experimental data,[149] as the LCT corrections are clearly higher than the SCT corrections.[106, 107, 149, 150]

4.1.3   Unimolecular Isomerization Rates

The reaction rates for the isomerization of the various sulfur oxide–water complexes incorporating the highest tunneling correction, i.e., $\kappa(\mu OMT)$, are depicted in Figure 4.14 on page 79. The rather straight lines, i.e., Arrhenius behavior, for the SO_3–$3H_2O$, SO_2–$3H_2O$ and SO_2–$2H_2O$ complexes again demonstrate that tunneling is negligible at temperatures above 100 K for these complexes. For the other complexes more or less pronounced curvature in the Arrhenius plot is indicative of a mechanism influenced by tunneling. However, the relative order in terms of rate constants is dominated by the barrier height shown in Table 4.1 on page 62 and Table 4.3 on the page before rather than the tunneling corrections shown in Table 4.2 on page 65 and Table 4.4 on the next page even at temperatures as low as 100 K. The only exception of this ordering is found for the SO_3–$1H_2O$ and SO_2–$1H_2O$ complexes at T<160 K. Here, the higher tunneling correction found for the latter

	Wigner	ZCT	SCT	LCT
n=1	24.9	2.7×10^{21}	4.8×10^{26}	6.1×10^{24}
	7.0	6.5×10^{3}	1.1×10^{6}	3.1×10^{5}
	3.7	19.2	113.4	35.3
n=2	3.7	3.2×10^{3}	1.9×10^{6}	3.8×10^{6}
	1.7	3.3	8.9	7.2
	1.3	1.6	2.2	1.8
n=2+1	3.9	6.1×10^{3}	2.6×10^{6}	8.3×10^{6}
	1.7	4.5	17.0	15.1
	1.3	1.8	2.9	2.2
n=3	1.7	1.5	2.0	3.4
	1.2	1.1	1.2	1.3
	1.1	1.0	1.1	1.1

Table 4.4: Tunneling correction factors κ at 100 K (top row), 200 K (middle) and 300 K (bottom) to the rate constants obtained from classical transition state theory for the reaction $SO_3 \cdot nH_2O \rightleftharpoons H_2SO_4 \cdot (n-1)H_2O$. B3LYP/6-31+G(d) was employed throughout. The Wigner correction[123] is calculated directly from the imaginary frequency at s=0 Bohr in Figure 4.13 on page 73 without using any information of the reaction path, zero-curvature tunneling (ZCT) involves tunneling along the minimum energy path, small-curvature tunneling (SCT)[228] involves adiabatic tunneling at the inner turning points of the concave side of the minimum energy path,[229] and large-curvature tunneling (LCT)[104] involves vibrationally non-adiabatic straight line tunneling through the reaction swath. The latter three corrections were all calculated employing the semi-classical approximation.[230]

outweighs the lower reaction barrier encountered for the former. Nevertheless, the absolute rate constants of about 10^{-30}s^{-1} corresponding to a half-life of many million years are much too low to be observed by any human being. From Figure 4.14 on the following page it seems that in our atmosphere only sulfur trioxide, but not sulfur dioxide is hydrated readily. On the other hand many megatons (cf. Figure 1.3 on page 12) of sulfur dioxide are emitted annually but merely any sulfur trioxide. All of the sulfur trioxide available for the hydration has to be formed *in situ*, therefore. The question that remains is, whether the amount of available SO_3 compared to the amount of available SO_2 is enough (or not), so that the predominant hydration channel in our atmosphere involves SO_3 (or SO_2).

4.1.4 Comparison of Pre-Association Reactions

The question on the predominant hydration channel in our atmosphere can be answered when comparing the equilibria constants K for the pre-association reactions

$$SO_2 + nH_2O \rightleftharpoons SO_2 \cdot nH_2O \rightleftharpoons \{H_2SO_3 \cdot (n-1)H_2O\}, \tag{4.1}$$

$$SO_3 + nH_2O \rightleftharpoons SO_3 \cdot nH_2O \rightleftharpoons H_2SO_4 \cdot (n-1)H_2O, \tag{4.2}$$
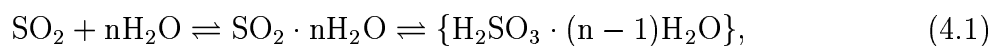
forming the unimolecular constants and substituting the observed values of about 10^5 molecules per cm^3 of SO_3 and 10^{10} molecules per cm^3 of SO_2[35] for the concentrations of SO_3 and SO_2, respectively. These equilibria constants K can be calculated from the well known thermodynamics-equation

$$K = exp(-\frac{\Delta G}{RT},) \tag{4.3}$$
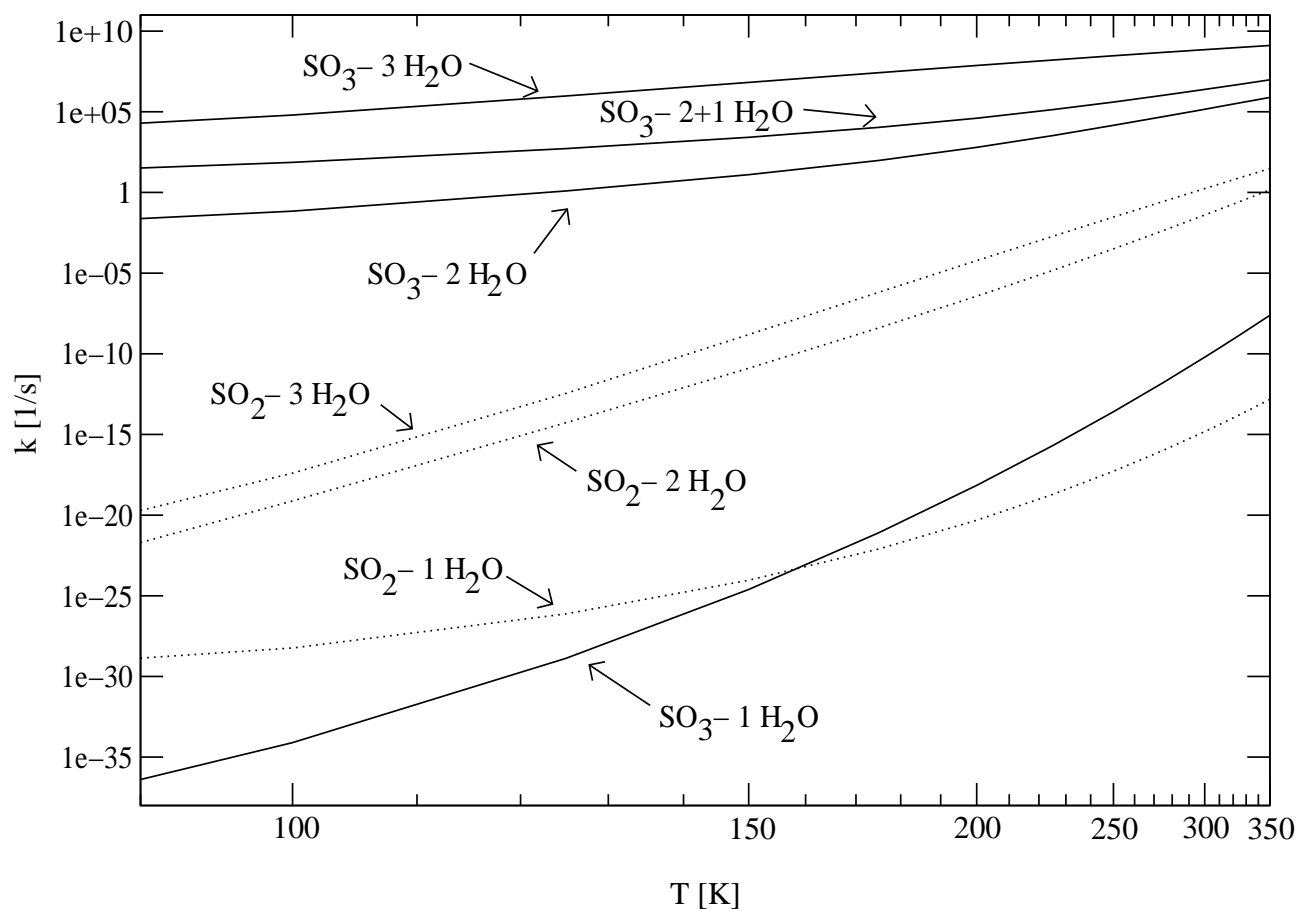
Figure 4.14: Arrhenius plot of the hydration reactions of sulfur trioxide (solid lines) and sulfur dioxide (dotted lines) in the presence of up to three water molecules in the unimolecular complex as calculated from VTST/μOMT on B3LYP/6-31+G(d) reaction hypersurfaces. Note that the range of times reaches from nanoseconds (10^{10}s^{-1}) via days (10^{-5}s^{-1}) and years (10^{-10}s^{-1}) to many millions of years ($<10^{-20}$s^{-1}).

where R is the gas-constant (1.98588 calK^{-1}mol^{-1}) and T is the temperature. ΔG can be calculated from the association energies listed in Table 4.1 on page 62 and Table 4.3 on page 75 and the thermal corrections available from the partition functions obtained in the course of a frequency calculation by Gaussian98.[140] Similar calculation schemes are also used by other groups to determine equilibrium constants for atmospheric association reactions.[6,241] The association energies were not corrected for the basis set superposition error (BSSE), e.g., by the Counterpoise method,[242–244] because BSSE becomes systematically small on using larger basis sets[245] and because BSSE can even be viewed as an "improvement" of the description of the cluster by the basis functions of the monomers.[246] Comparing the association energies (at 0 K) it becomes clear that hydrogen bonding preferentially stabilizes the sulfur trioxide–water complexes compared to the sulfur dioxide–water complexes. In the complexes with a single water water molecule 4–5 kcal/mol additional stabilization is found. Introducing a second water molecule about 1 kcal/mol additional stabilization is found. A third molecule contributes further 2.5 kcal/mol, so that in total 7.5–8.5 kcal/mol preference in hydration in favor of SO$_3$ is found for the complexes with three water molecules. On the other hand the thermal corrections (cf. Table 4.5 on the following page), containing especially translational entropy, disfavor the sulfur trioxide water complexes by 0.5–2.5 kcal/mol depending on the hydration state and the temperature. Nevertheless, the thermal effect is small compared to the electronic effect. Therefore, the equilibria constants are higher for the pre-association involving SO$_3$ rather than SO$_2$. These differences are especially evident at low temperatures, e.g., at 100 K the equilibrium constant for the formation of SO$_3\cdot3$H$_2$O is higher by 16 orders of magnitude than the one of SO$_2\cdot3$H$_2$O.

For a fast pre-association, which is the case for the barrierless aggregation of single molecules to van-der-Waals or hydrogen bonded complexes, the overall (concentration-dependent) rate constant can be written as the product of the unimolecular rate constant

	100 K	150 K	200 K	250 K	300 K	350 K
SO_2–$1H_2O$	3.57	4.81	6.04	7.24	8.42	9.56
SO_2–$2H_2O$	9.39	12.33	15.31	18.30	21.26	24.19
SO_2–$3H_2O$	14.22	18.62	23.09	27.57	32.03	36.45
SO_3–$1H_2O$	4.29	5.73	7.22	8.72	10.23	11.74
SO_3–$2H_2O$	9.88	12.80	15.79	18.80	21.80	24.78
SO_3–$(2+1)H_2O$	15.42	19.96	24.61	29.24	33.98	38.64
SO_3–$3H_2O$	15.44	19.98	24.67	29.40	34.13	38.85
SO_2–$1H_2O$	5.0×10^3	4.5	1.4×10^{-1}	1.9×10^{-2}	5.0×10^{-3}	2.0×10^{-3}
SO_2–$2H_2O$	5.9×10^{15}	1.7×10^6	2.6×10^1	3.3×10^{-2}	4.0×10^{-4}	1.8×10^{-5}
SO_2–$3H_2O$	6.8×10^{29}	3.0×10^{13}	1.6×10^5	1.8	9.1×10^{-4}	4.3×10^{-6}
SO_3–$1H_2O$	2.5×10^{12}	1.5×10^6	9.9×10^2	1.2×10^1	6.3×10^{-1}	7.7×10^{-2}
SO_3–$2H_2O$	3.5×10^{27}	1.3×10^{14}	2.0×10^7	1.6×10^3	3.1	3.7×10^{-2}
SO_3–$(2+1)H_2O$	1.2×10^{46}	1.3×10^{24}	9.9×10^{12}	2.2×10^6	6.9×10^1	4.5×10^{-2}
SO_3–$3H_2O$	8.0×10^{45}	9.6×10^{23}	7.2×10^{12}	1.4×10^6	4.7×10^1	3.1×10^{-2}

Table 4.5: Thermal correction from association energy (cf. Table 4.1 on page 62 and Table 4.3 on page 75) to association Gibbs free energy ΔG in kcal/mol as calculated at B3LYP/6-31+G(d) level of theory (top) and equilibrium constants in atm^{-n} for the pre-association reactions $SO_x + nH_2O \rightleftharpoons SO_x \cdot (H_2O)_n$ (x=2,3; n=1,2,3) calculated at B3LYP/6-31+G(d) level of theory (bottom).

(cf. Figure 4.14 on page 79) and the equilibrium constant for the pre-association (cf. Table 4.5 on the preceding page).[155]

The differences between the SO_3 and SO_2 hydration rate constants seen in Figure 4.14 on page 79 are further increased due to the pre-association. For a rate law depending first-order on SO_2 or SO_3 this implies that the SO_2 pressure has to be 10 orders of magnitude higher than the SO_3 pressure at 250 K and even 20 orders of magnitude higher at 150 K so that the SO_2 hydration becomes competitive. However, at 30 km altitude the steady state of SO_3 of about 10^5 molecules per cm^3 compared to SO_2 of about 10^{10} molecules per cm^3 is only lower by 5 orders of magnitude.[35] It is, therefore, save to assume that the dominant mechanism converting S(IV) to S(VI) species is *first* the oxidation of SO_2 by OH· and *second* the isomerization of a SO_3/H_2O cluster of a stoichiometry of 1:2 or higher, because the slow hydration of SO_2 is circumvented.

4.1.5   Experimental Verification

Conversion Time

Fortunately, at least for the SO_3 hydration experimentalists sought to imitate the reaction conditions in our atmosphere. In molecular beam studies the decay of SO_3 has been attributed mostly to the complexation of one H_2O and one SO_3 moiety, which rapidly isomerizes to H_2SO_4.[61,62] The conversion time set an upper limit of +13 kcal/mol on the reaction barrier to unimolecular isomerization.[62,63] The bimolecular hydration rate constant corresponding to this process was determined to be about $9.1 \times 10^{-13} cm^3 s^{-1}$ as early as 1975.[64] Newer studies carefully eliminating heterogeneous wall reactions have inferred upper limits of $2.4 \times 10^{-15} cm^3 s^{-1}$ and $5.7 \times 10^{-15} cm^3 s^{-1}$ for the homogeneous reaction.[34,65,66] All these studies assume a linear dependence of the SO_3 loss rate on water vapor pressure. More recent gas-phase studies yielded a second-order dependence of this

rate with respect to water vapor pressure[34,67] implying the involvement of water-dimers.[35] Experiments both under turbulent[35] and laminar[68] flow conditions yielded a nitrogen pressure independent conversion rate constant of SO_3 to sulfuric acid of 2.0–$3.0 \times 10^{-31} cm^6 s^{-1}$ at 300 K.

The Rate Law

According to their finding of second-order dependence on water vapor pressure and first-order dependence on SO_3 pressure, the formation rate of sulfuric acid can be written as third-order law

$$-\frac{d[SO_3]}{dt} = \frac{d[H_2SO_4]}{dt} = \kappa^{\mu OMT} \times K \times k^{CVTST} \times [SO_3][H_2O]^2, \qquad (4.4)$$

where the product of the tunneling correction factor ($\kappa^{\mu OMT}$), the equilibrium constant for the pre-association (K) and the unimolecular rate constant (k^{CVTST}) corresponds to the rate constants k. In order to compare my results with the experimentally determined rate constants all four mechanisms were assumed to be second-order in water pressure by converting the calculated ΔG values for the pre-association to equilibrium constants of units atm^{-2} instead of units atm^{-n}, which are then converted to cm^6 by multiplying with $(1.363 \times 10^{-22} T)^2$ $cm^6 atm^2$. The resulting plot together with the experimental findings are depicted in Figure 4.15 on page 87.

It is evident that the reaction involving just one water molecule is too slow by about 23 orders of magnitude in order to account for the experimental behavior. The reaction involving two water molecules agrees better, but is still slower by 3 orders of magnitude. Microsolvation of the two water bridge by just one additional water molecule further accelerates the reaction especially at low temperatures (around 250 K). At 350 K still an order of magnitude is missing in comparison to the reaction chamber results. The rotary mecha-

nism involving three water molecules is predicted to be faster than the observed results. At low temperatures the prediction is higher by 5 orders of magnitude, which might indicate that the association of the three water molecules in a bridge can not be accomplished before the unimolecular isomerization occurs. At high temperatures the prediction is slightly too high implying that this mechanism plays an important role in the homogeneous gas-phase conversion process of sulfur trioxide to sulfuric acid.

The Atmospheric Mechanism

Complexes with clusters of more than approximately twelve water molecules would be converted to sulfuric acid with nearly no energy barrier, i.e., ultrafast.[247] However, the water content of our atmosphere precludes formation of complexes with very large clusters. In binary sulfuric acid—water vapors the distribution of hydrates is such that at relative humidities of around 50% there are about 10^{10} hydrates with 1–3 water molecules, but only 10^8 with four and only 10^6 with six water molecules.[248] Relative humidities of over 300% are required that also complexes of four water molecules can be found to a similar extent to the 1–3 water molecule complexes with sulfuric acid.

The barriers for the unimolecular reaction (cf. Table 4.3 on page 75) for clusters with n>1 water molecules are all lower than +13 kcal/mol. +13 kcal/mol were found by Hofmann-Sievert and Castleman to be the upper limit for the actual unimolecular isomerization barrier from comparing RRKM rate constants with the collision deactivation of $5 \times 10^5 s^{-1}$ of chemically activated sulfur trioxide water complexes.[62] The fact that the unimolecular rate constant predicted in this work for n=3 varies between $1 \times 10^8 s^{-1}$ (200 K) and $2 \times 10^9 s^{-1}$ (350 K) demonstrates that my findings agree with the dominant reaction channel being isomerization rather than collision deactivation. The molecular beam result showing a ratio of 8:1 of the water monomer to the dimer, but only a ratio of 3:1 in the reaction products, with SO_3 clearly underlines that much faster reactions take place with

n>1 water molecules.[62] The pre-association equilibrium of SO_3 and n=1–3 water molecules acts as driving force for overcoming the barrier to isomerization. The association energies, i.e., binding energies of sulfur trioxide-water complexes, presented in Table 4.3 on page 75, are in reasonable agreement with experimental results.[64] For n>1 the gain in energy due to association is larger than the energy required to cross the transition state for the unimolecular step.

Apparent Activation Energies

Apparent activation energies E_a were then gained from the reaction rate constant graphs as a function of the temperature ($E_a = R\frac{T_1 T_2}{T_1 - T_2}\ln\frac{k_1}{k_2}$) instead of just summing the electronic energies at 0 K for the pre-association and the reaction barrier, as this additionally includes enthalpy and entropy effects as well as quantum effects like zero-point energy and tunneling. The activation energies in the temperature region investigated vary less than $\pm$ 1 kcal/mol. Comparing the experimentally determined apparent "activation" energies for the overall process of -13 kcal/mol[35,68] between 283 and 370 K with the here-determined energies of about +10 kcal/mol (n=1), -8 kcal/mol (n=2), -24 kcal/mol (n=2+1) and -27 kcal/mol (n=3), it is likely that the laboratory determined rate constant is in fact an averaged value that emerges from mixed participation of the latter three mechanisms.

4.1.6 Atmospheric Implications

In the troposphere, where the water content is rather high, most likely the fastest mechanism, namely the double-proton transfer with transient H_3O^+ rotation, will play the dominant role. However, the rate determining step under these water-rich conditions will be the oxidative step from SO_2 to SO_3.[35] Increasing the altitude to the stratosphere reduces the water content and the total pressure, which inhibits the formation of larger sulfur trioxide complexes with water. Therefore, the importance of water mediated double-proton

transfer increases. Additionally, heterogeneous processes on aerosol surfaces gain importance.[35] The half-life[155] of sulfur trioxide under upper stratospheric conditions[1,35] (10^{-2} atm, 250 K, 5 ppmv water vapor=10^{12} water molecules/cm^3) is predicted to be between 15 minutes (100% rotary mechanism) and 8 days (100% water mediated double proton transfer). Colder temperatures and increased water vapor pressure additionally decrease this half-life. This estimated homogeneous half-life is similar in magnitude to the predictions by Jayne et al.[35] for the heterogeneous processes. Therefore, I believe both homogeneous and heterogeneous reactions to be of equal importance as rate determining steps in the upper stratosphere for the oxidative conversion of DMS and SO$_2$ to sulfates.
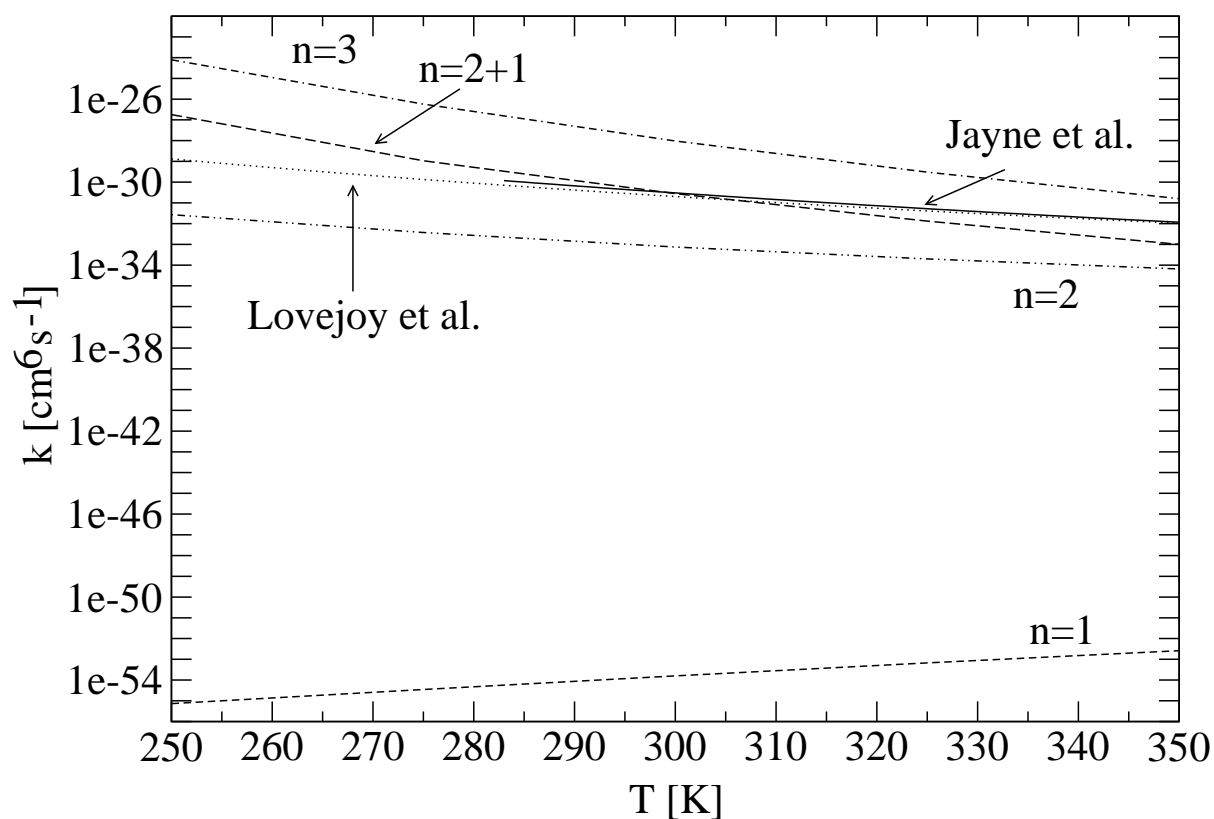
Figure 4.15: Bimolecular reaction rate constant for the reaction $SO_3 + nH_2O \rightarrow SO_3 \cdot nH_2O$ $\rightarrow H_2SO_4 \cdot (n-1)H_2O$ as a function of the temperature. Experimental data are directly taken from the references Jayne et al.[35] and Lovejoy et al.[68] Calculated values were obtained from B3LYP/6-31+G(d) hypersurfaces and single-level dynamics in the microcanonical optimized multidimensional tunneling framework of variational transition state theory.

4.2   Decomposition of Chlorine Nitrate

4.2.1   By Water

Stationary Structures

The optimized structures involving up to three water molecules can be seen in Figure 4.16. Similar chlorine nitrate–water systems have been investigated previously in other groups. Ying and Zhao have proved that the best binding site for water involves interaction between the water oxygen and the chlorine atom,[249] which is also found in this work. Xu and Zhao, McNamara and Hillier as well as Bianco and Hynes systematically studied the decomposition reaction involving a different number of microsolvating water molecules up to eight water molecules.[250–254] A general consensus is that the reaction barrier to chlorine nitrate decomposition vanishes on increasing the number of water molecules. Up to about six water molecules the reaction was shown to be completely non-ionic. Above six water molecules ions like H_2OCl^+ or H_3O^+ and NO_3^- were found to be stable intermediates and the barrier to decomposition was found to be close to zero. Whereas studies at the Hartree-Fock level of theory neglecting electron correlation find the chlorine atom of the reaction product within the reactive ring, it is shown here that at B3LYP/6-31+G(d) level of theory taking into account electron correlation the chlorine atom moves out of the ring in a secondary reaction leading to the global minimum. In case of two hydrolyzing water molecules (n=2) the HOCl moiety rotates, so that the hydroxyl group takes the role of the chlorine atom. In the case of three hydrolyzing water molecules (n=3) the HOCl moiety moves out of the ring completely in order to produce $HNO_3 \cdot 2H_2O$, which is more stable than $HNO_3 \cdot HOCl \cdot 2H_2O$.
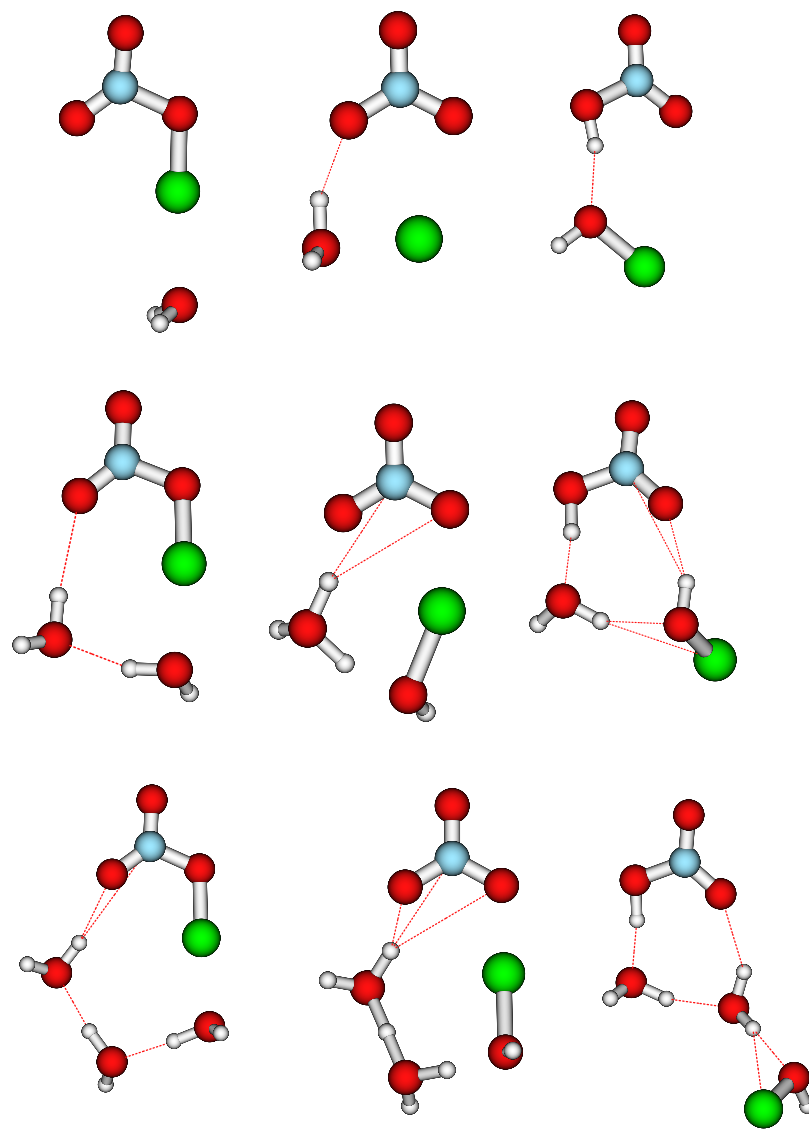
Figure 4.16: Stationary *in vacuo* structures involved in the hydrolysis of chlorine nitrate in the presence of one (top), two (middle) and three (bottom) water molecules as found at B3LYP/6-31+G(d) level of theory.

Reaction Energetics

The reaction barrier to decomposition is shown in Figure 4.17 and Table 4.6. The first striking feature is the enormous barrier, both in height and width, to decomposition involving one molecule of water. Looking at the corresponding geometries in Figure 4.16 reveals that the rather large OCl$\cdots$O distance of 4.29 (4.44) Å at B3LYP/6-31+G(d) (MP2/aug-cc-pVDZ) level of theory prohibits the formation of a hydrogen bond between water and and chlorine nitrate. Both hydrogen atoms of the water molecule are out of the plane built by the atoms of chlorine nitrate. Introducing a second water molecule fulfills a bifunctional role. On the one hand this water molecule acts as hydrogen bond donor to an oxygen atom of chlorine nitrate, and on the other hand it acts as hydrogen bond acceptor for a hydrogen bond with the first water molecule. One hydrogen atom of the first water molecule is forced, therefore, into the chlorine nitrate plane. As a result of the "closure" of the reactive ring by the second water molecule the barrier drops by about 32 kcal/mol according to the electronic structure methods taking electron correlation most carefully into account, namely CCSD(T)/aug-cc-pVDZ and G2(MP2). Introducing a third water molecule in the reactive ring relieves steric strain. This is quite unexpected, as a large ring containing 7 heavy atoms and 3 hydrogen-atoms is formed. Akhmatskaya et al. even stated that in the case of one participating water molecule "the transition state involves a six-membered ring, with presumably little strain, which suggests that inclusion of a further quantum mechanical water molecule would not greatly facilitate the reaction". From my calculations this statement now may be called obsolete.

On the course from the minimum geometry to the transition state the hydrogen bond angle involved in proton transfer changes to more favorable values, i.e., values close to the linear (180 degree) arrangement, in the three water system, whereas it changes to less favorable values in the two water system. For example one hydrogen bond angle increases

		B3LYP/ 6-31+G(d)	MP2/ aug-cc-pVDZ	CCSD(T)/ 6-31+G(d)	CCSD(T)/ aug-cc-pVDZ	G2(MP2)
n=1	$ClONO_2/H_2O$	5.24	3.76	4.80	–	–
	$ClONO_2 \cdot H_2O$	0.00	0.00	0.00	0.00	0.00
	TS	47.21	62.84	61.70	58.20	58.61
	$HNO_3 \cdot HOCl$	-1.02	2.20	-0.23	–	–
n=2	$ClONO_2/2H_2O$	15.60	–	–	–	–
	$ClONO_2 \cdot (H_2O)_2$	0.00	0.00	0.00	0.00	0.00
	TS	22.37	25.89	29.80	26.47	26.63
	$HNO_3 \cdot HOCl \cdot H_2O$	-5.77	-3.36	-4.55	–	–
n=3	$ClONO_2/3H_2O$	27.59	–	–	–	–
	$ClONO_2 \cdot (H_2O)_3$	0.00	0.00	0.00	–	0.00
	TS	14.96	18.83	23.00	–	19.95
	$HNO_3 \cdot HOCl \cdot (H_2O)_2$	-0.52	–	–	–	–

Table 4.6: Electronic energies in kcal/mol for the decomposition of chlorine nitrate by n water molecules. The first lines correspond to the separated molecules, the second lines correspond to the $ClONO_2 \cdot (H_2O)_n$ minima (set to 0.00 kcal/mol by definition), the third lines correspond to the transition states to the concerted nucleophilic substitution/proton transfer reaction (TS), and the last lines correspond to the $HNO_3 \cdot HOCl \cdot (H_2O)_{n-1}$ minima. CCSD(T) energies rely on MP2/aug-cc-pVDZ geometries. G2(MP2) values were calculated according to the literature,[147] but without zero-point correction.

from 173 to 178 degree (B3LYP) in the three water case, but it decreases only from 174 degree to 167 degree in the three water system. Overall this results in a reduction of the barrier by 7 kcal/mol.

Comparing the results obtained from different electronic structure methods it can be seen that hybrid density functional theory underestimates the reaction barriers, especially because the $OCl \cdots O$ distance is underestimated by about 0.15 Å in the minima, but overestimated by 0.05 Å in the transition states, when comparing to MP2/aug-cc-pVDZ geometries. Nevertheless, B3LYP/6-31+G(d) was used for the generation of the minimum energy path, as it is by far the cheapest method out of the methods listed in Table 4.6 for the calculation of electronic properties. In order to account for the discrepancies in the reaction barrier, the hypersurface was interpolated to G2(MP2) barriers.[131]
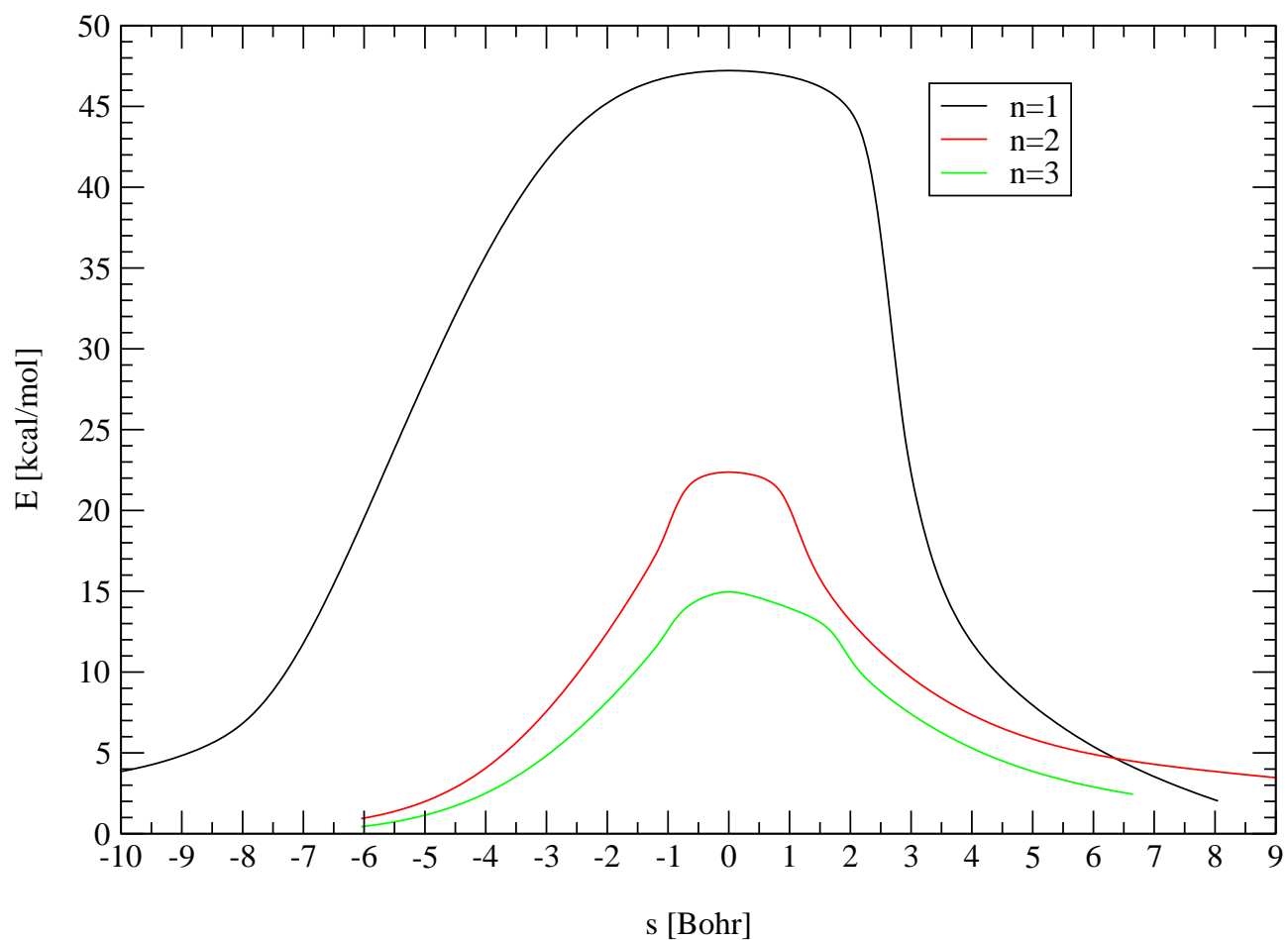
Figure 4.17: Energy along the classical reaction coordinate (MEP, IRC) as found at B3LYP/6-31+G(d) level of theory for the reaction $ClONO_2 \cdot nH_2O \rightarrow HOCl \cdot HNO_3 \cdot (n-1)H_2O$

Reaction Mechanism

From the mechanistic point of view the decomposition reaction is a nucleophilic substitu-
tion reaction coupled to a (multiple) proton transfer. The nucleophile is a water molecule
attacking the electrophile chlorine. The accompanying proton transfer enhances the nu-
cleophilicity of the attacking water molecule, as a species akin to the hydroxyl anion is
generated. At the same time the basicity of the leaving group, the nitrate anion, is re-
duced because of the proton transfer. As the reaction coordinate involves a single transition
state and no intermediates, a bimolecular reaction depending both on the concentrations
of the water molecules and chlorine nitrate molecules will result, and the correct nomen-
clature is S_N2. In order to take the coupled proton transfer (PT) into consideration the
nomenclature S_N2/PT will be used.

For an analysis of the reaction mechanism Figure 4.18, Figure 4.19 and Figure 4.20 can
be used. First, the water and the chlorine nitrate molecules change their relative orientation
by translational and rotational motions. Figure 4.20 shows that most reorientation is
required for the n=1 reaction, where the angle changes from 60 degree to 30 degree. Next
the chlorine atom is transferred from O4 to O6. Contrary to proton transfer there is no
minimum in the O—O distance required to trigger chlorine transfer. While the O_2NO—Cl
distance increases from 1.71 Å to 2.68 Å the proton to be transferred changes its distance
to the water oxygen only from 0.97 Å to 1.00 Å (n=1). The broad bump at negative
s values in Figure 4.19 corresponds to this movement. In comparison to hydrogen atom
transfer the reaction angle (cf. Figure 4.20) changes rather slowly in the case of chlorine
atom transfer. This indicates that chlorine movement is less coupled to other vibrational
degrees of freedom than hydrogen atom transfer. As the reaction coordinate motion at the
transition state still corresponds to chlorine movement, the "imaginary frequency" is rather
low, namely 172i cm^{-1} (n=1). The movement of the chlorine atom, which has a large van-
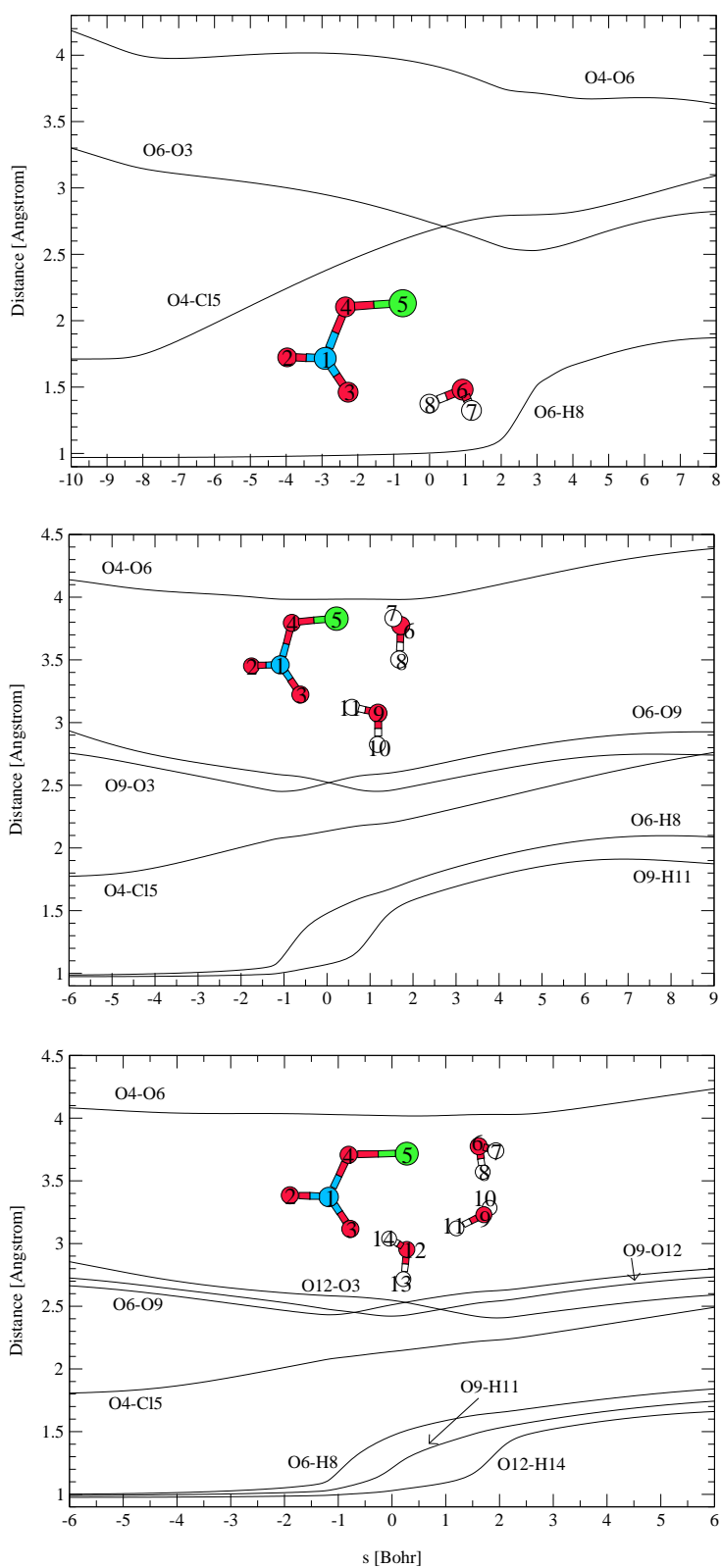
Figure 4.18: Distances [in Å] between selected two atoms along the minimum energy path [in Bohr] for the decomposition of chlorine nitrate by one (top), by two (middle) or by three (bottom) water molecules. The numbering scheme is shown as inset in the respective plots.
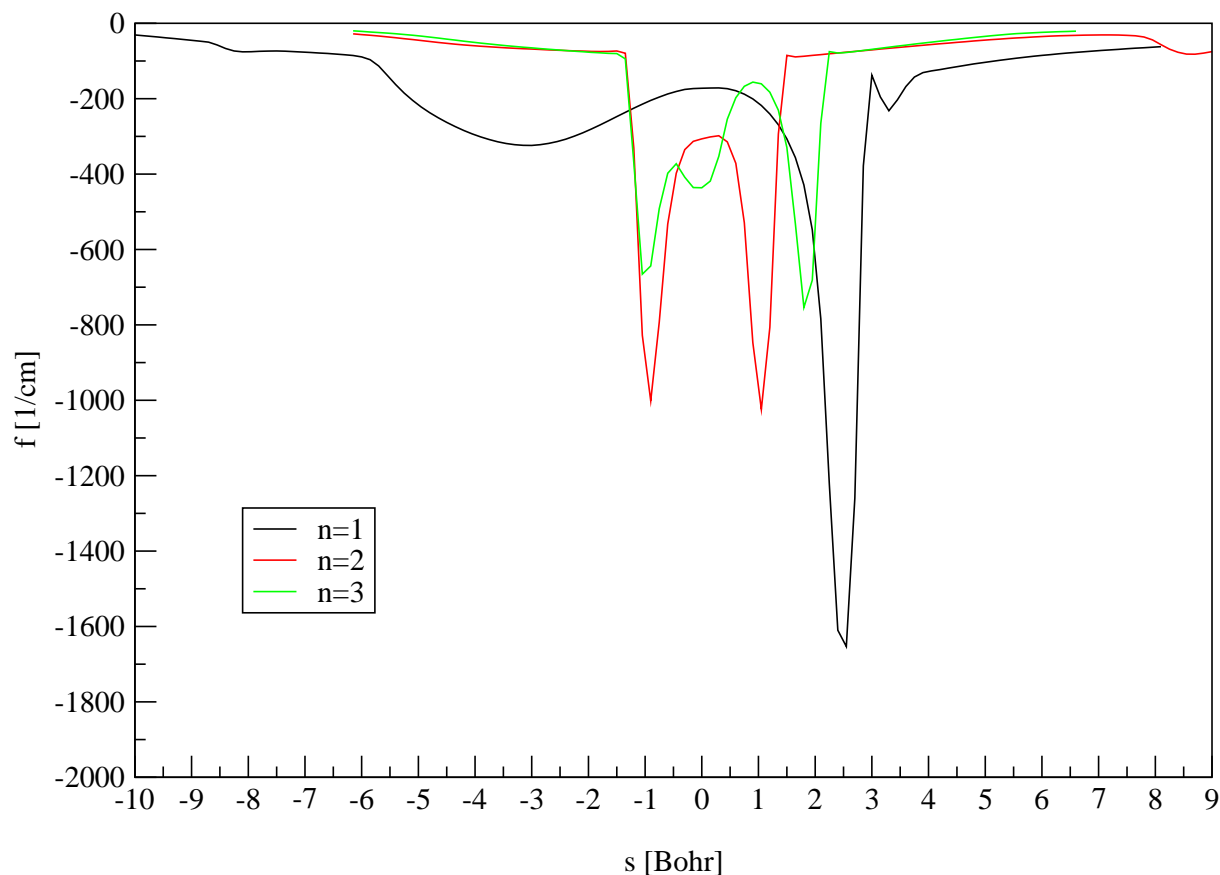
Figure 4.19: "Imaginary" frequency along the reaction coordinate. Negative s values correspond to $ClONO_2$–H_2O like species, s=0 Bohr corresponds to the transition state, and positive s values correspond to $HOCl$–HNO_3 like species.

der-Waals radius of 1.8 Å compared to 1.0 Å of the hydrogen atom, compresses the O—O distances involved in hydrogen bonding, which in turn triggers the asynchronous proton transfer events. On the second branch of the reaction coordinate the proton increases its distance suddenly to 1.87 Å, whereas the O_2NO—Cl distance increases only by 0.41 Å (n=1).

Concerning the reactions involving more than one water molecule the first proton is transferred before the transition state. The second proton transfer occurs exactly at the transition state for n=3. The last proton transfer to the nitrate anion occurs after having
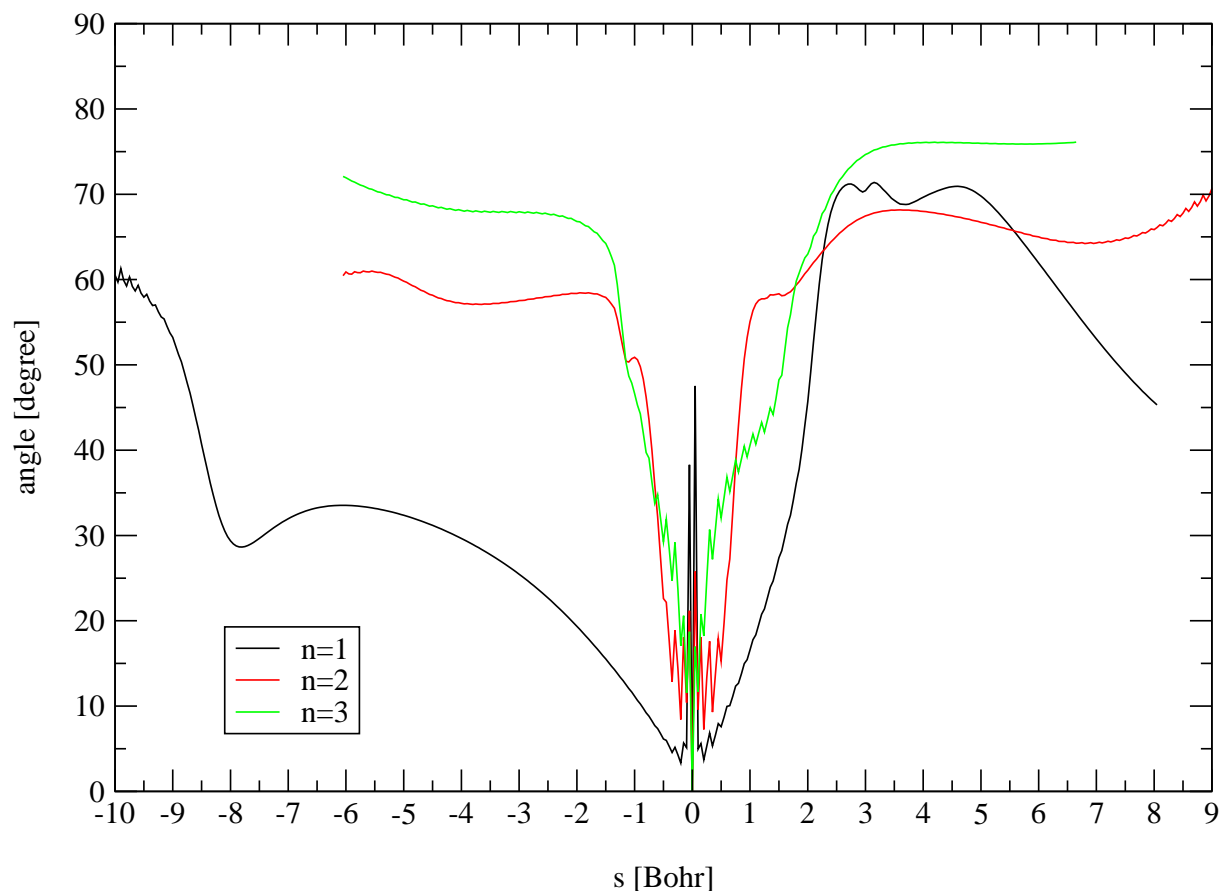
Figure 4.20: Angle between the reaction coordinate at the transition state, i.e., normal-mode vector of the "imaginary" frequency, and the gradient along the reaction path. Negative s values correspond to $ClONO_2$–H_2O like species, s=0 Bohr corresponds to the transition state, and positive s values correspond to $HOCl$–HNO_3 like species.

passed the transition state for all investigated reactions. Chlorine movement occurs at any stage of the reaction, i.e., synchronously to the proton transfer reactions. Therefore, the broad bump found for n=1 is absent in Figure 4.19 for n=2 and n=3. In the transition state itself the "moving" proton is found at the position that shows the maximal distance both to the hydroxyl like nucleophile and the leaving group nitrate. This ensures that both a strong nucleophile and a good leaving group govern the reaction.

	Wigner	ZCT	SCT	LCT
	1.3	1.5	1.5	3.1
n=1	1.1	1.1	1.1	1.1
	1.0	1.0	1.0	1.0
	1.8	1.5×10^3	4.1×10^7	2.1×10^9
n=2	1.2	2.2	4.5	3.3
	1.1	1.4	1.6	1.4
	2.6	3.7	1.7×10^1	9.9×10^3
n=3	1.3	1.3	1.4	1.5
	1.1	1.1	1.2	1.2

Table 4.7: Tunneling correction factors κ at 100 K (top row), 200 K (middle) and 300 K (bottom) to the rate constants obtained from classical transition state theory for the reaction $ClONO_2 \cdot nH_2O \rightleftharpoons HNO_3 \cdot HOCl \cdot (n\text{-}1)H_2O$. B3LYP/6-31+G(d) was employed throughout. The Wigner correction[123] is calculated directly from the imaginary frequency at s=0 Bohr in Figure 4.19 without using any information of the reaction path, zero-curvature tunneling (ZCT) involves tunneling along the minimum energy path, small-curvature tunneling (SCT)[228] involves adiabatic tunneling at the inner turning points of the concave side of the minimum energy path,[229] and large-curvature tunneling (LCT)[104] involves vibrationally non-adiabatic straight line tunneling through the reaction swath. The latter three corrections were all calculated employing the semi-classical approximation.[230]

The Influence of Tunneling

For n=1 tunneling plays only a marginal role due to the broad barrier caused by the movement of the chlorine atom. For n=2 and n=3 tunneling significantly influences the reaction rate only at temperatures T<175 K. At these temperatures the dominant mechanism corresponds to a direct corner cutting through the reaction swath. The representative tunneling energy, at which the average molecule enters the classically forbidden region, is 0.1, 5, 7 and 10 kcal/mol below the barrier top at 200 K, 175 K, 150 K and 100 K, respectively for n=2. The structures corresponding to the entering and exit point of the classically forbidden region at 100 K are depicted in Figure 4.21 on the next page. It can be seen that both proton transfer reactions occur in the classically forbidden regime. This is valid also at 175 K. On the other hand at 200 K the most probable tunneling energy is very close to the barrier top, so that none of the two protons can tunnel. There is a sharp crossover between classically dominated reaction and tunneling dominated reaction at about 175 K. For n=3 this transition occurs at 125 K. At temperatures above 125 K none of the protons tunnel, whereas at temperatures below 125 K all three protons tunnel through the reaction swath. No temperatures can be found, at which only one or two protons tunnel.

4.2.2   By Hydrochloric Acid

Reaction Mechanism and Energetics

The second reaction that is believed to be important in the conversion of chlorine nitrate to easily photolyzable substrates involves nucleophilic attack of the negatively polarized chlorine atom of HCl on the positively polarized chlorine atom of chlorine nitrate. The stationary structures for this type of reaction are depicted in Figure 4.22 on page 101. In principle this reaction is analogous to decomposition involving water molecules if the chlorine atom of HCl is viewed as valence-isoelectronically replacing the hydroxyl group of
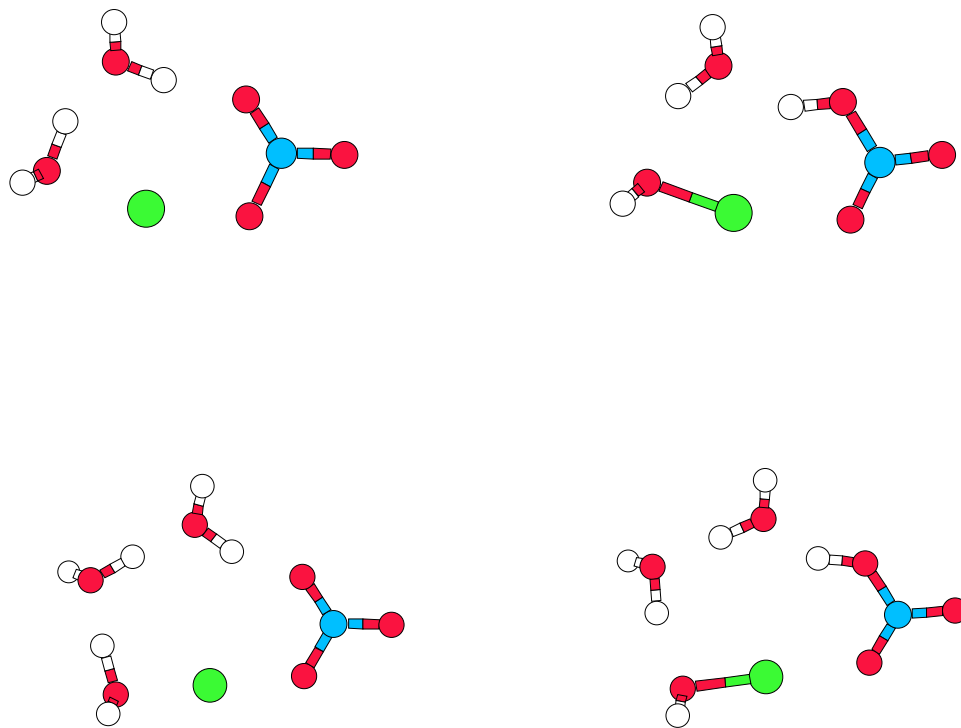
Figure 4.21: Geometries in the chlorine nitrate–2 water (top) and chlorine nitrate–3 water (bottom) system at which the minimum energy path is traversed by tunneling at 100 K.

	k [s^{-1}]	f [1]	κ [1]	K [cm^{3n}]
	$ClONO_2 \cdots H_2O$ (n=1)			
150 K	6.5×10^{-75}	0.992	1.19	7.9×10^{-20}
175 K	1.1×10^{-62}	0.992	1.14	1.3×10^{-20}
200 K	1.6×10^{-53}	0.992	1.10	3.6×10^{-21}
	$ClONO_2 \cdots 2\ H_2O$ (n=2)			
150 K	8.7×10^{-27}	0.999	905.4	6.7×10^{-36}
175 K	1.8×10^{-21}	0.999	27.05	2.8×10^{-38}
200 K	1.7×10^{-17}	0.999	6.22	4.5×10^{-40}
	$ClONO_2 \cdots 3\ H_2O$ (n=3)			
150 K	1.4×10^{-15}	0.730	11.96	1.3×10^{-47}
175 K	7.0×10^{-12}	0.794	2.65	5.4×10^{-52}
200 K	3.9×10^{-9}	0.845	1.82	2.8×10^{-55}

Table 4.8: Classical TST reaction rate constants k, variational correction factor f, tunneling correction factor κ and equilibrium constant K for the pre-association of chlorine nitrate and water. The reaction rate constant for the heterogeneous hydrolyses of chlorine nitrate can be obtained by multiplying k, f and κ yielding pressure independent units of s^{-1} for the unimolecular isomerization. The homogeneous gas-phase reaction rate constant can be obtained by multiplying k, f, κ and additionally K in partial pressure dependent units of $cm^{3n}\ s^{-1}$ (n is the number of participating water molecules).
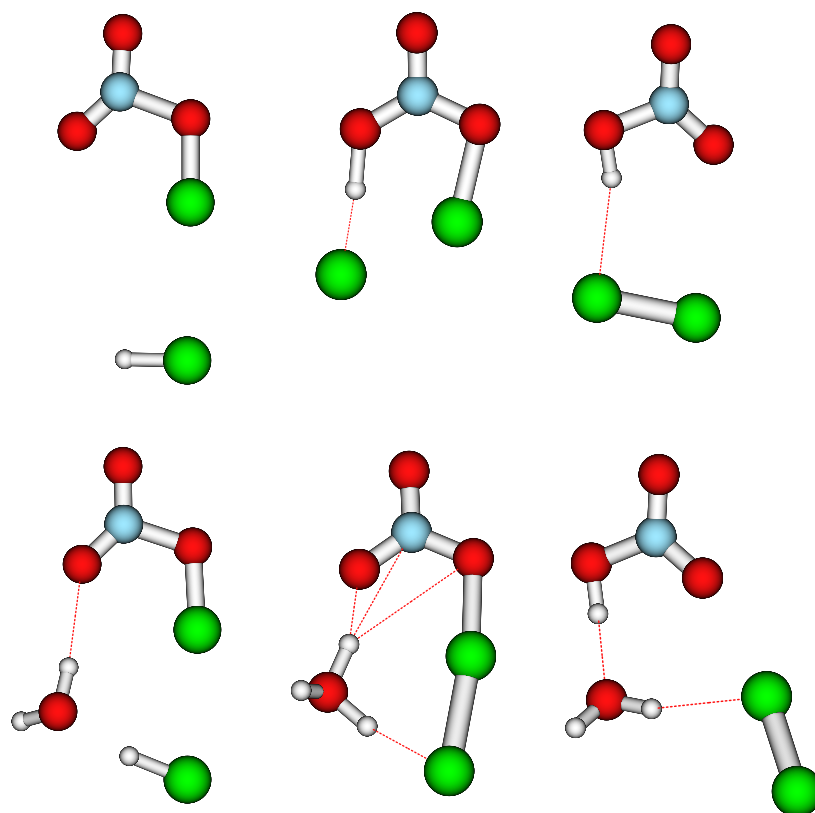
Figure 4.22: Stationary *in vacuo* structures involved in the decomposition of chlorine nitrate by HCl with (top) and without (bottom) the assistance of a water molecule as optimized at MP2/aug-cc-pVDZ level of theory.

water. A major difference is caused by the much larger van-der-Waals radius of the chlorine atom compared to the OH group. This results in an OCl–Cl bond of 4.99 Å in the $ClONO_2$–1HCl minimum, which is about 0.5 Å longer than the comparable bond in the $ClONO_2$–$1H_2O$ system. As a product rather stable molecular chlorine evolves instead of the rather unstable hypochlorous acid HOCl. Whereas the water reaction is rather thermoneutral as can be seen in Table 4.6 on page 91, the HCl reaction is clearly exothermic as can be seen in Table 4.9 on page 105. According to the Hammond principle[255, 256] this implies that the transition state will be late on the reaction coordinate and therefore similar to the products. In fact in the transition state the Cl–Cl bond is already apparent. On the other hand in the decomposition by water the transition state is central. The larger similarity to the exothermic products in the decomposition by HCl compared to the decomposition by water finally leads to a barrier lower by 12 kcal/mol for n=0 and even 16 kcal/mol for n=1 at both G2(MP2) and CCSD(T)/aug-cc-pVDZ//MP2/aug-cc-pVDZ level of theory (cf. Table 4.6 on page 91 and Table 4.9 on page 105).

The late nature of the transition states is also demonstrated from Figure 4.25 on page 106. In the decomposition involving HCl the proton is transferred before the transition state, which is contrary to decomposition involving a molecule of water. The proton translocation is superposed to movement of the chlorine atoms, as can be seen in Figure 4.23 on the following page. This results in a much thinner barrier compared to the reaction caused by water as can be seen on comparing Figure 4.24 on page 104 with Figure 4.17 on page 92.

The imaginary frequency of 1096i cm^{-1} compared to 172i cm^{-1} of the saddle points on the hypersurfaces of $ClONO_2$–1HCl (cf. Figure 4.25 on page 106) and $ClONO_2$–$1H_2O$, respectively, is a further hint at pronounced hydrogen atom movement in the transition state region. On the other hand hydrogenic motion is missing in the transition state of the decomposition involving both a water and HCl molecule. The imaginary frequency of
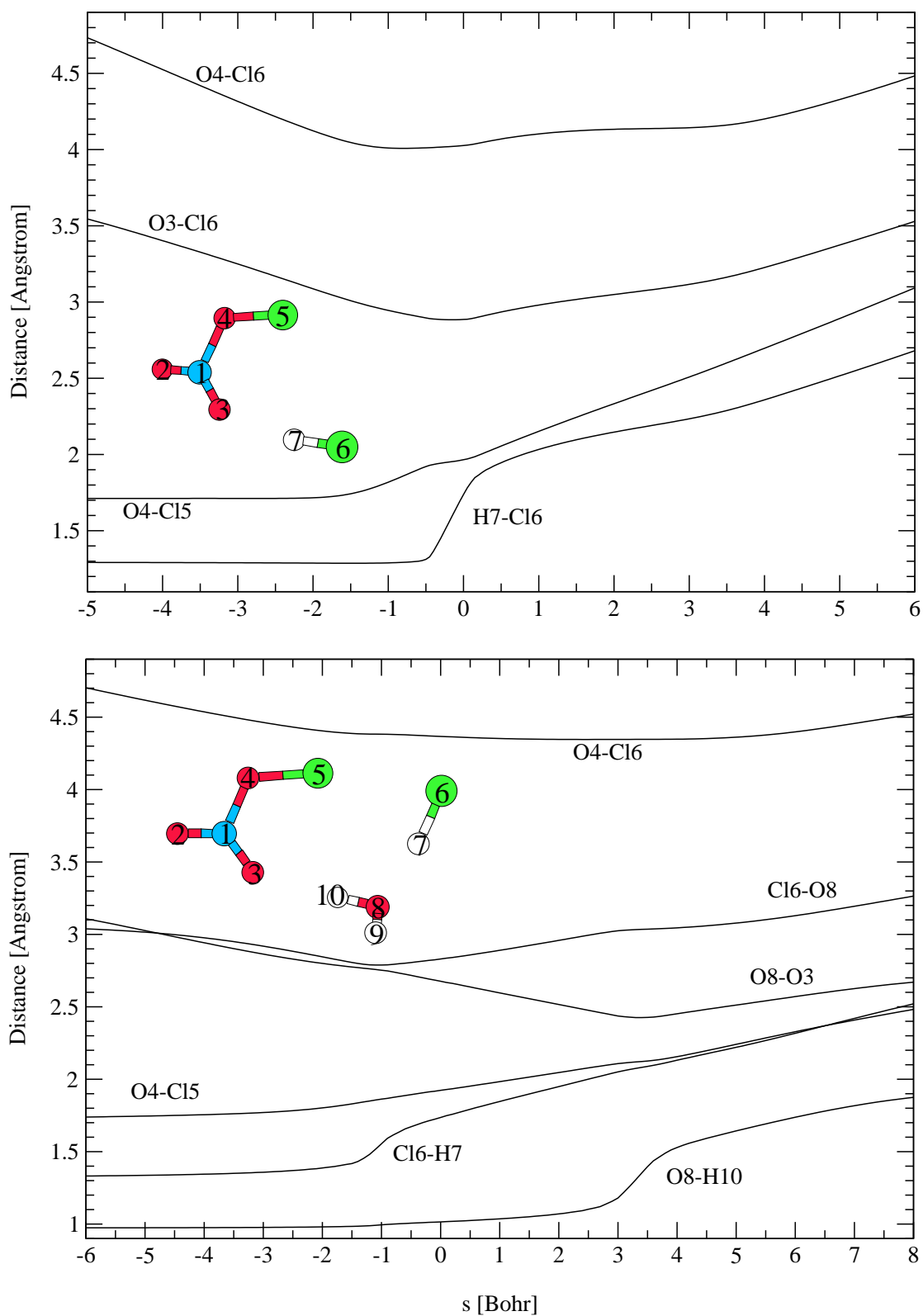
Figure 4.23: Distances [in Å] between selected two atoms along the minimum energy path [in Bohr] for the decomposition of chlorine nitrate by HCl (top) and by HCl/H$_2$O (bottom). The numbering scheme is shown as inset in the respective plots.
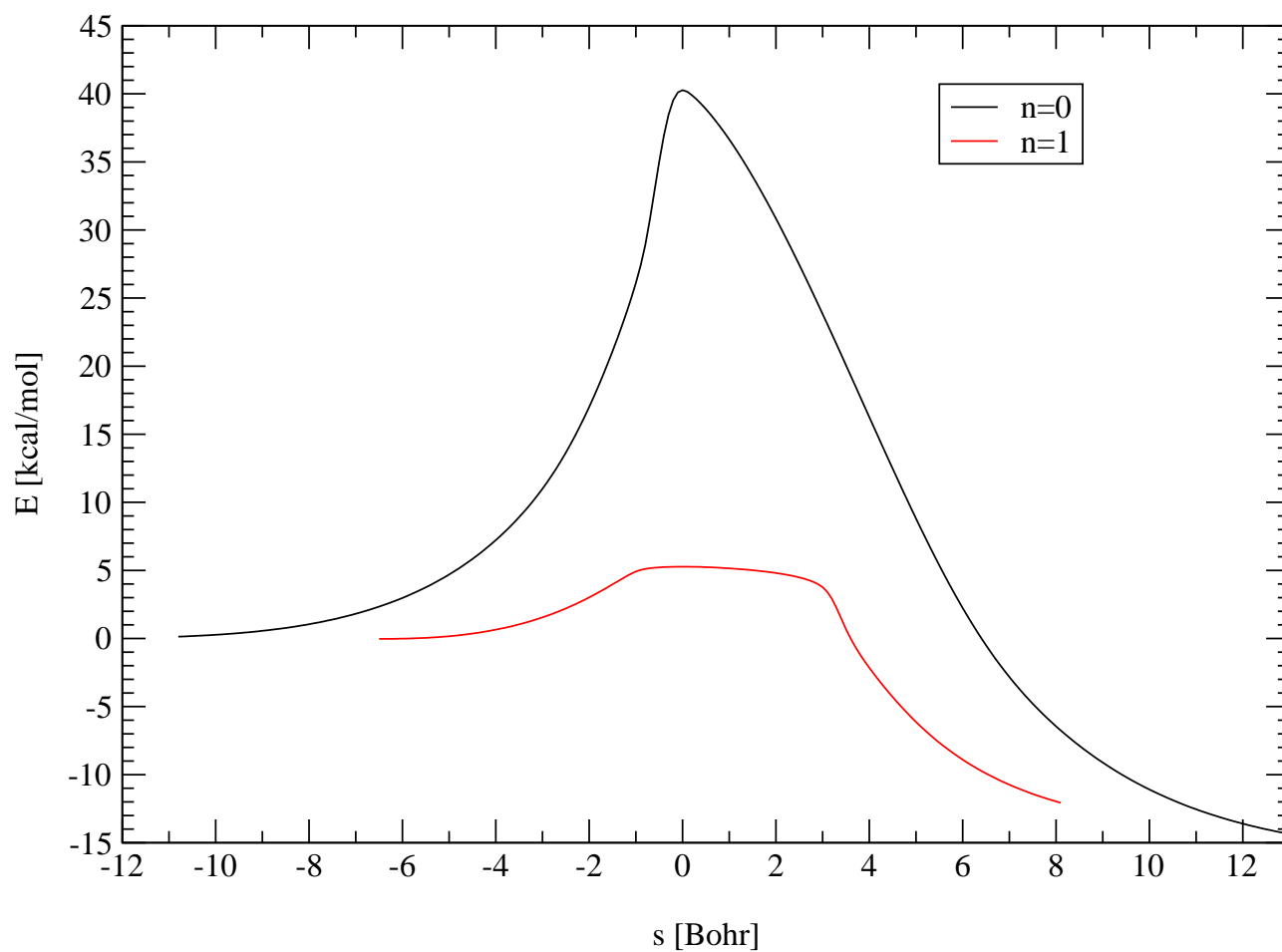
Figure 4.24: Energy along the classical reaction coordinate (MEP, IRC) as found for the decomposition of chlorine nitrate by HCl with (n=1) and without (n=0) the assistance of a water molecule as calculated at B3LYP/6-31+G(d) level of theory.

		B3LYP/ 6-31+G(d)	MP2/ aug-cc-pVDZ	CCSD(T)/ aug-cc-pVDZ	G2(MP2)
n=1	$ClONO_2$/HCl	1.27	1.88	2.19	2.21
	$ClONO_2$·HCl	0.00	0.00	0.00	0.00
	TS	40.27	47.83	44.75	46.07
	HNO_3·Cl_2	-16.08	-12.25	-14.31	-17.70
n=2	$ClONO_2$/HCl/H_2O	11.46	11.33	12.10	11.36
	$ClONO_2$·HCl·H_2O	0.00	0.00	0.00	0.00
	TS	5.27	10.87	11.10	10.77
	HNO_3·Cl_2·H_2O	-18.02	-14.18	-15.71	-19.47

Table 4.9: Electronic energies in kcal/mol for the decomposition of chlorine nitrate by HCl unassisted (n=0) and assisted by one water molecule (n=1). The first lines correspond to the separated molecules, the second lines correspond to the $ClONO_2$·HCl·nH_2O minima (set to 0.00 kcal/mol by definition), the third lines correspond to the transition states to the concerted nucleophilic substitution/proton transfer reaction (TS), and the last lines correspond to the HNO_3·Cl_2·nH_2O minima. CCSD(T) energies rely on MP2/aug-cc-pVDZ geometries. G2(MP2) values were calculated according to the literature,[147] but without zero-point correction.

117i cm^{-1} is even lower than the comparable frequency of 307i cm^{-1} in the decomposition induced by two water molecules. In this case heavy atom movement, namely approaching of the chlorine atoms and hydrogen bond compression of the OH···O bond occurs. This results in the rather flat and broad transition state region for n=1 in Figure 4.24 on the preceding page. Stabilization of the unimolecular complex on both branches does not start until the hydrogen atoms are transferred.

The Influence of Tunneling

Concerning the tunneling corrections as listed in Table 4.10 on page 107 this implies that tunneling is very important for n=0, but negligible for n=1. Again, this is in strict contrast to the comparable reactions involving decomposition by water.

The combined effect of reaction barriers and these tunneling corrections is shown in the unimolecular isomerization rate constants in Figure 4.26 on page 108. This Figure also
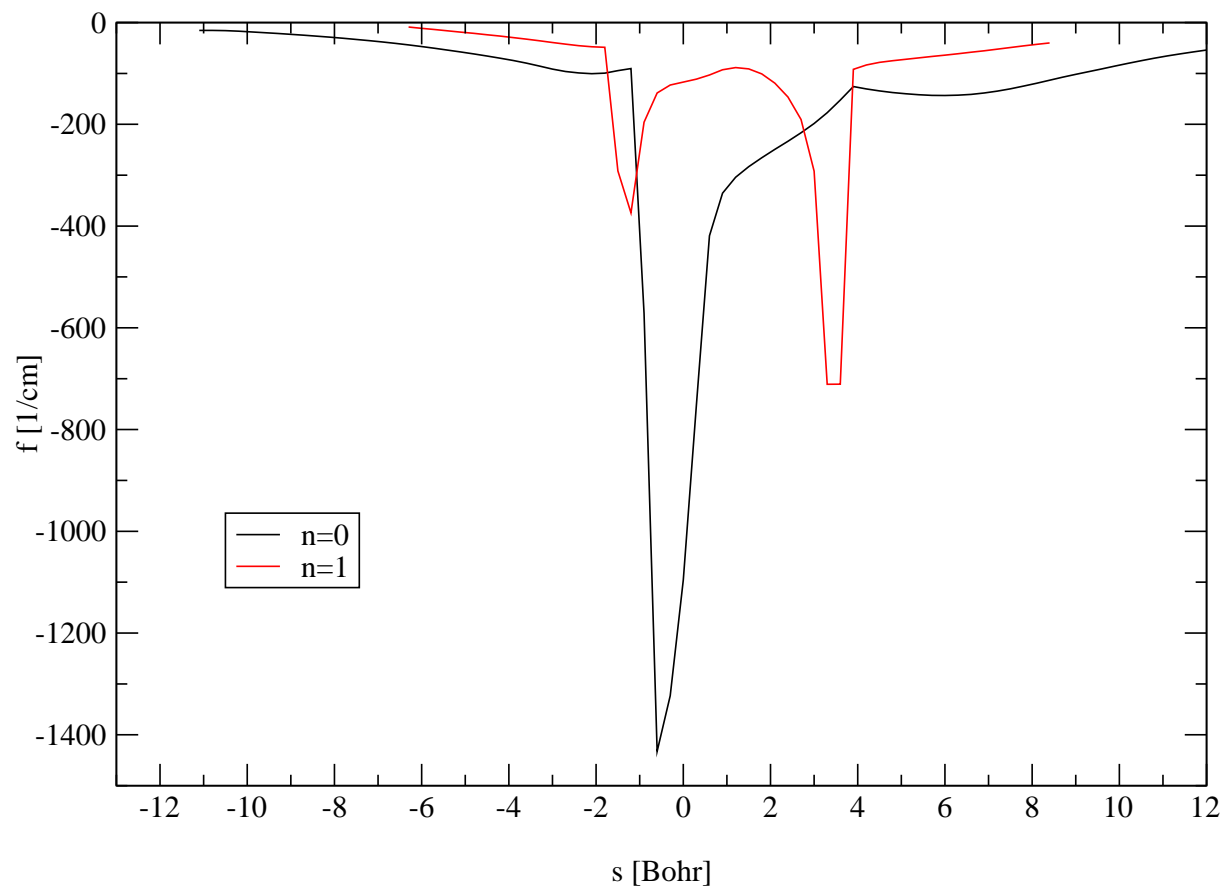
Figure 4.25: "Imaginary" frequency along the reaction coordinate as calculated at B3LYP/6-31+G(d) level of theory. Negative s values correspond to $ClONO_2$–HCl like species, s=0 Bohr corresponds to the transition state, and positive s values correspond to Cl_2–HNO_3 like species. The water-free reaction is labeled by n=0, the water-assisted reaction by n=1.

	Wigner	ZCT	SCT	LCT
n=0	5.6	22.3	977.7	2.0×10^{6}
	4.4	5.7	47.0	2.6×10^{3}
	3.6	3.2	12.9	74.9
n=1	1.1	1.2	1.4	1.3
	1.0	1.1	1.3	1.3
	1.0	1.1	1.2	1.1

Table 4.10: Tunneling correction factors κ at 150 K (top row), 175 K (middle) and 200 K (bottom) to the rate constants obtained from classical transition state theory for the decomposition of chlorine nitrate by HCl unassisted (n=0) and assisted by one water molecule (n=1). B3LYP/6-31+G(d) was employed throughout. The Wigner correction[123] is calculated directly from the imaginary frequency at s=0 Bohr in Figure 4.25 on the page before without using any information of the reaction path, zero-curvature tunneling (ZCT) involves tunneling along the minimum energy path, small-curvature tunneling (SCT)[228] involves adiabatic tunneling at the inner turning points of the concave side of the minimum energy path,[229] and large-curvature tunneling (LCT)[104] involves vibrationally non-adiabatic straight line tunneling through the reaction swath. The latter three corrections were all calculated employing the semi-classical approximation.[230]

contains the rate constants calculated for the decomposition reactions by water for direct comparison.

4.2.3 Influence of Pre-Association

Similar to the hydration of sulfur oxides also in the case of the decomposition of chlorine nitrate the concentration dependence is important. At finite temperatures the association energies given in Table 4.6 on page 91 and Table 4.9 on page 105 have to be corrected because of vibrational and rotational excitation or entropy. The corrections needed to obtain Gibbs free energies ΔG for the reactions

$$ClONO_2 + nH_2O \rightleftharpoons ClONO_2 \cdot (H_2O)_n \qquad (4.5)$$
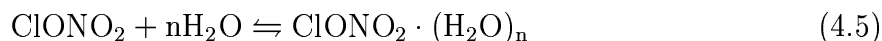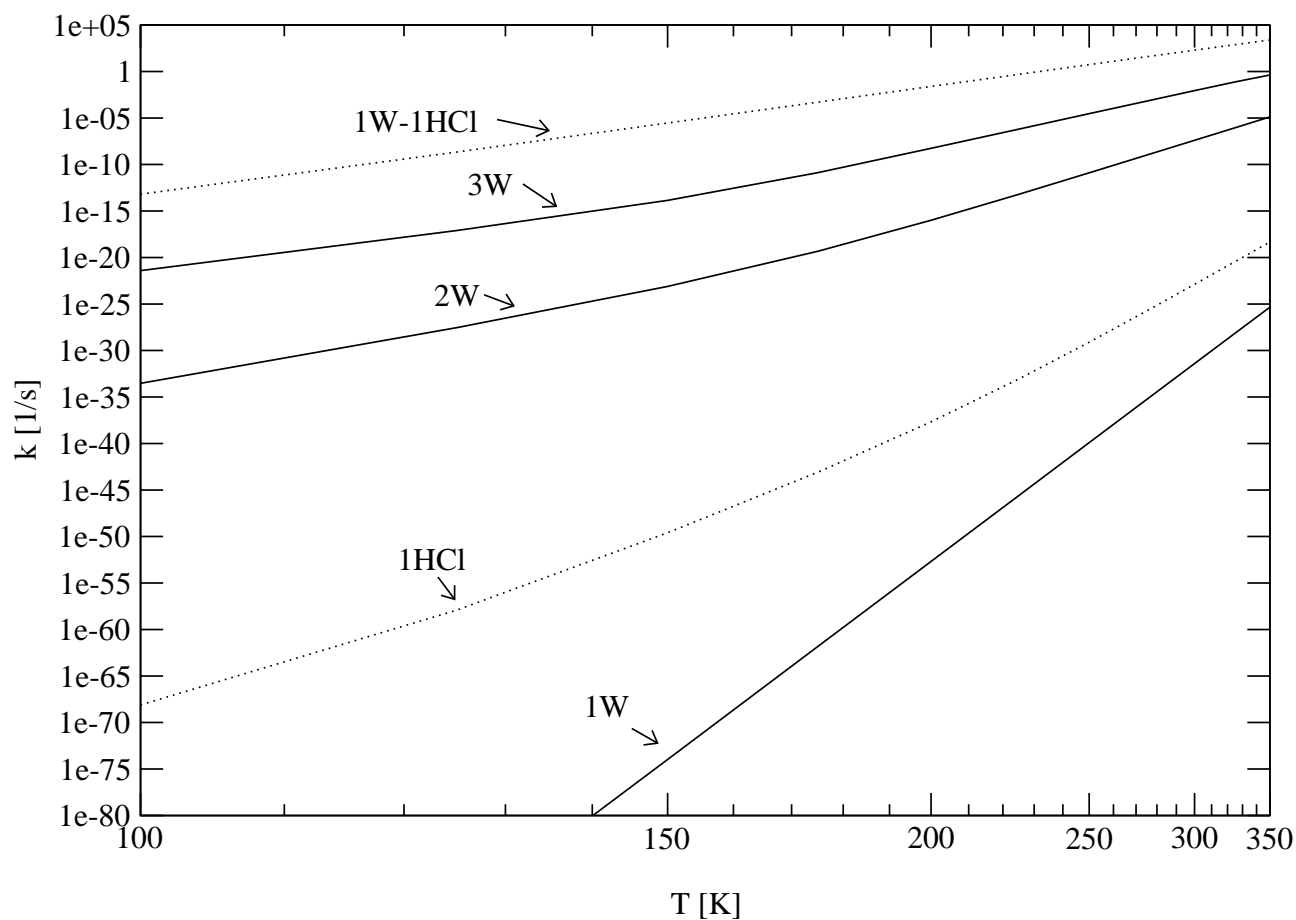
Figure 4.26: Arrhenius plot of the decomposition of chlorine nitrate with water alone (solid lines) and HCl (dotted lines) in the presence of up to three water molecules in the unimolecular complex as calculated from VTST/μOMT on B3LYP/6-31+G(d) reaction hypersurfaces. The reaction barrier is interpolated to G2(MP2)[147] Note that the range of times reaches from nanoseconds (10^{10}s^{-1}) via days (10^{-5}s^{-1}) and years (10^{-10}s^{-1}) to many millions of years ($<10^{-20}\text{s}^{-1}$). "W" stands for decomposition by water, and "HCl" stands for decomposition by hydrochloric acid.

with n=1–3 and

$$ClONO_2 + HCl + nH_2O \rightleftharpoons ClONO_2 \cdot HCl \cdot (H_2O)_n \qquad (4.6)$$
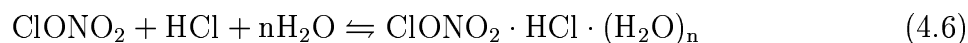
with n=0,1 are given in Table 4.11 on the next page. From these association Gibbs free energies equilibria constants were obtained analogously to the hydration of sulfur oxides. When comparing the HCl and the pure water decomposition reaction again, it is found that the association energies clearly favor the chlorine nitrate–water complexes, whereas the thermal corrections favor the chlorine nitrate–HCl complexes. That is, the higher the temperature the more likely a complex containing HCl instead of water will be formed. However, at the temperatures investigated here the clearly dominating contribution stems from the association energies and not the thermal corrections. Therefore, all equilibria constants of the chlorine nitrate water complexes are clearly higher than their pendants of the chlorine nitrate–HCl complexes. The difference amounts to 6 orders of magnitude at 100 K and still one order of magnitude at 350 K irrespective of n. The "break even" point, at which incorporation of HCl into the complex has the same probability than formation of a pure water–chlorine nitrate complex, can be extrapolated to approximately 800 K. Nevertheless in our atmosphere HCl is much less abundant than water. Whereas about 10^{14} molecules of water per cm^3 are observed in the atmosphere only 10^9 molecules HCl and 10^8 molecules $ClONO_2$ per cm^3 are observed.[57,73,257,258] This difference in abundance has the result that even at temperatures of 800 K the chlorine nitrate–water complexes are expected to be found more frequently by a factor of 10^5 than the chlorine nitrate–HCl complexes in the equilibrium. At 100 K and 200 K the differences in the equilibria constants further enhance this factor to 10^{11} and 10^8, respectively, as under such conditions the equilibrium pressure of the complex is directly proportional to the equilibrium constant and the pressures of the educts.

	100 K	150 K	200 K	250 K	300 K	350 K
$ClONO_2$–$1H_2O$	3.64	4.84	6.04	7.22	8.37	9.50
$ClONO_2$–$2H_2O$	9.66	12.71	15.79	18.87	21.93	24.96
$ClONO_2$–$3H_2O$	14.74	19.23	23.80	28.38	32.94	37.47
$ClONO_2$–$1HCl$	2.54	3.56	4.54	5.50	6.42	7.33
$ClONO_2$–$1H_2O$–$1HCl$	8.27	11.12	13.99	16.86	19.70	22.51
$ClONO_2$–$1H_2O$	3.2×10^3	3.8	1.3×10^{-1}	1.9×10^{-2}	5.2×10^{-3}	2.2×10^{-3}
$ClONO_2$–$2H_2O$	9.8×10^{12}	1.6×10^4	6.2×10^{-1}	1.4×10^{-3}	2.4×10^{-5}	1.4×10^{-6}
$ClONO_2$–$3H_2O$	1.3×10^{28}	1.5×10^{12}	1.4×10^4	2.0×10^{-1}	1.3×10^{-4}	6.7×10^{-7}
$ClONO_2$–$1HCl$	1.7×10^{-3}	4.6×10^{-4}	2.7×10^{-4}	2.0×10^{-4}	1.8×10^{-4}	1.6×10^{-4}
$ClONO_2$–$1H_2O$–$1HCl$	9.5×10^6	3.1	1.7×10^{-3}	1.9×10^{-5}	9.8×10^{-7}	1.2×10^{-7}

Table 4.11: Thermal correction from association energy (cf. Table 4.6 on page 91 and Table 4.9 on page 105) to association Gibbs free energy ΔG in kcal/mol as calculated at B3LYP/6-31+G(d) level of theory (top) and equilibrium constants in atm^{-n} for the pre-association reactions given in Equation 4.5 on page 107 and Equation 4.6 on the page before calculated at B3LYP/6-31+G(d) level of theory (bottom).

Homogeneous versus Heterogeneous Reaction

The required pre-association in the homogeneous case explains why the heterogeneous reaction is so much more effective in converting chlorine nitrate. Assuming 10^{14} water molecules per cm^3, which corresponds to a partial pressure of about 0.003 mbar, the half-life of chlorine nitrate can be estimated to be many thousand years. On the other hand the heterogeneous reaction does not depend on the concentration of the surrounding species, as long as there is transport to the surface. The half-life drastically reduces then to a few hours depending on the temperature and the reaction mechanism. Therefore, the homogeneous reaction can fortunately not compete with the heterogeneous hydrolysis. Loading of midlatitudes with liquid-like aerosol surface due to anthropogenic emission or natural events like eruptions of vulcanoes[30] is expected to cause lower ozone budgets not only above Antarctica. Recently ozone losses have been found also above Artica.[259]

Nevertheless, the competition between HCl and H_2O reaction channels is of course determined by the likelihood of the adsorption of the rivaling species on the surface. Under

the assumption that the adsorption energy on polar stratospheric clouds can be replaced by the here calculated association energies the factor of 10^8 can be used for the discussion of the heterogeneous reactions. In order to be able to be competitive in the stratosphere with the pure water reaction, the HCl reaction has to be 8 orders of magnitude faster at 200 K in the isomerization step. Comparing the decomposition reactions involving 1H$_2$O–1HCl or 1HCl with the reactions involving 2H$_2$O or 1H$_2$O, respectively, in Figure 4.26 on page 108 demonstrates that this is clearly the case at temperatures lower than 200 K, where the difference amounts to more than 10 orders of magnitude. On increasing the temperature to 400 K this difference is reduced slowly to about 5 orders of magnitude, which means that the decomposition channel free of HCl dominates. At intermediate temperatures between 200 K and 300 K I expect the two reaction channels to be competitive. The dominant reaction channel is likely to be determined by air-parcel composition variations, e.g., induced by wind, temperature changes or human influences. Especially in type II PSCs containing almost 100% of water the competition may be turned to the favor of the water channel. Statements of experimental atmospheric chemists that the water channel is the dominant contribution to ozone depletion at water-rich conditions[55–57] underline the significance of these results.

4.2.4   Discussion of Results

Consistent with ^{18}O-substitution experiments[260] and with recent theoretical results[249–251] my calculations support a S$_N$2 type attack of water on the Cl—ONO$_2$ bond that is favoured by a concerted proton transfer (PT) generating a stronger, hydroxyl like, nucleophile. Also mass spectroscopic and infrared studies indicated this change in the degree of polarization of this bond leading to enhanced electrophilicity of the chlorine atom.[76,261] Unlike HCl adsorption on the basal plane of ice[58] a full ionization of the substrate is not observed. The asynchronous, but concerted nature of the molecular movements precludes interme-

diary formation of $[H_2OCl]^+$, a species discussed in context of the so-called "ion-catalyzed mechanism" in the literature.[253, 262] An important aspect of the mechanism investigated here is the water-mediated nature of the proton transfer ("bifunctional catalysis") and the catalytic effect exerted by single water molecules. In a very interesting study Beichert and Schrems showed that such a catalytic effect is also exerted by HSO_4^-, but not H_2SO_4, on the decomposition of chlorine nitrate by HCl.[263] As the ozone layer above midlatitude is presently undamaged, the authors conclude that the surface of midlatitude-aerosol is made from undissociated sulfuric acid. Furtheron they state that there is a penetration-barrier that prevents HCl and $ClONO_2$ from direct contact with HSO_4^- found in the bulk-aerosol. Also the NO_3^- anion has been shown both in experiments[264] and from *ab initio* calculations[265] to enhance the rate of decomposition of $ClONO_2$ by HCl. In other studies it has been shown that introducing even more water molecules further diminishes the reaction barrier so that a fast reaction is expected because of preferential solvation of the transition state.[250, 251, 253, 254, 266] In the case of the barrierless reaction in large water clusters the hydrolysis would supposedly even be collision-limited. A similar barrierless situation for the decomposition of $ClONO_2$ by HCl has been found by McNamara, Tresadern and Hillier in the presence of only two water molecules.[267] Whereas these authors were able to locate a transition state for the decomposition in the $ClONO_2 \cdot HCl \cdot 2H_2O$ system at B3LYP/6-311++G(d,p) and MP2/6-311++G(3df,3pd) level of theory, I could not find such a transition state at both B3LYP/6-31+G(d) and MP2/aug-cc-pVDZ level of theory. Furtheron these authors show that in large water cluster the ionic attack of Cl^- on $ClONO_2$ is responsible for the barrierless reaction. However, as both the ionization of HCl interacting with ice surfaces[268] the reaction of Cl^- with $ClONO_2$[269] and Cl_2 desorption are rapid, and would, therefore, finally lead to massive ozone depletion, I suppose that such mechanisms can not be operative in our atmosphere. On the other hand Bianco and Hynes find a (zero-point energy corrected) reaction barrier of 6.4 kcal/mol for the decomposition

of $ClONO_2$ by HCl in a cluster of nine water molecules,[270] which seems to be rather high in view of the results by McNamara and in my work. The experiments in the group of nobel-laureate Mario J. Molina in a fast flow reactor for the HCl reaction on different ice surfaces yielding large reaction probabilities γ are more consistent with the interpretation of an ionic reaction mechanism involving HCl solvation in a liquid-like surface layer.[271]

Numerous laboratory experiments have also focussed on determining the reaction probabilities γ for chlorine nitrate hydrolysis (without HCl) on different ice and acid/ice surfaces at temperatures between 140 K and 200 K.[73,74,272–275] A common conclusion arising due to these experiments is the sensitivity of γ on equilibrium water vapour pressures, which are lowest for surfaces coated with acids like nitric acid trihydrate. Also lower temperatures due to climate changes have been related to higher water vapour pressures in PSC leading to increased levels of active chlorine species.[276]

The result shown in Figure 4.26 on page 108 clearly shows why such experimental finding were made. Coating of the water-surface reduces the number of freely available water molecules, which drastically reduces the rate of conversion. On trying to correlate the observed ozone depletions with the decomposition rate of chlorine nitrate, it was found that a rate constant of $5.0 \times 10^{-5} s^{-1}$ best reproduces the observations. Such a rate constant can be explained by a mechanism involving three water molecules or one water molecule and one HCl molecule according to Figure 4.26 on page 108 in the temperature region between 150 K and 250 K. I propose, therefore, the reaction mechanism depicted in Figure 4.27 on the next page to be responsible for the observed ozone depletion. Interestingly, a recent uptake study of chlorine containing species on water clusters revealed a similar binding at a ratio of 1:3.[277]

As complexation with only three water molecules is required to explain the satellite, ground-based, and balloon measured ozone profiles[49] by ozone column models,[57] the number of freely available water molecules in PSCs is probably limited to about three. This
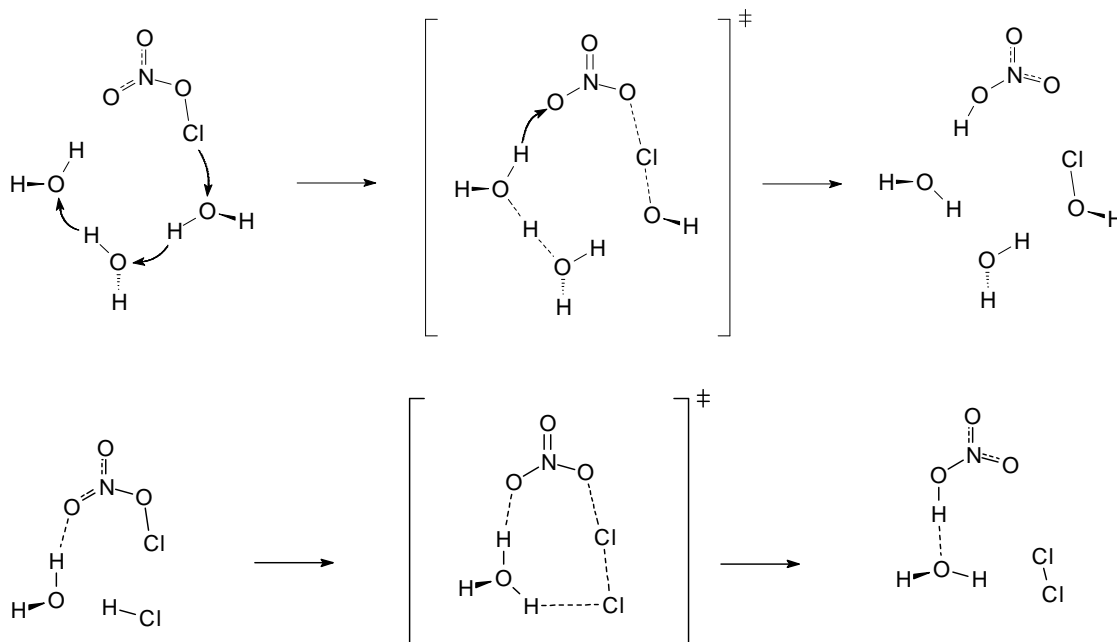
Figure 4.27: Reaction mechanism proposed to be responsible for observed ozone depletion above Antarctica. The decomposition of chlorine nitrate can take place via water-mediated triple proton transfer along three water molecules (top) or water/HCl-mediated double proton transfer (bottom).

prevents the very fast conversion expected for larger water clusters. Increasing water content in the atmosphere in the future could result in an acceleration of the decomposition and consequently also drastically lower ozone levels. An increase from 6000 ppbv to 6700 ppbv water at 20 km altitude was measured between 1979 and 1997.[257,278] Therefore, the parameter appropriate for future ozone column models describing $ClONO_2$ hydrolysis will be found, to my opinion, to be shifted to values clearly higher than $5.0 \times 10^{-5} s^{-1}$ in the future. I am not sure whether the dominant effect in the coupled system of stratospheric ozone-loss, stratospheric cooling and stratospheric water vapour change[276] is the effect of water vapour changes to cooling,[278] the effect of temperature-change on ozone depletion[279] as proposed recently or rather the effect of water vapour changes to ozone-depletion via an accelerated decay of chlorine reservoir species investigated in this study. An increase in water vapour was demonstrated to determine the amount of water co-condensing with H_2SO_4 vapour and to result in a large decrease of the lifetime of $ClONO_2$,[280] which puts additional emphasis to this conclusion.

According to the here-determined rate constants during a 30 second passage time of $ClONO_2$ (assuming immediate uptake on PSC) about 5% $ClONO_2$ will be converted, i.e., $\gamma=0.05$. A passage time of 4 minutes would lead to $\gamma=0.3$. These γ values agree with the reaction probabilities of chlorine nitrate on different PSC model surfaces found in the laboratory[73,74,272-275] and, therefore, validate the abovementioned conclusions.

Chapter 5

Short Summary

Variational transition state theory and multidimensional tunneling methods on hybrid density functional theory generated hypersurfaces have been used to investigate the temperature dependence of the reaction rate constants of water-mediated proton transfer reactions relevant to the chemistry of our atmosphere, namely the hydration of sulfur dioxide and sulfur trioxide and the decomposition of chlorine nitrate. Highly accurate reaction barriers were calculated using *ab initio* methods taking into account most of the electron correlation, namely CCSD(T)/aug-cc-pVDZ//MP2/aug-cc-pVDZ and G2(MP2).

On comparing the determined rate constants with laboratory and atmospheric data, the following points could be established:

- All of the investigated reactions are highly sensitive to changes in humidity, as water acts as efficient catalyst, i.e., the barrier to the reaction is reduced drastically.

- Present-day atmospheric chemistry can only be explained when a limited number of water molecules is available for the formation of molecular clusters.

- Both in the troposphere and in the stratosphere SO_3 is hydrated rather than SO_2. SO_2 emissions have to be oxidized, therefore, before being subject to hydration.

- A mechanism involving two or three water molecules is relevant for the production of sulfate aerosols, which play a decisive role in the context of global climate change and acid rain.

- A third water molecule has the function of assisting double-proton transfer rather than acting as active participant in triple-proton transfer in the case of the hydration of sulfur oxides.

- The observed ozone depletion above Arctica and Antarctica can be explained either by decompositon of chlorine nitrate in the presence of three water molecules (triple proton transfer) or by decomposition of chlorine nitrate in the presence of one molecule of HCl and one molecule of water (double proton transfer).

- The preassociation reaction required for homogeneous gas-phase conversion of chlorine reservoir species to active chlorine species increases the half-life of the reservoir species enormously in comparison to the unimolecular heterogeneous reaction. Thats why the ozone layer above midlatitudes shows no depletion.

- The nucleophilic attack is *concerted* with the proton transfer(s), i.e., no reaction intermediates like ions exist.

- The multiple proton transfers occur *asynchronously* according to the hydrogen bond compression mechanism in a linear $OH\cdots O$ arrangement at a heavy atom distance of 2.5 Å.

Chapter 6

Kurzzusammenfassung

Mit Hilfe der variationellen Theorie des aktivierten Komplexes und mehrdimensionaler Tunnelmethoden auf der Basis von Hybriddichtefunktional-Hyperflächen wurde die Temperaturabhängigkeit der Geschwindigkeitskonstanten von wasserunterstützten Protonenübertragungsreaktionen untersucht, die eine wesentliche Rolle in der Chemie unserer Atmosphäre spielen, nämlich die Wasseranlagerungen an Schwefeldioxid bzw. Schwefeltrioxid sowie die Zersetzung von Chlornitrat. Sehr genaue Berechnungen der Barrierenhöhen dieser Reaktionen wurden mittels *ab initio* Methoden durchgeführt, die den größten Teil der Elektronenkorrelation berücksichtigen, d.h., CCSD(T)/aug-cc-pVDZ//MP2/aug-cc-pVDZ und G2(MP2).

Beim Vergleich der hier bestimmten Geschwindigkeitskonstanten mit Daten aus dem Labor und aus der Atmophäre konnten folgende Punkte herausgearbeitet werden:

- Alle untersuchten Reaktionen hängen stark von der Luftfeuchtigkeit ab, weil Wasser als effizienter Katalysator agiert, also die Reaktionsbarriere stark erniedrigt.

- Die derzeitige atmosphärische Chemie kann nur erklärt werden, wenn eine begrenzte Anzahl von Wassermolekülen zur Bildung molekularer Cluster zur Verfügung steht.

- Sowohl in der Troposphäre als auch in der Stratosphäre wird SO$_3$, und nicht SO$_2$, hydratisiert. SO$_2$ Emissionen müssen dementsprechend vor der Wasseranlagerung oxidiert werden.

- Ein Mechanismus mit zwei oder drei Wassermolekülen ist entscheidend für die Bildung von Sulfatärosolen, die eine wesentliche Rolle im Zusammenhang mit globaler Klimaveränderung und saurem Regen spielen.

- Ein drittes Wassermolekül hat im Fall der Wasseranlagerung an Schwefeloxide die Funktion eine zweifache Protonenübertragung zu unterstützen anstatt selbst aktiv an einer dreifachen Protonenübertragung mitzuwirken.

- Der beobachtete Ozonabbau über der Arktis und Antarktis ist entweder über den Zerfall von Chlornitrat in der Anwesenheit von drei Wassermolekülen (dreifache Protonenübertragung) oder in der Anwesenheit von einem Molekül HCl und einem Molekül Wasser (zweifache Protonenübertragung) zu erklären.

- Das für eine homogene Gasphasen-Umwandlung von inaktiven zu aktiven Chlorsubstanzen benötigte vorgelagerte Assoziationsgleichgewicht erhöht die Halbwertszeit von ClONO$_2$ bzw. HCl im Vergleich zur heterogenen Umwandlung extrem. Aus diesem Grund findet über mittleren Breiten fast kein Ozonabbau statt.

- Der nukleophile Angriff ist *konzertiert* mit der Protonenübertragung, d.h., keine ionischen Reaktionsintermediate treten auf.

- Die mehrfachen Protonenübertragungen geschehen *asynchron*, wobei jeder Einzelschritt in einer auf 2.5 Å verkürzten Wasserstoffbrücke in einer linearen OH$\cdots$O Anordnung stattfindet.

Chapter 7

References

Bibliography

1. T. E. Graedel and P. J. Crutzen. Chemie der Atmosphäre, Bedeutung für Klima und Umwelt. Spektrum, Akademischer Verlag, Heidelberg, Berlin, Oxford, (1994).

2. D. M. Murphy, D. S. Thomson, and M. J. Mahoney. In situ measurements of organics, meteoritic material, mercury, and other elements in aerosols at 5 to 19 kilometers. *Science* **282**, 1664–1669 (1998).

3. A. Jenkins. End of the acid reign? *Nature* **401**, 537–538 (1999).

4. J. L. Stoddard *et al.* Regional trends in aquatic recovery from acidification in North America and Europe. *Nature* **401**, 575–578 (1999).

5. T. E. Graedel. Corrosion-related aspects of the chemistry and frequency of occurrence of precipitation. *J. Electrochem. Soc.* **133**, 2476–2482 (1986).

6. V. Vaida and J. E. Headrick. Physicochemical properties of hydrated complexes in the Earth's atmosphere. *J. Phys. Chem. A* **23**, 5401–5412 (2000).

7. R. J. Charlson, J. E. Lovelock, M. O. Andreae, and S. G. Warren. Oceanic phytoplankton, atmospheric sulphur, cloud albedo and climate. *Nature* **326**, 655–661 (1987).

8. R. P. Kiene. Sulphur in the mix. *Nature* **402**, 363–365 (1999).

9. R. Simó and C. Pedrós-Alió. Role of vertical mixing in controlling the oceanic production of dimethyl sulphide. *Nature* **402**, 396–399 (1999).

10. B. J. Huebert. Sulphur emissions from ships. *Nature* **400**, 713–714 (1999).

11. K. Capaldo *et al.* Effects of ship emissions on sulphur cycling and radiative climate forcing over the ocean. *Nature* **400**, 743–746 (1999).

12. L. Granat, H. Rodhe, and R. O. Hallberg. Nitrogen, Phophorous, and Sulfur: Global Cycles, volume 32. Ecological Bulletins, Stockholm, (1976).

13. W. R. Stockwell and J. G. Calvert. The mechanism of the HO-SO2 reaction. *Atmos. Environ.* **17**, 2231–2235 (1983).

14. R. Steudel. Schwefelsäure aus Schwefeltrioxid und Wasser — eine überraschend komplexe Reaktion. *Angew. Chem.* **107**, 1433–1435 (1995).

15. W.-K. Li and M. L. McKee. Theoretical study of OH and H_2O addition to SO_2. *J. Phys. Chem. A* **101**, 9778–9782 (1997).

16. A. D. Clarke *et al.* Particle nucleation in the tropical boundary layer and its coupling to marine sulfur sources. *Science* **282**, 89–92 (1998).

17. A. Kukui, V. Bossoutrout, G. Laverdet, and G. Le Bras. Mechanism of the reaction of CH_3SO with NO_2 in relation to atmospheric oxidation of dimethyl sulfide: Experimental and theoretical study. *J. Phys. Chem. A* **104**, 935–946 (2000).

18. A. Laaksonen, V. Talanquer, and D. W. Oxtoby. Nucleation: Measurements, theory, and atmospheric applications. *Annu. Rev. Phys. Chem.* **46**, 489–524 (1995).

19. T. Koop, H. P. Ng, L. T. Molina, and M. J. Molina. A new optical technique to study aerosol phase transitions: The nucleation of ice from H_2SO_4 aerosols. *J. Phys. Chem. A* **102**, 8924–8931 (1998).

20. R. F. Niedziela *et al.* A temperature and composition-dependent study of H_2SO_4 aerosol optical constants using fourier transform and tunable diode laser infrared spectroscopy. *J. Phys. Chem. A* **103**, 8030–8040 (1999).

21. M. J. Molina *et al.* Physical chemistry of the $H_2SO_4/HNO_3/H_2O$ system: Implications for polar stratospheric clouds. *Science* **261**, 1418–1423 (1993).

22. O. B. Toon and M. A. Tolbert. Spectroscopic evidence against nitric acid trihydrate in polar stratospheric clouds. *Nature* **375**, 218–221 (1995).

23. T. Koop and K. S. Carslaw. Melting of $H_2SO_4 \cdot 4H_2O$ particles upon cooling: Implications for polar stratospheric clouds. *Science* **272**, 1638–1641 (1996).

24. J. Schreiner *et al.* Chemical analysis of polar stratospheric cloud particles. *Science* **283**, 968–970 (1999).

25. R. J. Charlson *et al.* Climate forcing by anthropogenic aerosols. *Science* **255**, 423–430 (1992).

26. J. T. Kiehl. Solving the aerosol puzzle. *Science* **283**, 1273–1274 (1999).

27. J. M. Haywood, V. Ramaswamy, and B. J. Soden. Tropospheric aerosol climate forcing in clear-sky satellite observations over the oceans. *Science* **283**, 1299–1303 (1999).

28. H. Rodhe. Clouds and climate. *Nature* **401**, 223–225 (1999).

29. M. C. Facchini, M. Mircea, S. Fuzzi, and R. J. Charlson. Cloud albedo enhancement by surface-active organic solutes in growing droplets. *Nature* **401**, 257–259 (1999).

30. P. McCormick, L. W. Thomason, and C. R. Trepte. Atmospheric effects of the Mt Pinatubo eruption. *Nature* **373**, 399–404 (1995).

31. S. C. Solomon, M. A. Bullock, and D. H. Grinspoon. Climate change as a regulator of tectonics on venus. *Science* **286**, 87–90 (1999).

32. R. W. Carlson, R. E. Johnson, and M. S. Anderson. Sulfuric acid on Europa and the radiolytic sulfur cycle. *Science* **286**, 97–99 (1999).

33. A. P. Showman and R. Malhotra. The Galilean satellites. *Science* **286**, 77–84 (1999).

34. X. Wang, Y. G. Jin, M. Suto, and L. C. Lee. Rate constant of the gas phase reaction of SO_3 with H_2O. *J. Chem. Phys.* **89**, 4853–4860 (1988).

35. J. T. Jayne *et al.* Pressure and temperature dependence of the gas-phase reaction of SO_3 with H_2O and the heterogeneous reaction of SO_3 with H_2O/H_2SO_4 surfaces. *J. Phys. Chem. A* **101**, 10000–10011 (1997).

36. J. E. Hansen *et al.* Climate forcings in the Industrial era. *Proc. Natl. Acad. Sci.* **95**, 12753–12758 (1998).

37. J. T. Houghton, G. J. Jenkins, and J. J. Ephraums. Climate Change: The IPCC Scientific Assessment. Cambridge University Press, Cambridge, UK, (1990).

38. S. E. Schwartz and P. R. Buseck. Absorbing phenomena. *Science* **288**, 989–990 (2000).

39. A. S. Ackerman *et al.* Reduction of tropical cloudiness by soot. *Science* **288**, 1042–1047 (2000).

40. A. Tabazadeh *et al.* Quantifying denitrification and its effect on ozone recovery. *Science* **288**, 1407–1411 (2000).

41. J. Hansen, M. Sato, J. Glascoe, and R. Ruedy. A common-sense climate index: Is climate changing noticeably? *Proc. Natl. Acad. Sci.* **95**, 4113–4120 (1998).

42. J. G. Farman, B. G. Gardiner, and J. D. Shanklin. Large losses of total ozone in Antarctica reveal seasonal ClO_x/NO_x interaction. *Nature* **315**, 207–210 (1985).

43. S. Solomon. Progress towards a quantitative understandig of antarctic ozone depletion. *Nature* **347**, 347–354 (1990).

44. P. O. Wennberg *et al.* Removal of stratospheric O_3 by radicals: In situ measurements of OH, HO_2, NO, NO_2, ClO and BrO. *Science* **266**, 398–404 (1994).

45. P. J. Crutzen *et al.* A reevaluation of the ozone budget with HALOE UARS data: No evidence for the ozone deficit. *Science* **268**, 705–708 (1995).

46. K. S. Carslaw *et al.* Increased stratospheric ozone depletion due to mountain-induced atmospheric waves. *Nature* **391**, 675–678 (1998).

47. D. W. Fahey and A. R. Ravishankara. Summer in the stratosphere. *Science* **285**, 208–211 (1999).

48. D. J. Hofman *et al.* Ozone profile measurements at McMurdo Station, Antarctica during the spring of 1987. *J. Geophys. Res.* **94**, 16527–16536 (1989).

49. W. J. Randel *et al.* Trends in the vertical distribution of ozone. *Science* **285**, 1689–1692 (1999).

50. J. G. Anderson, W. H. Brune, and M. H. Proffitt. Ozone destruction by chlorine radicals within the Antarctic vortex: The spatial and temporal evolution of $ClO-O_3$ anticorrelation based on in situ ER-2 data. *J. Geophys. Res.* **94**, 11465–11479 (1989).

51. M. A. Tolbert. Sulfate aerosols and polar stratospheric cloud formation. *Science* **264**, 527–528 (1994).

52. S. Solomon, R. R. Garcia, F. S. Rowland, and D. J. Wuebbles. On the depletion of antarctic ozone. *Nature* **321**, 755–758 (1986).

53. P. J. Crutzen and F. Arnold. Nitric acid cloud formation in the cold antarctic stratosphere: A major cause for the springtime 'ozone hole'. *Nature* **324**, 651–655 (1986).

54. R. J. Cicerone. Changes in stratospheric ozone. *Science* **237**, 35–42 (1987).

55. M. J. Molina, T.-L. Tso, L. T. Molina, and F. C.-Y. Wang. Antarctic stratospheric chemistry of chlorine nitrate, hydrogen chloride, and ice: Release of active chlorine. *Science* **238**, 1253–1257 (1987).

56. M. A. Tolbert, M. J. Rossi, R. Malhotra, and D. M. Golden. Reaction of chlorine nitrate with hydrogen chloride and water at antarctic stratospheric temperatures. *Science* **238**, 1258–1260 (1987).

57. M. B. McElroy, R. J. Salawitch, S. C. Wofsy, and J. A. Logan. Reduction of antarctic ozone due to synergistic interactions of chlorine and bromine. *Nature* **321**, 759–762 (1986).

58. B. J. Gertner and J. T. Hynes. Molecular dynamics simulation of hydrochloric acid ionization at the surface of stratospheric ice. *Science* **271**, 1563–1566 (1996).

59. C. T. McElroy, C. A. McLinden, and J. C. McConnell. Evidence for bromine monoxide in the free troposphere during the arctic polar sunrise. *Nature* **397**, 338–341 (1999).

60. C. A. Pommerening, S. M. Bachrach, and L. S. Sunderlin. Addition of protonated water to SO_3. *J. Phys. Chem. A* **103**, 1214–1220 (1999).

61. R. G. Keesee, R. Sievert, and A. W. Castleman, Jr. Mass spectral and electric deflection study of acetic acid clusters and sulfur trioxide/water clusters. *Ber. Bunsen.-Ges. Phys. Chem.* **88**, 273–274 (1984).

62. R. Hofmann-Sievert and A. W. Castleman, Jr. Reaction of SO_3 with water clusters and the formation of H_2SO_4. *J. Phys. Chem.* **88**, 3329–3333 (1984).

63. P. M. Holland and A. W. Castleman, Jr. Gas phase complexes: Considerations of the stability of clusters in the sulfur trioxide–water system. *Chem. Phys. Lett.* **56**, 511–514 (1978).

64. A. W. Castleman, Jr. *et al.* Kinetics of association reactions pertaining to H_2SO_4 aerosol formation. *Int. J. Chem. Kinet. Symp.* **1**, 629–640 (1975).

65. T. Reiner and F. Arnold. Laboratory flow reactor measurements of the reaction SO_3 + H_2O + M. implications for gaseous H_2SO_4 and aerosol formation in the plumes of jet aircraft. *Geophys. Res. Lett.* **20**, 2659–2662 (1993).

66. T. Reiner and F. Arnold. Laboratory investigations of gaseous sulfuric acid formation via $SO_3 + H_2O + M \rightarrow H_2SO_4 + M$: measurement of the rate constant and product identification. *J. Chem. Phys.* **101**, 7399–7407 (1994).

67. C. E. Kolb *et al.* Gas phase reaction of sulfur trioxide with water vapor. *J. Am. Chem. Soc.* **116**, 10314–10315 (1994).

68. E. R. Lovejoy, D. R. Hanson, and L. G. Huey. Kinetics and products of the gas-phase reaction of SO_3 with water. *J. Phys. Chem.* **100**, 19911–19916 (1996).

69. T. S. Chen and P. L. Moore Plummer. Ab initio MO investigation of the gas-phase reaction $SO_3 + H_2O \rightarrow H_2SO_4$. *J. Phys. Chem.* **89**, 3689–3693 (1985).

70. M. Hofmann and P. v. R. Schleyer. Acid rain: Ab initio investigation of the $H_2O \cdot SO_3$ complex and its conversion into H_2SO_4. *J. Am. Chem. Soc.* **116**, 4947–4952 (1994).

71. K. Morokuma and C. Muguruma. Ab initio molecular orbital study of the mechanism of the gas phase reaction $SO_3 + H_2O$: Importance of the second water molecule. *J. Am. Chem. Soc.* **116**, 10316–10317 (1994).

72. E. J. Meijer and M. Sprik. A density functional study of the addition of water to SO_3 in the gas phase and in aqueous solution. *J. Phys. Chem. A* **102**, 2893–2898 (1998).

73. D. R. Hanson and A. R. Ravishankara. Investigation of the reactive and nonreactive processes involving $ClONO_2$ and HCl on water and nitric acid doped ice. *J. Phys. Chem.* **96**, 2682–2691 (1992).

74. J. P. D. Abbatt and M. J. Molina. Heterogenous interactions of $ClONO_2$ and HCl on nitric acid trihydrate at 202 K. *J. Phys. Chem.* **96**, 7674–7679 (1992).

75. R. P. Wayne. Chemistry of Atmospheres. An Introduction to the Chemistry of Atmospheres of Earth, the Planets, and their Satellites, second edition. Clarendon Press, Oxford, (1991).

76. A. B. Horn, J. R. Sodeau, T. B. Roddis, and N. A. Williams. Mechanism of the heterogeneous reaction of hydrogen chloride with chlorine nitrate and hypochlorous acid on water ice. *J. Phys. Chem. A* **102**, 6107–6120 (1998).

77. M. A. Alberty and S. D. VanDeveer. Modeling the Global Environment: Is the Montreal Protocol a Useful Precedent? Harrison Program on the Future Global Agenda, (1995).

78. A. H. Zewail. Femtochemistry: Recent progress in studies of dynamics and control of reactions and their transition states. *J. Phys. Chem.* **100**, 12701–12724 (1996).

79. A. H. Zewail. Femtochemistry: Atomic-scale dynamics of the chemical bond. *J. Phys. Chem. A* **104**, 5660–5694 (2000).

80. A. H. Zewail. The Chemical Bond: Structure and Dynamics. Academic Press, San Diego, (1992).

81. A. Douhal, S. K. Kim, and A. H. Zewail. Femtosecond molecular-dynamics of tautomerization in model base-pairs. *Nature* **378**, 260–263 (1995).

82. M. Chachisvillis, T. Fiebig, A. Douhal, and A. H. Zewail. Femtosecond dynamics of a hydrogen-bonded model base pair in the condensed phase: Double proton transfer in 7-azaindole. *J. Phys. Chem. A* **102**, 669–673 (1998).

83. N. Pugliano and R. J. Saykally. Measurement of quantum tunneling between chiral isomers of the cyclic water trimer. *Science* **257**, 1937–1940 (1992).

84. R. J. Saykally and G. A. Blake. Molecular interactions and hydrogen bond tunneling: Some new perspectives. *Science* **259**, 1570–1575 (1993).

85. K. Liu *et al.* Dynamics of structural rearrangements in the water trimer. *J. Am. Chem. Soc.* **116**, 3507–3512 (1994).

86. K. Liu, J. D. Cruzan, and R. J. Saykally. Water clusters. *Science* **271**, 929–933 (1996).

87. K. Liu, M. G. Brown, and R. J. Saykally. Terahertz laser vibration-rotation tunneling spectroscopy and dipole moment of a cage form of the water hexamer. *J. Phys. Chem. A* **101**, 8995–9010 (1997).

88. K. Liu, M. G. Brown, J. D. Cruzan, and R. J. Saykally. Terahertz laser spectroscopy of the water pentamer: Structure and hydrogen bond rearrangement dynamics. *J. Phys. Chem. A* **101**, 9011–9021 (1997).

89. J. D. Cruzan, M. R. Viant, M. G. Brown, and R. J. Saykally. Terahertz laser vibration-rotation tunneling spectroscopy of the water tetramer. *J. Phys. Chem. A* **101**, 9022–9031 (1997).

90. M. R. Viant *et al.* Pseudorotation in water trimer isotopomers using terahertz laser spectroscopy. *J. Phys. Chem. A* **101**, 9032–9041 (1997).

91. G. D. Billing and K. V. Mikkelsen. chapter Collisional approach, 18–24. John Wiley & Sons, Inc., Copenhagen and Arhus (1996).

92. H. Eyring. The activated complex in chemical reactions. *J. Chem. Phys.* **3**, 107–115 (1935).

93. S. Glasstone, K. Laidler, and H. Eyring. The Theory of Rate Processes. McGraw-Hill, New York, (1941).

94. K. J. Laidler and M. C. King. The development of transition state theory. *J. Phys. Chem.* **87**, 2657–2664 (1983).

95. D. G. Truhlar, W. L. Hase, and J. T. Hynes. Current status of transition state theory. *J. Phys. Chem.* **87**, 2664–2682 (1983).

96. D. G. Truhlar, A. D. Isaacson, and B. C. Garrett. chapter Generalized Transition State Theory, 65–137. CRC Press, Boca Raton, FL (1985).

97. M. M. Kreevoy and D. G. Truhlar. chapter Transition State Theory, 13–95. John Wiley & Sons, Inc., New York (1986).

98. S. C. Tucker and D. G. Truhlar. chapter Dynamical Formulation of Transition State Theory: Variational Transition States and Semiclassical Tunneling, 291–346. NATO ASI Series C 267. Kluwer, Dordrecht, The Netherlands (1989).

99. D. G. Truhlar, B. C. Garrett, and S. J. Klippenstein. Current status of transition-state theory. *J. Phys. Chem.* **100**, 12771–12800 (1996).

100. T. Loerting. Beschreibung des konzertierten intramolekularen Austausches von Wasserstoffatomen in zyklischen Molekülen im Zuge der Theorie des aktivierten Komplexes. Master's thesis, University of Innsbruck, Innsbruck, (1997).

101. W. H. Miller, N. C. Handy, and J. E. Adams. Reaction path Hamiltonian for polyatomic molecules. *J. Chem. Phys.* **72**, 99–112 (1980).

102. B. C. Garrett, D. G. Truhlar, R. S. Grev, and A. W. Magnuson. Improved treatment of threshold contributions in variational transition-state theory. *J. Phys. Chem.* **84**, 1730–1748 (1980).

103. Y.-P. Liu *et al.* Molecular modeling of the kinetic isotope effect for the [1,5]-sigmatropic rearrangement of cis-1,4-pentadiene. *J. Am. Chem. Soc.* **115**, 2408–2415 (1993).

104. B. C. Garrett, T. Joseph, T. N. Truong, and D. G. Truhlar. Application of the large-curvature tunneling approximation to polyatomic molecules: abstraction of H or D by methyl radical. *Chem. Phys.* **136**, 271–283 (1989).

105. D. G. Truhlar and M. S. Gordon. From force fields to dynamics: Classical and quantal paths. *Science* **249**, 491–498 (1990).

106. T. Loerting, K. R. Liedl, and B. M. Rode. Large curvature tunneling effects reveal concerted hydrogen exchange rates in cyclic hydrogen fluoride clusters comparable to carboxylic acid dimers. *J. Am. Chem. Soc.* **120**, 404–412 (1998).

107. T. Loerting, K. R. Liedl, and B. M. Rode. Predictions of rate constants and estimates for tunneling splittings of concerted proton transfer in small cyclic water clusters. *J. Chem. Phys.* **109**, 2672–2679 (1998).

108. Y.-P. Liu *et al.* Direct dynamics calculation of the kinetic isotope effect for an organic hydrogen-transfer reaction, including corner-cutting tunneling in 21 dimensions. *J. Am. Chem. Soc.* **115**, 7806–7817 (1993).

109. A. Gonzalez-Lafont, T. N. Truong, and D. G. Truhlar. Interpolated variational transition-state theory: Practical methods for estimating variational transition-state properties and tunneling contributions to chemical reaction rates from electronic structure calculations. *J. Chem. Phys.* **95**, 8875–8894 (1991).

110. J. C. Corchado *et al.* Dual-level reaction-path dynamics (the /// approach to VTST with semiclassical tunneling). application to OH + NH3 → H2O + NH2. *J. Phys. Chem.* **99**, 687–694 (1995).

111. F. Graf, R. Meyer, T.-K. Ha, and R. R. Ernst. Dynamics of hydrogen bond exchange in carboxlic acid dimers. *J. Chem. Phys.* **75**, 2914–2918 (1992).

112. A. Karpfen. Ab initio studies on hydrogen-bonded clusters: Structure and vibrational spectra of cyclic hydrogen fluoride $(HF)_n$ complexes. *Int. J. Quantum Chem., Quantum Chem. Symp.* **24**, 129–140 (1990).

113. A. Stöckli *et al.* Hydrogen bond dynamics in isotopically substituted benzoic acid dimers. *J. Chem. Phys.* **93**, 1502–1520 (1990).

114. B. C. Garrett and C. F. Melius. 35–54. NATO ASI Series C 339. Kluver Academic, Netherlands (1991).

115. L. Meschede and H. H. Limbach. Dynamic NMR study of the kinetic HH/HD/DD isotope effects on the double proton transfer in cyclic bis(p-fluorophenyl) formamidine dimers. *J. Phys. Chem.* **95**, 10267–10280 (1991).

116. G. Scherer and H. H. Limbach. Dynamic NMR study of the tautomerism of bicyclic oxalamidines: Kinetic HH/HD/DD isotope and solvent effects. *J. Am. Chem. Soc.* **116**, 1230–1239 (1994).

117. A. Karpfen and O. Yanovitskii. Cooperativity in hydrogen bonded clusters: An improved ab intio SCF study on the structure and energetics of neutral, protonated and deprotonated chains and of neutral, cyclic hydrogen fluoride oligomers. *J. Mol. Struct. (Theochem)* **314**, 211–227 (1994).

118. F. Aguilar-Parrilla, O. Klein, J. Elguero, and H. H. Limbach. A dynamic ^{15}N NMR study of kinetic hydrogen/deuterium isotope and tunnel effects on the triple proton transfer in crystalline 3,5-dimethylpyrazole. *Ber. Bunsen.-Ges. Phys. Chem.* **101**, 889–901 (1997).

119. H. Benedict *et al.* Solid state ^{15}N NMR and theoretical studies of primary and secondary geometric H/D isotope effects on low-barrier NHN-hydrogen bonds. *J. Am. Chem. Soc.* **120**, 2939–2950 (1998).

120. T. H. Dunning, Jr. *et al.* Theoretical studies of the energetics and dynamics of chemical reactions. *Science* **240**, 453–459 (1988).

121. D. J. Wales. Structure, dynamics, and thermodynamics of clusters: Tales from topographic potential surfaces. *Science* **271**, 925–929 (1996).

122. D. J. Wales, M. A. Miller, and T. R. Walsh. Archetypal energy landscapes. *Nature* **394**, 758–760 (1998).

123. E. Wigner. Über das Überschreiten von Potentialschwellen bei chemischen Reaktionen. *Z. Phys. Chem. B* **32**, 203–216 (1932).

124. M. Page and J. W. McIver, Jr. On evaluating the reaction path Hamiltonian. *J. Chem. Phys.* **88**, 922–935 (1988).

125. V. S. Melissas, D. G. Truhlar, and B. C. Garrett. Optimized calculations of reaction paths and reaction-path functions for chemical reactions. *J. Chem. Phys.* **96**, 5758–5772 (1992).

126. K. K. Baldridge, M. S. Gordon, R. Steckler, and D. G. Truhlar. Ab initio reaction paths and direct dynamics calculations. *J. Phys. Chem.* **93**, 5107–5119 (1989).

127. C. Gonzalez and H. B. Schlegel. An improved algorithm for reaction path following. *J. Chem. Phys.* **90**, 2154–2161 (1989).

128. C. Gonzalez and H. B. Schlegel. Reaction path following in mass-weighted internal coordinates. *J. Phys. Chem.* **94**, 5523–5527 (1990).

129. C. Gonzalez and H. B. Schlegel. Improved algorithms for reaction path following: Higher-order implicit algorithms. *J. Chem. Phys.* **95**, 5853–5860 (1991).

130. P. Y. Ayala and H. B. Schlegel. A combined method for determining reaction paths, minima, and transition state geometries. *J. Chem. Phys.* **107**, 375–384 (1997).

131. Y.-Y. Chuang and D. G. Truhlar. Improved dual-level direct dynamics method for reaction rate calculations with inclusion of multidimensional tunneling effects and validation for the reaction of H with trans-N_2H_2. *J. Phys. Chem. A* **101**, 3808–3814 (1997).

132. V. A. Benderskii, D. E. Makarov, and C. A. Wight. Chemical Dynamics at Low Temperatures, volume LXXXVIII of *Advances in Chemical Physics*. John Wiley & Sons, Inc., New York, (1994).

133. B. C. Garrett and D. G. Truhlar. A least-action variational method for calculating multidimensional tunneling probabilities for chemical reactions. *J. Chem. Phys.* **79**, 4931–4938 (1983).

134. W.-P. Hu, Y.-P. Liu, and D. G. Truhlar. Variational transition-state theory and semiclassical tunneling calculations with interpolated corrections: A new approach to interfacing electronic structure theory and dynamics for organic reactions. *J. Chem. Soc., Faraday Trans.* **90**, 1715–1725 (1994).

135. W.-P. Hu, I. Rossi, J. C. Corchado, and D. G. Truhlar. Molecular modeling of cobustion kinetics. The abstraction of primary and secondary hydrogens by hydroxyl radical. *J. Phys. Chem. A* **101**, 6911–6921 (1997).

136. E. Rosenman and M. L. McKee. Reaction path dynamics and theoretical rate constants for the $CH_3F + Cl \rightarrow HCl + CH_2F$ reaction by direct dynamics method. *J. Am. Chem. Soc.* **119**, 9033–9038 (1997).

137. A. Fernández-Ramos *et al.* Direct dynamics study of the dissociation and elimination channels in the thermal decomposition of methyl nitrite. *J. Am. Chem. Soc.* **120**, 7594–7601 (1998).

138. O. Roberto-Neto, E. L. Coitiño, and D. G. Truhlar. Dual-level direct dynamcis calculations of deuterium and carbon-13 kinetic isotope effects for the reaction Cl + CH_4. *J. Phys. Chem. A* **102**, 4568–4578 (1998).

139. J. C. Corchado *et al.* Dual-level direct dynamics calculations of the reaction rates for a Jahn-Teller reaction: Hydrogen abstraction from CH_4 or CD_4 by $O(^3P)$. *J. Phys. Chem. A* **102**, 4899–4910 (1998).

140. M. J. Frisch *et al.* Gaussian 98, Revision A.7. Gaussian, Inc., Pittsburgh PA, (1998).

141. I. N. Levine. Quantum Chemistry. Prentice Hall International, Inc., London, (1991).

142. F. Jensen. Introduction to Computational Chemistry. Wiley VCH, D-69469 Weinheim, Germany, (1999).

143. A. D. Becke. Density-functional thermochemistry. III. The role of exact exchange. *J. Chem. Phys.* **98**, 5648–5652 (1993).

144. C. Møller and M. S. Plesset. Note on an approximation treatment for many-electron systems. *Phys. Rev.* **46**, 618–622 (1934).

145. K. Raghavachari, G. W. Trucks, J. A. Pople, and M. Head-Gordon. A fifth-order perturbation comparison of electron correlation theories. *Chem. Phys. Lett.* **157**, 479–483 (1989).

146. T. H. Dunning, Jr. Gaussian basis sets for use in correlated molecular calculations. I. The atoms boron through neon and hydrogen. *J. Chem. Phys.* **90**, 1007–1023 (1989).

147. L. A. Curtiss, K. Raghavachari, and J. A. Pople. Gaussian-2 theory using reduced Møller-Plesset orders. *J. Chem. Phys.* **98**, 1293–1298 (1993).

148. C. Märker *et al.* A critical analysis of electronic density functionals for structural, energetic, dynamic and magnetic properties of hydrogen fluoride clusters. *J. Comput. Chem.* **18**, 1695–1719 (1997).

149. T. Loerting and K. R. Liedl. Toward elimination of discrepancies between theory and experiment: Double proton transfer in dimers of carboxylic acids. *J. Am. Chem. Soc.* **120**, 12595–12600 (1998).

150. T. Loerting and K. R. Liedl. Temperature dependent ways of proton transfer – a benchmark study on cyclic HF oligomers. *J. Phys. Chem. A* **103**, 9022–9028 (1999).

151. A. D. Becke. Density-functional thermochemistry. V. Systematic optimization of exchange-correlation functionals. *J. Chem. Phys.* **107**, 8554–8560 (1997).

152. Y.-Y. Chuang *et al.* Polyrate8.2. University of Minnesota, Minneapolis, (1999).

153. J. C. Corchado, E. L. Coitiño, Y.-Y. Chuang, and D. G. Truhlar. Gaussrate8.2. University of Minnesota, Minneapolis, (1999).

154. K. A. Nguyen, I. Rossi, and D. G. Truhlar. A dual-level shephard interpolation method for generating potnetial energy surfaces for dynamics calculations. *J. Chem. Phys.* **103**, 5522–5530 (1995).

155. P. W. Atkins. Physical Chemistry. Oxford University Press, Walton Street, Oxford OX2 6DP, fourth edition, (1990).

156. L. Masgrau, À. González-Lafont, and J. M. Lluch. Effect of a complex formation on the calculated low-pressure rate constant of a bimolecular gas-phase reaction governed by tunneling. *J. Comput. Chem.* **20**(16), 1685–1692 (1999).

157. R. C. Millikan and K. S. Pitzer. The infrared spectra of dimeric and crystalline formic acid. *J. Am. Chem. Soc.* **80**, 3515–3521 (1958).

158. C. C. Costain and G. P. Srivastava. Microwave rotation spectra of hydrogen-bonded molecules. *J. Chem. Phys.* **41**, 1620–1627 (1964).

159. J. E. Bertie and K. H. Michaelian. The Raman spectra of gaseous formic acid -h_2 and -d_2. *J. Chem. Phys.* **76**, 886–894 (1982).

160. C. C. Wilson, N. Shankland, and A. J. Florence. Direct determination of the temperature dependence of proton transfer in the benzoic acid dimer by single crystal neutron diffraction. *Chem. Phys. Lett.* **253**, 103–107 (1996).

161. C. C. Wilson, N. Shankland, and A. J. Florence. A single-crystal neutron diffraction study of the temperature dependence of hydrogen-atom disorder in benzoic acid dimers. *J. Chem. Soc., Faraday Trans.* **92**, 5051–5057 (1996).

162. T. Neuheuser, B. A. Hess, C. Reutel, and E. Weber. Ab initio calculations of supramolecular recognition modes. cyclic versus noncyclic hydrogen bonding in the formic acid/formamide system. *J. Phys. Chem.* **98**, 6459–6467 (1994).

163. W. Qian and S. Krimm. Origin of the C=O stretch mode splitting in the formic acid dimer. *J. Phys. Chem.* **100**, 14602–14608 (1996).

164. W. Qian and S. Krimm. A model for the interactions of the hydrogen bond that incorporates its spectroscopic properties. *J. Phys. Chem. A* **102**, 5825–5827 (1997).

165. K. R. Liedl, S. Sekusak, and E. Mayer. Has the dimer of carbonic acid a lower energy than its constituents water and carbon dioxide? *J. Am. Chem. Soc.* **119**, 3782–3784 (1997).

166. W. Qian and S. Krimm. Electrostatic model for the interaction force constant of the formic acid dimer. *J. Phys. Chem. A* **102**, 659–667 (1998).

167. W. Hage, K. R. Liedl, A. Hallbrucker, and E. Mayer. Carbonic-acid in the gas-phase and its astrophysical relevance. *Science* **279**, 1332–1335 (1998).

168. B. H. Meier, F. Graf, and R. R. Ernst. Structure and dynamics of intramolecular hydrogen bonds in carboxylic acid dimers: A solid state NMR study. *J. Chem. Phys.* **76**, 767–774 (1982).

169. S. Nagaoka *et al.* A study on the proton transfer in the benzoic acid dimer by ^{13}C high-resolution solid-state NMR and proton T_1 measurements. *Chem. Phys. Lett.* **80**, 580–584 (1981).

170. S. Nagaoka *et al.* An NMR relaxation study on the proton transfer in the hydrogen bonded carboxylic acid dimers. *J. Chem. Phys.* **79**, 4694–4703 (1983).

171. T. Agaki *et al.* A study of hydrogen bond dynamics in carboxylic acids by NMR T_1 measurements: Isotope effects and hydrogen-bond length dependence. *Chem. Phys. Lett.* **139**, 331–335 (1987).

172. M. A. Neumann *et al.* Proton dynamics and the tautomerization potential in benzoic acid crystals. *Ber. Bunsen.-Ges. Phys. Chem.* **102**, 325–334 (1998).

173. B. H. Meier *et al.* Neutron scattering study of dynamically disorederd hydrogen bonds: Terephthalic acid. *Chem. Phys. Lett.* **103**, 169–174 (1983).

174. J. L. Skinner and H. P. Trommsdorf. Proton transfer in benzoic acid crystals: A chemical spin-boson problem. Theoretical analysis of nuclear magnetic resonance, neutron scattering, and optical experiments. *J. Chem. Phys.* **89**, 897–907 (1988).

175. A. J. Horsewill *et al.* The quantum dynamics of proton transfer in the hydrogen bond. *Ber. Bunsen.-Ges. Phys. Chem.* **102**, 317–324 (1998).

176. J. M. Clemens, R. M. Hochstrasser, and H. P. Trommsdorf. Direct studies of proton tunneling in hydrogen bonded mixed molecular crystals by optical excitation. *J. Chem. Phys.* **80**, 1744–1753 (1984).

177. G. R. Holtom, H. P. Trommsdorf, and R. M. Hochstrasser. Impurity-induced double proton transfer in benzoic acid crystals. *Chem. Phys. Lett.* **131**, 44–50 (1986).

178. R. M. Hochstrasser and H. P. Trommsdorff. Observation of delocalized states of the proton in carboxylic acid dimers in condensed matter. *Chem. Phys.* **115**, 1–6 (1987).

179. M. Pierre, H. P. Trommsdorff, and R. M. Hochstrasser. volume 17 of *Proceedings in Physics*, chapter Optical studies of proton tunneling and relaxation in benzoic acid, 186–191. Springer, Berlin (1987).

180. C. Rambaud *et al.* Tunneling dynamcis of delocalized protons in benzoic acid dimers: A study of the temperature dependence by time and frequency domain optical spectroscopy. *Chem. Phys.* **136**, 335–347 (1989).

181. A. Heuer and U. Haeberlen. The dynamics of hydrogens in double well potentials: The transition of the jump rate from the low temperature quantum-mechanical to the high temperature activated regime. *J. Chem. Phys.* **95**, 4201–4214 (1991).

182. A. Oppenländer, C. Rambaud, H. P. Trommsdorff, and J. C. Vial. Translational tunneling of protons in benzoic acid crystals. *Phys. Rev. Lett.* **63**, 1432–1435 (1989).

183. A. J. Horsewill, P. J. McDonald, and D. Vijayaraghavan. Hydrogen bond dynamics in benzoic acid dimers as a function of hydrostatic pressure measured by nuclear magnetic resonance. *J. Chem. Phys.* **100**, 1889–1894 (1994).

184. D. F. Brougham, A. J. Horsewill, and R. I. Jenkinson. Proton transfer dynamics in the hydrogen bond: A direct measurement of the incoherent tunneling rate by NMR and the quantum-to-classical transition. *Chem. Phys. Lett.* **272**, 69–74 (1997).

185. V. P. Sakun, M. V. Vener, and N. D. Sokolov. Proton tunneling assisted by the intermolecular vibration excitation. temperature dependence of the proton spin-lattice relaxation time in benzoic acid powder. *J. Chem. Phys.* **105**, 379–387 (1996).

186. R. Meyer and R. R. Ernst. Transitions induced in a double minimum system by interaction with a quantum mechanical heat bath. *J. Chem. Phys.* **93**, 5518–5532 (1990).

187. D. F. Brougham *et al.* The correlation between hydrogen bond tunneling dynamics and the structure of benzoic acid dimers. *J. Chem. Phys.* **105**, 979–982 (1996).

188. S. Hayashi, J. Umemura, S. Kato, and K. Morokuma. Ab initio molecular orbital study on the formic acid dimer. *J. Phys. Chem.* **88**, 1330–1334 (1984).

189. Y.-T. Chang, Y. Yamaguchi, W. H. Miller, and H. F. Schaefer, III. An analysis of the infrared and Raman spectra of the formic acid dimer $(HCOOH)_2$. *J. Am. Chem. Soc.* **109**, 7245–7253 (1987).

190. N. Shida, P. F. Barbara, and J. Almlöf. A reaction surface Hamiltonian treatment of the double proton transfer of formic acid dimer. *J. Chem. Phys.* **94**, 3633–3643 (1991).

191. Y. Kim. Direct dynamics calculations of the double proton transfer in formic acid dimer. *J. Am. Chem. Soc.* **118**, 1522–1528 (1996).

192. N. Shida, J. Almlöf, and P. F. Barbara. Tunneling paths in intramolecular proton transfer. *J. Phys. Chem.* **95**, 10457–10464 (1991).

193. V. A. Benderskii, S. Y. Grebenshchikov, D. E. Makarov, and E. V. Vetoshkin. Tunneling trajectories of two proton-transfer. *Chem. Phys.* **185**, 101–112 (1994).

194. Z. Smedarchina, A. Fernandez-Ramos, and M. A. Rios. A comparison of two methods for direct tunneling dynamics: Hydrogen exchange in the glycolate anion as a test case. *J. Chem. Phys.* **106**, 3956–3964 (1997).

195. A. Fernández-Ramos, Z. Smedarchina, M. Z. Zgierski, and W. Siebrand. Mode-specific tunneling splittings in 9-hydroxyphenalenone: Comparison of two methods for direct tunneling dynamics. *J. Chem. Phys.* **109**, 1004–1013 (1998).

196. Z. Smedarchina, W. Caminati, and F. Zerbetto. Tunneling splittings from ab initio data: indoline, a test case. *Chem. Phys. Lett.* **237**, 279–285 (1995).

197. Z. Smedarchina, W. Siebrand, and M. Z. Zgierski. An instanton approach to intramolecular hydrogen exchange: Tunneling splittings in malonaldehyde and the hydrogenoxalate anion. *J. Chem. Phys.* **103**, 5326–5334 (1995).

198. Z. Smedarchina, W. Siebrand, and M. Z. Zgierski. Mode-specific hydrogen tunneling in tropolone: An instanton approach. *J. Chem. Phys.* **104**, 1203–1212 (1996).

199. W. H. Miller. Periodic orbit description of tunneling in symmetric and asymmetric double-well potentials. *J. Phys. Chem.* **83**, 960–963 (1979).

200. G. C. Hancock *et al.* Reaction-path analysis of the tunneling splitting in fluxional molecules: Application to the degenerate rearrangement of hydrogen fluoride dimer. *J. Chem. Phys.* **85**, 4997–5003 (1986).

201. G. C. Hancock and D. G. Truhlar. Reaction-path analysis of the effect of monomer excitation on the tunneling splitting of the hydrogen fluoride dimer. *J. Chem. Phys.* **90**, 3498–3505 (1989).

202. Y. Volobuev, W. C. Necoechea, and D. G. Truhlar. Tunneling splittings in predissociated HF dimer. *J. Phys. Chem. A* **101**, 3045–3048 (1997).

203. N. Makri and W. H. Miller. Basis set methods for describing the quantum mechanics of a "system" interacting with a harmonic bath. *J. Chem. Phys.* **86**, 1451–1457 (1987).

204. D. J. Wales. Some estimates of tunneling splittings in small clusters. *J. Am. Chem. Soc.* **115**, 11191–11201 (1993).

205. W. T. Duncan and T. N. Truong. Thermal and vibrational-state selected rates of the $CH_4+Cl \rightleftharpoons HCl+CH_3$ reaction. *J. Chem. Phys.* **103**, 9642–9652 (1995).

206. J. K. Gregory and D. C. Clary. Calculations of the tunneling splittings in water dimer and trimer using diffusion monte carlo. *J. Chem. Phys.* **102**, 7817–7829 (1995).

207. J. J. Paz, M. Moreno, and J. M. Lluch. Bidimensional tunneling splitting in the A $^1B_2$ and X $^1A_1$ states of tropolone. *J. Chem. Phys.* **103**, 353–359 (1995).

208. V. A. Benderskii *et al.* Tunneling splitting in vibrational spectra of non-rigid molecules. I. Perturbative instanton approach. *Chem. Phys.* **219**, 119–142 (1997).

209. V. A. Benderskii, E. V. Vetoshkin, L. von Laue, and H. P. Trommsdorff. Tunneling splitting in vibrational spectra of non-rigid molecules. II. Excited states. *Chem. Phys.* **219**, 143–160 (1997).

210. V. L. Klochikin and L. I. Trakhtenberg. Tunneling splitting in vibrational spectra of molecules. *Chem. Phys. Lett.* **285**, 34–40 (1998).

211. I. Ohmine and S. Saito. Water dynamics: Fluctutation, relaxation, and chemical reactions in hydrogen bond network rearrangement. *Acc. Chem. Res.* **32**, 741–749 (1999).

212. K. R. Liedl, S. Sekusak, R. T. Kroemer, and B. M. Rode. New insights into the dynamics of concerted proton tunneling in cyclic water and hydrogen fluoride clusters. *J. Phys. Chem. A* **101**, 4707–4716 (1997).

213. N. Makri and W. H. Miller. A semiclassical tunneling model for use in classical trajectory simulations. *J. Chem. Phys.* **91**, 4026–4036 (1989).

214. S. Nagaoka, N. Hirota, T. Matsushita, and K. Nishimoto. An ab initio calculation on proton transfer in the benzoic acid dimer. *Chem. Phys. Lett.* **92**, 498–502 (1982).

215. C. Scheurer and P. Saalfrank. Density matrix model for hydrogen transfer in the benzoic acid dimer. *Chem. Phys. Lett.* **245**, 201–208 (1995).

216. C. Scheurer and P. Saalfrank. Hydrogen transfer in vibrationally relaxing benzoic acid dimers: Time-dependent density matrix dynamics and infrared spectra. *J. Chem. Phys.* **104**, 2869–2882 (1995).

217. L. Turi. Ab initio molecular orbital analysis of dimers of cis-formic acid. Implications for condensed phases. *J. Phys. Chem.* **100**, 11285–11291 (1996).

218. D. Sundholm, M. R. Sundberg, and R. Uggla. Intermolecular interactions in p-chlorobenzoic acid dimers. *J. Phys. Chem. A* **102**, 7137–7142 (1998).

219. D. Antoniou and S. D. Schwartz. Proton transfer in benzoic acid crystals: Another look using quantum operator theory. *J. Chem. Phys.* **109**, 2287–2293 (1998).

220. K. R. Liedl, R. T. Kroemer, and B. M. Rode. Hydrogen transitions between $(HF)_n$ C_{nh} structures (n=2–5) via D_{nh} transition states as models for hydrogen tunneling in hydrogen fluoride clusters. *Chem. Phys. Lett.* **246**, 455–462 (1995).

221. P. Schuster *et al.* Chemical and Biochemical Reactivity, The Jerusalem Symposia on Quantum Chemistry and Biochemistry, volume VI, chapter Potential Curves for Proton Transfer Along Hydrogen Bonds, 257–282. The Israel Academy of Sciences and Humanities, Jerusalem (1974).

222. R. P. Bell. The Tunnel Effect in Chemistry. Chapman and Hall, London and New York, (1980).

223. D. Gerritzen and H. H. Limbach. Kinetic isotope effects and tunneling in cyclic double and triple proton transfer between acetic scid and methanol in tetrahydrofuran studied by dynamic ^{1}H and ^{2}H nmr spectroscopy. *J. Am. Chem. Soc.* **106**, 869–879 (1984).

224. J. Catalán, J. Palomar, and J. L. G. de Paz. Intramolecular proton or hydrogen-atom transfer in the ground and excited states of 2-hydroxybenzoyl compounds. *J. Phys. Chem. A* **101**, 7914–7921 (1997).

225. A. V. Smirnov *et al.* Excited state intramolecular H atom transfer of hypericin and hypocrellin A investigated by fluorescence upconversion. *J. Phys. Chem. A* **103**, 7949–7957 (1999).

226. P. Mueller. Glossary of terms used in physical organic chemistry. *Pure. Appl. Chem.* **66**, 1077–1184 (1994).

227. K. P. C. Vollhardt. Organic Chemistry. W. H. Freeman and Company, New York, (1994).

228. G. C. Lynch, D. G. Truhlar, and B. C. Garrett. Test of the accuracy of small-curvature and minimum-energy reference paths for parametrizing the search for least-action tunneling paths: (H,D) + H'Br -> (H,D)Br + H'. *J. Chem. Phys.* **90**, 3102–3109 (1989).

229. R. A. Marcus and M. E. Coltrin. A new tunneling path for reactions such as H+H_2 $\rightleftharpoons$ H_2+H. *J. Chem. Phys.* **67**, 2609 (1977).

230. M. S. Child. Semiclassical Mechanics with Molecular Applications, volume 25 of *International Series of Monographs on Chemistry*. Oxford Science Publications, Oxford, (1991).

231. L. Schriver, D. Carrere, A. Schriver, and K. Jaeger. Matrix-isolation photolysis of SO_2, O_3 and H_2O: Evidence for the H_2O:SO_3 complex. *Chem. Phys. Lett.* **181**, 505–511 (1991).

232. J. A. Phillips, M. Canagaratna, H. Goodfriend, and K. R. Leopold. Microwave detection of a key intermediate in the formation of atmospheric sulfuric acid: The structure of H_2O—SO_3. *J. Phys. Chem.* **99**, 501–504 (1995).

233. A. R. Bandy and J. C. Ianni. Study of the hydrates of H_2SO_4 using density functional theory. *J. Phys. Chem. A* **102**, 6533–6539 (1998).

234. P. Beichert and O. Schrems. Complexes of sulfuric acid with hydrogen chloride, water, nitric acid, chlorine nitrate and hydrogen peroxide: An ab initio investigation. *J. Phys. Chem. A* **102**, 10540–10544 (1998).

235. H. Arstila, K. Laasonen, and A. Laaksonen. Ab initio study of gas-phase sulphuric acid hydrates containing 1 to 3 water molecules. *J. Chem. Phys.* **108**, 1031–1039 (1998).

236. A. Givan, L. A. Larsen, A. Loewenschuss, and C. J. Nielsen. Infrared matrix isolation study of H_2SO_4 and its complexes with H_2O. *J. Chem. Soc., Faraday Trans.* **94**, 827–835 (1998).

237. R. L. Kuczkowski, R. D. Suenram, and F. J. Lovas. Microwave spectrum, structure, and dipole moment of sulfuric acid. *J. Am. Chem. Soc.* **103**, 2561–2566 (1981).

238. L. Kurdi and E. Kochanski. Theoretical studies of sulfuric acid monohydrate: Neutral or ionic complex? *Chem. Phys. Lett.* **158**, 111–115 (1989).

239. T. Loerting *et al.* On the surprising kinetic stability of carbonic-acid (H_2CO_3). *Angew. Chem. Int. Ed.* **39**, 891–894 (2000).

240. D. E. Folmer, E. S. Wisniewski, S. M. Hurley, and A. W. Castleman, Jr. Femtosecond cluster studies of the solvated 7-azaindole excited state double-proton transfer. *Proc. Natl. Acad. Sci.* **96**, 12980–12986 (1999).

241. S. Aloisio and J. S. Francisco. Reaction rate constant determination of association reactions using theoretical calculations: A case study of the $HO_2 + NO_2$ reaction. *J. Phys. Chem. A* **104**, 6212–6217 (2000).

242. S. F. Boys and F. Bernardi. The calculation of small molecular interactions by the differences of separate total energies. Some procedures with reduced errors. *Mol. Phys.* **19**, 553–566 (1970).

243. F. B. van Duijneveldt, J. G. C. M. van Duijneveldt-van de Rijdt, and J. H. van Lenthe. Ab initio calculations on the geometry and oh vibrational frequency shift of cyclic water trimer. *Chem. Phys.* **175**, 271–281 (1993).

244. F. B. van Duijneveldt. Molecular Interactions: From van der Waals to Strongly Bound Complexes, chapter Basis Set Superposition Error, 81–104. John Wiley & Sons, Chichester (1997).

245. A. K. Rappé and E. R. Bernstein. Ab initio calculation of nonbonded interactions: Are we there yet? *J. Phys. Chem. A* **104**, 6117–6128 (2000).

246. K. R. Liedl. Dangers of counterpoise corrected hypersurfaces - advantages of basis set superposition improvement. *J. Chem. Phys.* **108**, 3199–3204 (1998).

247. E. V. Akhmatskaya *et al.* Formation of H_2SO_4 from SO_3 and H_2O, catalysed in water clusters. *Chem. Comm.* , 707 (1997).

248. A. Jaecker-Voirol, P. Mirabel, and H. Reiss. Hydrates in supersaturated binary sulfuric acid-water vapor: A reexamination. *J. Chem. Phys.* **87**, 4849–4852 (1987).

249. L. Ying and X. Zhao. Theoretical studies of $XONO_2$–H_2O (X=Cl, H) complexes. *J. Phys. Chem. A* **101**, 6807–6812 (1997).

250. R. Bianco and J. T. Hynes. Ab initio model study of the mechanism of chlorine nitrate hydrolysis on ice. *J. Phys. Chem. A* **102**, 309–314 (1998).

251. R. Bianco, B. J. Gertner, and J. T. Hynes. Proton transfer reactions at the surface of ice, heterogeneous reactions involved in stratospheric ozone depletion. *Ber. Bunsen.-Ges. Phys. Chem.* **102**, 518–526 (1998).

252. S. C. Xu and X. S. Zhao. Theoretical investigation of the reaction of $ClONO_2$ with H_2O on water clusters. *J. Phys. Chem. A* **103**, 2100–2106 (1999).

253. J. McNamara and I. H. Hillier. Exploration of the mechanism of the hydrolysis of chlorine nitrate in small water clusters using electronic structure methods. *J. Phys. Chem. A* **103**, 7310–7321 (1999).

254. J. P. McNamara, G. Tresadern, and I. H. Hillier. The facile decomposition of chlorine nitrate in small water clusters. *Chem. Phys. Lett.* **310**, 265–270 (1999).

255. G. S. Hammond. A correlation of reaction rates. *J. Am. Chem. Soc.* **77**, 334–338 (1955).

256. D. Farcasiu. The use and misuse of the Hammond postulate. *J. Chem. Edu.* **52**, 76–79 (1975).

257. S. J. Oltmans and D. J. Hofmann. Increase in lower-stratospheric water vapour at a mid-latitude northern hemisphere site from 1981 to 1994. *Nature* **374**, 146–149 (1995).

258. S. Payan *et al.* First direct simultaneous HCl and $ClONO_2$ profile measurements in the arctic vortex. *Geophys. Res. Lett.* **25**, 2663–2666 (1998).

259. A. E. Waibel *et al.* Arctic ozone loss due to denitrification. *Science* **283**, 2064–2069 (1999).

260. D. R. Hanson. Reactivity of $ClONO_2$ on $H_2^{18}O$ ice and organic liquids. *J. Phys. Chem.* **99**, 13059–13061 (1995).

261. H. A. Donsig, D. Herridge, and J. C. Vickerman. Static SIMS studies of reactions on mimics of polar stratospheric clouds III: Mechanism of chlorine nitrate decomposition and reaction. *J. Phys. Chem. A* **103**, 9211–9220 (1999).

262. J. R. Sodeau, A. B. Horn, S. F. Banham, and T. G. Koch. Ionization of chlorine nitrate on ice at 180 K. *J. Phys. Chem.* **99**, 6258–6262 (1995).

263. P. Beichert and O. Schrems. Ab initio calculations of the catalytic impact of H_2SO_4 and HSO_4^- on the reaction of HCl with $ClNO_3$. *Phys. Chem. Chem. Phys.* **1**, 5459–5462 (1999).

264. J. M. V. Doren, A. A. Viggiano, and R. A. Morris. Rate enhancement of the reaction of HCl with $ClONO_2$ by ions: Implications for the mechanisms of stratospherically important heterogeneous reactions. *J. Am. Chem. Soc.* **116**, 6957–6958 (1994).

265. A. M. Mebel and K. Morokuma. Theoretical study of the reaction of HCl with $ClONO_2$ catalyzed by NO_3^-. "Attachment-detachment" mechansim for the anion-catalyzed neutral reactions. *J. Phys. Chem.* **100**, 2985–2992 (1996).

266. E. V. Akhmatskaya *et al.* Hydrolysis of SO_3 and $ClONO_2$ in water clusters. a combinded experimental and theoretical study. *J. Chem. Soc., Faraday Trans.* **93**, 2775–2779 (1997).

267. J. P. McNamara, G. Tresadern, and I. H. Hillier. Exploration of the mechanism of the activation of $ClONO_2$ by HCl in small water clusters using electronic structure methods. *J. Phys. Chem. A* **104**, 4030–4044 (2000).

268. M. Svanberg, J. B. C. Petterson, and K. Bolton. Coupled QM/MM molecular dynamics simulations of HCl interacting with ice surfaces and water clusters — evidence of rapid ionization. *J. Phys. Chem. A* **104**, 5787–5798 (2000).

269. H. Wincel, E. Mereand, and A. W. Castleman, Jr. Gas-phase reactions of $ClONO_2$ with $Cl^-(D_2O)_{n=0-3}$ and NO_2^-. *J. Phys. Chem. A* **101**, 8248–8254 (1997).

270. R. Bianco and J. T. Hynes. A theoretical study of the reaction of $ClONO_2$ with ice. *J. Phys. Chem. A* **103**, 3797–3801 (1999).

271. S.-H. Lee *et al.* The HCl+$ClONO_2$ reaction on various water ice surfaces. *Chem. Phys. Lett.* **315**, 7–11 (1999).

272. R. Oppliger, A. Allanic, and M. J. Rossi. Real-time kinetics of the uptake of $ClONO_2$ on ice and in the presence of HCl in the temperature range 160 K $\leq$ T $\leq$ 200 K. *J. Phys. Chem. A* **101**, 1903–1911 (1997).

273. S. B. Barone, M. A. Zondlo, and M. A. Tolbert. A kinetic and product study of the hydrolysis of $ClONO_2$ on type Ia polar stratospheric cloud materials at 185 K. *J. Phys. Chem. A* **101**, 8643–8652 (1997).

274. B. S. Berland, M. A. Tolbert, and S. M. George. Surface sensitive studies of the reactive uptake of chlorine nitrate on ice. *J. Phys. Chem. A* **101**, 9954–9963 (1997).

275. A. B. Horn, J. R. Sodeau, T. B. Roddis, and N. A. Williams. Low temperature reaction of chlorine nitrate with water ice. Formation of molecular nitric acid. *J. Chem. Soc., Faraday Trans.* **94**, 1721–1724 (1998).

276. D. B. Kirk-Davidoff, E. J. Hintsa, J. G. Anderson, and D. W. Keith. The effect of climate change on ozone depletion through changes in stratospheric water vapour. *Nature* **402**, 399–401 (1999).

277. R. S. MacTaylor, J. J. Gilligan, D. J. Moody, and A. W. Castleman, Jr. Molecular activation by surface coordination: New model for HCl reactivity on water-ice polar stratospheric clouds. *J. Phys. Chem. A* **103**, 4196–4201 (1999).

278. P. M. de F. Forster and K. P. Shine. Stratospheric water vapour changes as a possible contributer to observed stratospheric cooling. *Geophys. Res. Lett.* **26**, 3309–3312 (1999).

279. D. L. Hartmann *et al.* Can ozone depletion and global warming interact to produce rapid climate change? *Proc. Natl. Acad. Sci.* **97**, 1412–1417 (2000).

280. D. J. Hofmann and S. J. Oltmans. The effect of stratospheric water vapor on the heterogeneous reaction rate of $ClONO_2$ and H_2O for sulfuric acid aerosol. *Geophys. Res. Lett.* **19**, 2211–2214 (1992).

Appendix A

List of Tables

List of Tables

Appendix B

List of Figures

List of Figures

Appendix C

Abbreviations

6-31+G(d)	Pople basis set containing both diffuse and polarization functions (double zeta)
μOMT	microcanonical optimized multidimensional tunneling
aug-cc-pVDZ	correlation consistent Dunning basis set (double zeta)
aug-cc-pVTZ	correlation consistent Dunning basis set (triple zeta)
BAD	benzoic acid dimer
B3LYP	Becke's three parameter hybrid functional using the Lee-Yang-Parr correlation functional
CCSD(T)	coupled cluster singles, doubles, and perturbative triples method
DMS	dimethyl sulfide
FAD	formic acid dimer
G2(MP2)	Gaussian-2 theory using reduced Møller-Plesset orders
IRC	intrinsic reaction coordinate
LCT	large curvature tunneling
MEP	minimum energy path
MP2	Møller-Plesset second-order perturbation theory
PES	potential energy (hyper)surface
PSC	polar stratospheric cloud
PT	proton transfer
RRKM	Rice, Ramsperger, Kassel and Marcus theory
SCT	small curvature tunneling
S_N2	bimolecular nucleophilic substitution
TS	transition state
(V)TST	(variational) transition state theory
ZCT	zero curvature tunneling

Appendix D

About Me

Curriculum Vitae

Name	**Mag. Thomas Loerting**
Date of Birth	October 29, 1973
Place of Birth	Innsbruck
Father	Werner Sigfried Loerting
Mother	Gerda Loerting
Nationality	Austria
1980–1984	primary school in Innsbruck (VS Neu-Arzl)
1984–1992	high school in Innsbruck (BRG Reithmannstraße)
since 1988	working experience as metal-worker
6/1992	high school graduation with distinction
1992–1997	chemistry and mathematics diploma studies
	(Leopold-Franzens University Innsbruck)
since 1995	university tutor for inorganic, organic and theoretical chemistry,
	system administrator for Windows and Linux systems
9/1996–12/1997	master thesis at the Institute for General, Inorganic and
	Theoretical Chemistry supervised by Prof. Bernd M. Rode
	("Characterization of the concerted intramolecular exchange of
	hydrogen atoms in cyclic clusters by transition state theory")
12/1997	MSc with distinction
	(quantum-chemical calculations, vibrational spectroscopy)
since 1998	PhD studies at the Institute for General, Inorganic and
	Theoretical Chemistry supervised by Prof. Klaus R. Liedl
1/1999–8/1999	compulsory military service as medical assistant (military hospital Innsbruck)
since 10/1999	scholarship holder of the Austrian Academy of Sciences

Publication List

Mag. Thomas Loerting

1998   "Large Curvature Tunneling Effects Reveal Concerted Hydrogen Exchange
Rates in Cyclic Hydrogen Fluoride Clusters Comparable to Carboxylic Acid Dimers",
Thomas Loerting, Klaus R. Liedl, Bernd M. Rode,
J. Am. Chem. Soc., 120 (1998) 404–412.

"Predictions of rate constants and estimates for tunneling splittings
of concerted proton transfer in small cyclic water clusters",
Thomas Loerting, Klaus R. Liedl, Bernd M. Rode,
J. Chem. Phys., 109 (1998) 2662–2671.

"Toward Elimination of Discrepancies between Theory and Experiment:
Double Proton Transfer in Dimers of Carboxylic Acids",
Thomas Loerting, Klaus R. Liedl,
J. Am. Chem. Soc., 120 (1998) 12595–12600.

1999   "Temperature dependent ways of proton transfer -
A benchmark study on cyclic HF oligomers",
Thomas Loerting, Klaus R. Liedl,
J. Phys. Chem. A, 103 (1999) 9022–9028.

2000 | "On the surprising kinetic stability of carbonic acid (H_2CO_3)",

Thomas Loerting, Christofer Tautermann, Romano T. Kroemer,

Ingrid Kohl, Andreas Hallbrucker, Erwin Mayer, Klaus R. Liedl,

Angew. Chem. Int. Ed., 39 (2000) 891–894,

Angew. Chem., 112 (2000) 919–922.

"On the competing hydrations of sulfur dioxide and

sulfur trioxide in our atmosphere",

Thomas Loerting, Romano T. Kroemer, Klaus R. Liedl,

Chem. Comm., (2000) 999–1000.

"Toward Elimination of Discrepancies between Theory and Experiment:

The Rate Constant of the Atmospheric Conversion of SO_3 to H_2SO_4",

Thomas Loerting, Klaus R. Liedl,

Proc. Natl. Acad. Sci. USA, 97 (2000) in press.

"Prediction of the structure of human Janus kinase 2 (JAK2) comprising

the two carboxy-terminal domains reveals a mechanism for autoregulation",

Klaus Lindauer, Thomas Loerting, Klaus R. Liedl, Romano T. Kroemer,

submitted.

2000 | "Understanding Ozone Depletion: The Reaction Rate Constant

of Chlorine Nitrate Hydrolysis",

Thomas Loerting, Klaus R. Liedl,

submitted.

"The structure, modeling and dynamics of hindered 5,6-diarylacenaphthenes",

Wendy Cross, Geoffrey E. Hawkes, Romano T. Kroemer, Klaus R. Liedl,

Thomas Loerting, Rima Nasser, Robin G. Pritchard, Melanie Steele,

Michael Watkinson, Andrew Whiting,

submitted.

28th July 2000

Tunneling is like winning the lottery without having to buy a ticket

Viktor I. Goldanskii